Frequency Stability in Future Grids: The Role of Non-Synchronous Generation and Storage Systems

Dipl.-Ing. Alexander Rainer, BSc

0861368 (TUG)

5003234 (UOW)

Thesis submitted in partial fulfilment of the requirements for the degree of

Doctor of Philosophy

in Electrical Engineering

under the Joint PhD program

Supervisors

Ao.Univ.-Prof. Dipl.-Ing. Dr.techn. Herwig Renner
Institute for Electrical Power Systems
Graz University of Technology
Austria

Prof. Sarath Perera
Associate Professor Ashish Agalgaonkar
School of Electrical, Computer and Telecommunications Engineering
University of Wollongong
Australia

March 2022

Acknowledgements

In many ways, a doctoral thesis is an effort that would be impossible to complete without the people surrounding one. I am grateful that I had the opportunity to conduct this research under a Joint PhD program at the Graz University of Technology and University of Wollongong. This made it possible for me to stay abroad for almost two years – learning so much along the way.

First, I want to sincerely thank my supervisors Prof. Herwig Renner of the Graz University of Technology and Prof. Sarath Perera of the University of Wollongong that made everything possible and helped immensely from start to finish. Without your dedication and support to start this joint endeavour this would not have been possible. My deepest gratitude to you both for your insights, your wisdom, and patience.

I would also like to thank my co-supervisor, Associate Professor Ashish P. Agalgaonkar at the University of Wollongong for always having an open ear and getting me excited for cricket.

My research at the University of Wollongong was financially supported by the Postgraduate Award (UPA). Without it, my stay in Australia wouldn't have been possible.

To the wonderful current and former colleagues at the Institute of Electrical Power System at the Graz University of Technology, especially Philipp, Manuel, Stefan, Mike, and Elisabeth. You often knew exactly how to motivate me or get the ideas floating in my head. Thank you for the good times and the camaraderie during hard times.

To my newfound friends at the University of Wollongong, especially Maryam, who made my stay unforgettable.

I must thank my parents, Renate and Detlef for supporting my goals and giving me the opportunities to pursue this path. I extend my gratitude to my sister Anja for the continuous encouragement.

Finally, I want to thank my partner Mirza for being my rock, for your unconditional love and support. Thank you, for carrying me when things seemed too hard.

Affidavit

I *declare that I have authored this thesis independently, that I have not used other than the declared sources/resources, and that I have explicitly indicated all material which has been quoted either literally or by content from the sources used. The text document uploaded to TUGRAZonline is identical to the present doctoral thesis.*

13.04.2023

Date, Signature

Certification

I, Alexander Rainer, declare that this thesis submitted in fulfilment of the requirements for the conferral of the degree Doctor of Philosophy in Electrical Engineering, from the University of Wollongong, is wholly my own work unless otherwise referenced or acknowledged. This document has not been submitted for qualifications at any other academic institution except the partner institution University of Technology Graz for the completion of the Joint PhD program.

13.04.2023

Date, Signature

Abstract

In recent years, electricity generation employing renewable energy sources such as wind and solar dramatically increased and will continue to grow substantially in the future. Such developments cause a shift from conventional synchronous generators with well-known inherent behaviour to inverter-based generation with the behaviour strongly depending on the implemented control algorithms. Associated with this trend towards inverter based renewable energy generation is the reduction of system inertia leading to concerns on higher frequency gradients which can result in lower frequency nadirs and higher frequency zeniths in the event of network contingencies.

This thesis illustrates how the introduction of battery storage systems (BSS) into the power system can help to keep grids stable. With BSS, Fast Frequency Response (FFR) can be introduced as a new service that takes advantage of their fast reaction times. FFR is the incorporation of rapid active power increase or decrease by generation or load in a frame of two seconds or less, to correct a supply-demand imbalance and assist in managing power system frequency. In the context of this thesis, artificial inertia is treated as a subset of FFR. A central aim of the work presented in this thesis is to examine how different BSS activation mechanisms compare with each other and how effective these mechanisms are under different conditions. For that, the difference between activation methods and technologies that can provide FFR are highlighted leading to the development of four different controllers. The basic principles for these controllers are derived from existing concepts for FFR. The controllers considered include a proportional controller, artificial inertia controller, event detection controller, and an improved proportional controller. In the research, improvements to these BSS activation methods were undertaken and further developed. The performance of the controllers was tested utilising simulations for different grid conditions and scenarios in combination with conventional measures such as Frequency Containment Reserve (FCR).

A grid was modelled based on the South Australian transmission network to investigate the performance of the controllers in a grid with low levels of inertia and high frequency deviations associated with network disturbances. The results showed that the addition of a BSS can help mitigate the negative impact of high rates of change of frequency and that all tested controllers had a significant impact on the maximum frequency deviation.

The controllers were further tested with a measured signal from the grid separation event in the Central European system on January 8th, 2021. The measured frequency signal was first used as an input to observe the reaction a BSS, employing the proposed controllers, would have had if it had been connected during the disturbance and if the controllers operate as expected under real conditions. The disturbance was then simulated with a simplified model of the Central European grid and three different stages of BSS adoption in the system. The results highlighted that in a grid with higher levels of inertia than in the test grid examined based on the South Australian network, artificial inertia had a miniscule effect on the frequency deviation. The event detection controller and the improved proportional controller had the highest impact on the frequency. It was also be shown that the benefit of additional BSS, following a certain development stage, is diminishing.

The simulations highlighted the fact that the parametrisation of the controllers is of essential importance and needs to be adjusted depending on the grid situation and the limited rated power and storage capacity of the BSS. Parameter variation studies were carried out which showed that artificial inertia with an increased delay has a superior effect on the frequency than very fast acting artificial inertia.

Overall, the proposed novel controllers show a promising improvement over the standard droop controller. This also highlights the fact that existing frameworks for FFR can be further improved.

Key Words: Fast Frequency Response, Inertia, Frequency Stability, Battery Storage Systems, Renewable Energy, Power System Simulation

Table of Content

List of Figures

List of Tables

Abbreviations

AEMC	Australian Energy Market Commission
AEMO	Australian Energy Market Operator
AI	Artificial Inertia
BSS	Battery Storage System
CE	Central Europe
CFFR	Containment Fast Frequency Response
EFFR	Emergency Fast Frequency Response
EMT	Electromagnetic Transients
ENTSO-E	European Network of Transmission System Operators for Electricity
ERCOT	Electric Reliability Council Texas
FCAS	Frequency Control Ancillary Services
FCR	Frequency Containment Reserve
FFR	Fast Frequency Response
GB	Great Britain
LFSM-O	Limited Frequency Sensitivity Mode – Over frequency
LFSM-U	Limited Frequency Sensitivity Mode – Under frequency
LRET	Large-scale Renewable Energy Target
NEM	National Electricity Market (Australia)
NER	National Electricity Rules (Australia)
NERC	North American Electric Reliability Corporation
PCC	Point of common coupling
PLL	Phase Locked-Loop
PMU	Phasor Measurement Unit
PV	Photovoltaic
RAVG	Rolling Average
RMS	Root Mean Square
RoCoF	Rate of Change of Frequency
SA	South Australia
SCR	Short Circuit Ratio
SG	Synchronous Generator

SoC	State of Charge
TAS	Tasmania
TSO	Transmission System Operator
UFLS	Under Frequency Load Shedding

Chapter 1
Introduction

The demand for electrical energy has steadily increased over the years and will continue to do so in the future. A reliable supply of electricity is ever so important as the dependency on it increases and technological developments advance. The trend towards increased renewable energy sources is gradually causing a shift from conventional synchronous generators with well-known behaviour to inverter-based generation with characteristics dependent on the design and parametrisation of the associated controllers. Associated with this trend is the reduction of system inertia leading to concerns on higher frequency gradients (Rate of Change of Frequency - RoCoF) in the event of network contingencies such as the loss of a large synchronous generator, an interconnector or a system split such as the 2006 event as detailed in [1]. Out of the several available flexibility measures to address such concerns, as in [2] and [3], energy storage technologies provide remarkably promising response options because of their unique ability to decouple power generation and load over time [4]. In addition to load levelling [5], battery storage systems (BSS) can be used for transient and steady-state voltage control [6]. For example, the BSS as a part of Hornsdale Power Reserve in South Australia has been active since 2017 and has already assisted in preventing a system-wide blackout [7].

1.1 Background

In recent years, electricity generation employing renewable energy sources such as wind and solar dramatically increased and will continue to grow substantially in the future. This trajectory is caused by an increased public interest in climate change, governmental incentives, and technological advancements. [8] takes a closer look at this development as graphically illustrated in Figure 1.1 and Figure 1.2. The report covers 96% of the global GPD and represents 96% of the global population. The findings of the report show that renewable energy generating capacity experienced an estimated 257 GW of additional capacity. In total, the globally installed renewable energy power generation increased by almost 9.9% compared to 2019. Especially solar PV generation increased significantly and accounted for more additional power capacity (net of decommissioned capacity) than any other generating technology. Solar PV-rooftop systems have also become increasingly efficient over the years and prices of such installations continue to drop [9], [10]. Globally, the newly installed renewable power capacity consists of 54% solar PV, 36% wind and 7.7% hydropower in 2020 [8].

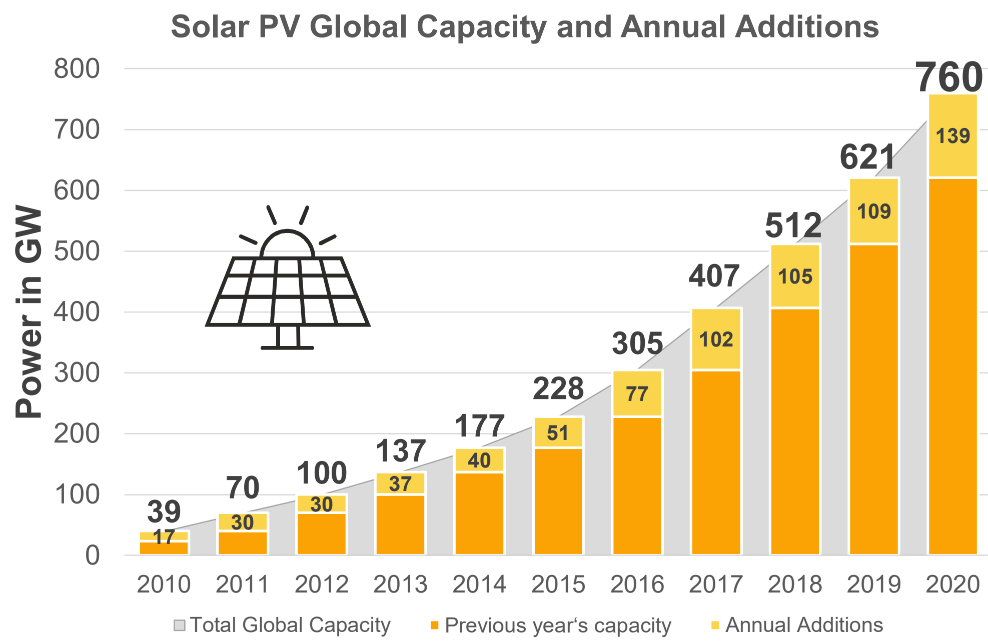

Figure 1.1: Solar PV Global Capacity and Annual Additions, 2010-2020 [8]

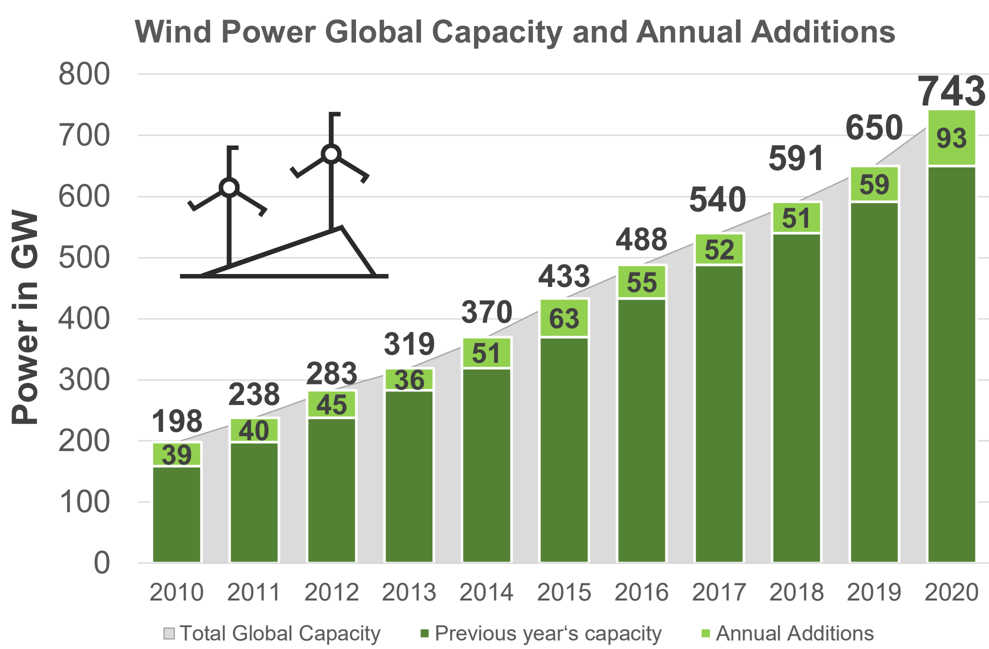

Figure 1.2: Wind Power Global Capacity and Annual Additions, 2010-2020 [8]

A country that is leading in renewable energy generation is Australia where renewable energy investments gained momentum following the legislation of the revised Large-scale Renewable Energy Target (LRET) in mid-2015. The target set in the LRET is to generate 33,000 GWh by 2020 with additional renewable energy generation compared to the 1997 baseline level established under the Renewable Energy Target legislation [11].

Generally, as pictorially illustrated in Figure 1.3, such developments cause a shift from conventional synchronous generators with well-known behaviour to inverter-based generation with characteristics dependent on the design and parametrisation of the controller, implemented functionalities and the specifications of the power electronic interfaces [12].

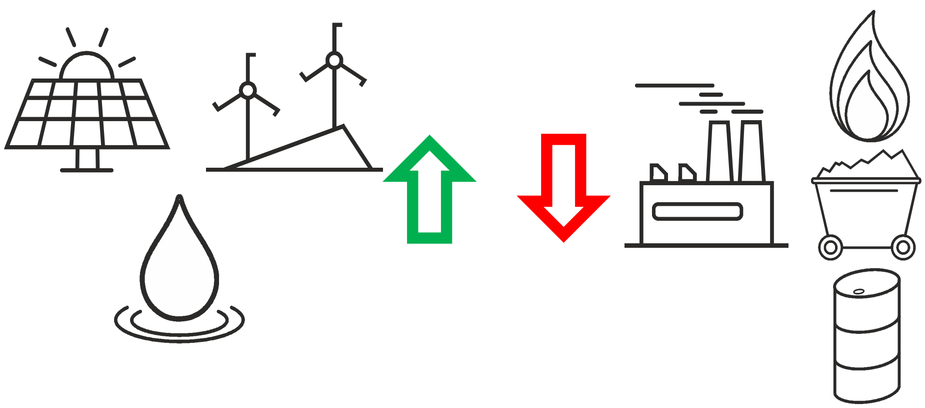

Figure 1.3: Change in Generation

Associated with this trend towards inverter based renewable energy generation is the reduction of system inertia leading to concerns on higher frequency gradients (Rate of Change of Frequency - RoCoF) which can result in lower frequency nadirs and higher frequency zeniths in the event of network contingencies. Such contingencies can be the loss of a large synchronous generator or an interconnector, like in South Australia where a RoCoF of 4 Hz/s was detected during the 2016 black system event [13]. Under these conditions, 49 Hz (where load shedding would usually start) would be reached within a quarter of a second, making it impossible for generators to react to the disturbance in time. Figure 1.4 illustrates the frequency after a loss of generation with varying degrees of system inertia. The figure also differentiates between the response with frequency Containment Reserve (FCR), also known as primary frequency control, and without FCR.

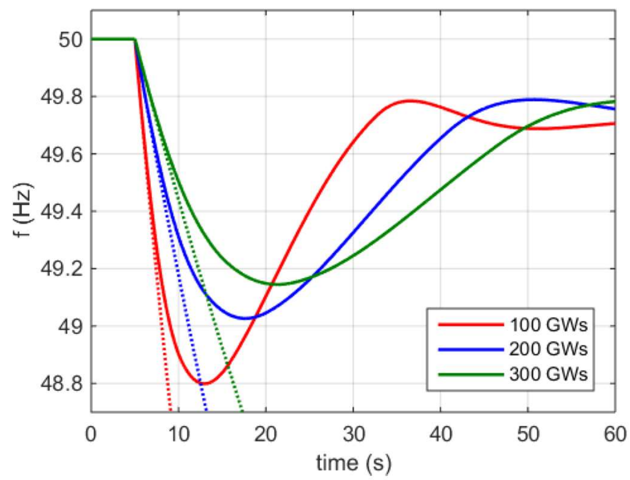

Figure 1.4: Frequency after a loss of generation with varying degrees of system inertia; dotted lines without FCR and solid with FCR [14]

Figure 1.4 illustrates the frequency response of a system that experiences a loss of generation with different levels of inertia ranging from 100 GWs to 300 GWs. It is clearly visible that reduced levels of inertia (100 GWs) lead to a lower instantaneous frequency drop. According to [15], five major synchronous systems have already implemented lower floors for the systems inertia to limit RoCoF. Inertia floors result in minimum requirements of synchronous generation that needs to be connected at any time. Table 1 summarises these floors and classifies them in relation to grid capacity that is linked to the peak demand. The table also features the relevant data on maximum RoCoF and the associated contingency. Australia features constraints in at-risk regions such as South Australia (SA) and Tasmania (TAS). Astonishingly, SA and TAS allow for much higher RoCoF values than the other countries. Missing data in the original table included in [15] was filled with data from [16] and [17].

Table 1.1: Inertia floors present in the regions ERCOT, Great Britain (GB), Ireland, NORDIC System and Australia: South Australia (SA) and Tasmania (TAS) [15]

	ERCOT	GB	Ireland	NORDIC	SA	TAS
Inertia floor	100 GWs	135 GWs	23 GWs	125 GWs	6 GWs	3.8 GWs
Peak demand	~73 GW	~60 GW	~6.5 GW	~72 GW	~2.6 GW [16]	~1.6 GW [16]
Contingency	2.75 GW	1.25 GW	0.5 GW	1.65 GW	0.35 GW	0.45 GW [17]
RoCoF	~1 Hz/s	0.125 Hz/s	0.5-1 Hz/s	0.5 Hz/s	3 Hz/s	3 Hz/s

The fast activation times and the converter-based connection of BSS to the grid offer new possibilities to provide load/frequency responses that are not only faster than conventional mechanism like FCR but might also be able to utilise controllers that offer better suited responses that circumvent the limits synchronous generators have. For example, governor activation times were sufficient in the past but in relation to increasing RoCoF even fast acting gas power plants will be too slow. As a result, cascading outages and widespread blackouts may occur [18].

1.2 Problem Statement

Electricity grids of the future are going to be weaker and more susceptible to disturbances. Disturbances that are now considered as small and not having a significant effect on the stability of the interconnected grid are going to have a significant impact. System splits and islanding scenarios will become more challenging because of unevenly distributed non-synchronous generation in interconnected systems. To secure a reliable electricity supply for future generation, it is important to develop solutions on how to deal with a decreasing penetration level of synchronous generators and how to address the adverse effects that this causes. In response to the decreasing levels of inertia, the earlier research focused on supplying artificial/virtual/synthetic inertia by non-synchronous generation. Although the slowing of the RoCoF by emulating the behaviour of synchronous machines is a step in the right direction, the capabilities of inverter-based generation and storage systems make advanced response possible. Additionally, inertia is only active during changing frequency because of its df/dt dependency and thus does not help with rebalancing the power. Over the recent years, the service identified as Fast Frequency Response (FFR) evolved as a new system service to support conventional frequency containment mechanisms where faster reaction times are necessary.

The provision of frequency response by wind turbines is already well established, for example in [19] and [20]. Compared to, for example, wind turbines, BSS offer less limitations and provide a wider range of power output and capacity. Their output is not limited by mechanical systems or external factors such as the weather (other than the BSS capacity and their operating constraints).

Two major studies have investigated the general feasibility of FFR for a respective region and summarized technical requirements. Firstly, the North American Electric Reliability Corporation published a white paper “Fast Frequency Response Concepts and Bulk Power System Reliability Needs” in March 2020 [21] which summarises FFR capabilities of wind turbines, solar PV, BSS, and load resources, and gives examples from manufactures who have developed ways to inject power rapidly into the power system.

Dynamic grid studies were undertaken under the assumption that all inverter-based generators that replaced synchronous generation are equipped with some form of (primary) frequency response. Varying degrees of system inertia and delays for the frequency responses were considered and the responses used were directly taken from the industry examples. The white paper does not compare FFR provided by different types of generation and does not conclude which response might be best suited for future grids.

Secondly, General Electric conducted a major study for the Australian Energy Market Operator (AEMO) in 2017 “Technology Capabilities for Fast Frequency Response” [22]. This report emphasises on explaining the various technologies capable of delivering FFR. Different activation methods are explained in detail and frequency and RoCoF measurements are elaborated. The report uses the SA grid with a frequency event that occurred on 1st November 2015 as an example for dynamic simulations. The goal of the simulations was to determine the size of FFR needed for such a contingency. A droop controller with a deadband was utilised to control the power injection dependent on the frequency deviation. Even though the report goes into much detail explaining different activation types, no other activation types were considered in the study besides the aforementioned controller.

Other studies such as [23] and [24] go into great detail on the effectiveness of BSS systems with frequency deviation dependent droop controllers, and in case of [24] the combination of controllers with droop characteristics for frequency deviation and RoCoF.

The above studies give a general overview but lack detailed simulations considering different types of controllers. Also, the studies also do not investigate whether a proportional (droop) controller is best suited for the application of concern leading to the problem area of alternative controller topologies that be developed which are able to provide an improved response. Further, the above studies do not investigate the shut-down period of BSS systems leading to another problem area. The proportional controllers used in these studies would provide a power output as long as there is a frequency deviation. Depending on the state of charge at the time of the frequency event, and the capacity of the BSS, the BSS could run dry abruptly. In a grid with a limited capacity of BSS contributing to frequency stability, a suboptimal operation of BSS with sudden shut-down may not significantly impact on the stability of the system but in future grids with less conventional generation and a higher dependency on BSS to support the grid frequency, these effects will have a substantial impact.

Although use of BSS to assist with frequency stability has been discussed in the recent years, research has not focused on investigation of different methods that can be used to activate such schemes and hence no acknowledge exists on their optimum use. Except for a few exceptions, BSS systems are generally considered too expensive to install. The challenges introduced by the increasing deployment of wind and solar generation and the reducing prices of BSS are making them more viable in the future. Considering the above, this thesis makes a substantial contribution to better understand the optimal usage of BSS schemes to address frequency stability related and other issues.

1.3 Research Questions and Methodology

This thesis focuses on how FFR provided by utility scale BSS can meet the additional measures to stabilise the frequency in case of a major event. Existing control strategies for FFR will be analysed to identify possibilities for improvement.

- **How is Fast Frequency Response defined?**
  The usage of the term Fast Frequency Response in legislation, research and applications will be evaluated. Existing frameworks are summarized, and a clear definition of Fast Frequency Response is presented (see Section 2.2 Fast Frequency Response).

- **How does Fast Frequency Response compare to and interact with conventional frequency contingency mechanisms?**
  FFR provided by battery storage systems can react much faster to frequency changes but can only participate for a short time compared to conventional generators that participate in frequency control. These up- and downsides need to be taken into consideration when introducing this new service and simulations will be carried out to investigate the interaction between new and old services (see Section 4.4 Frequency Response of the Network with Different Battery Controllers).

- **What are the key characteristics of a frequency contingency events and what is considered as favourable influences?**
  To assess the effectiveness of the novel controllers introduced, it is important to clarify the parameters of a frequency disturbance. These parameters include Rate of Change of Frequency, frequency nadir/zenith and settling time (see Section 2.1 Frequency Stability).

- **What are control types for FFR?**
  FFR can be activated by direct event detection and autonomous activation that are based on identification of disturbances or by continuous controller operation (see Section 2.3 Activation Methods).

- **Can FCR be provided by battery storage systems?**
  The use of frequency deviation proportional controllers that can otherwise be found as governors in generators are used in literature and application examples as a possible control strategy for battery storage systems. A frequency measurement from the Central European grid will be utilised to illustrate the limitations of this approach (see Section 3.1.2.1 C1 - Proportional Controller).

- **How can controllers be optimised for an overall better frequency contingency response?**
  Due to the non-linearity of the system, controller parameters and activation times have a significant impact on the overall performance of the controller and the stability of the system. Parameter sensitivity studies will be carried out to examine the impact of fast activation against slightly delayed activations (see Chapter 6 Network and Battery Energy Storage System Performance Sensitivity to Controller Parameter Variations).

Following the identification of the research questions above the relevant detailed work was undertaken as summarised below:

Preliminary work undertaken investigates frequency control and the effects of reducing inertia levels in frequency stability. Existing FFR definitions were analysed and a clear definition of FFR in the context of this thesis was formulated. With the insights gained from the literature research, several FFR controller models for BSS were developed utilising DIgSILENT PowerFactory noting that it is now a widely used software tool an increasing number of researchers and grid operators use. It is a well-recognised DIgSILENT PowerFactory offers a wide variety of functions and an extensive list of pre-modelled power system elements. Once a grid model is established, it is possible to run fault and load flow calculations or dynamic simulations all with the same grid model. The software also offers the facility for custom development of dynamic models that can be used during dynamic simulations. For example, these models can represent equipment types that are not predefined or need a higher level of detail, or controllers for different types of grid elements.

This work uses a root mean square (RMS) simulation which covers a time range that includes electromechanical transients. The dynamic RMS simulation works with time-varying complex root mean square values. It uses a symmetrical representation of the electricity grid and is the usual method for calculating electromechanical processes. Typically, issues of transient stability (such as critical fault explanation time), stability in the medium time range (e.g., optimisation of rotating reserve and load shedding) and oscillatory stability (e.g., inter-area oscillations) are investigated using RMS simulation. In contrast, an electromagnetic transients (EMT) simulation uses the instantaneous values of voltages and currents. This means that DC balancing elements or harmonics can also be considered. However, the computational effort and the computational times are correspondingly higher.

A sub-grid with a weak connection to the main grid was used to test the controllers under different generation scenarios. These scenarios range from low to high levels of renewable generation. Frequency stability is often investigated with the most severe outage. In case of this grid configuration, this outage is the loss of the interconnection during import. The results highlight the differences between the types of controllers and indicated a strong dependency of the controller parameters. This was examined further by performing a parameter variation study.

Finally, the controllers were tested under realistic conditions. Frequency measurement from the European grid during the January 8th, 2021, disturbance, was used to highlight the performance of the controllers compared to the actual reaction of the grid.

1.4 Thesis Outline and Contributions

Chapter 2 gives an overview of frequency stability and how it is currently managed in power systems followed by how FFR is particularly achieved by grid operators. How FFR will be used within the context of the work covered in the thesis is detailed and how it will be delivered is illustrated.

Chapter 3 describes the controller models that are used in the research. These controller models are based on the findings presented in Chapter 2 to illustrate the currently proposed controller methods by the grid operators. Initial investigations of these controller models emphasizes that these basic controllers can be improved. Two novel controller models are introduced. One of these controllers is based on an event detection algorithm that analyses the frequency and estimates how severe the frequency event is going to be. According to this analysis, a power output is activated rapidly, making possible a fast reaction to fast frequency changes. The second novel controller utilises a rolling average setpoint control to reduce the power output over time. Additionally, these novel controllers have a mechanism that blocks the reaction of the controller to not adversely affect the frequency restoration process.

The first objective of Chapter 4 is to develop a model a grid that features high levels of renewable energy generation with a weak connection to the main grid, so that a disconnection from the main grid is a scenario that can be investigated. Such a grid would exhibit high RoCoF and is in danger of a widespread blackout following the disconnection from the main grid during times of peak import or export. The established grid is then used to test the established controllers developed in Chapter 3 and analyses the effectiveness of FFR using a battery system. This work provides answers to the question how different BSS activation mechanisms compare with each other.

The aim of Chapter 5 is to utilise a real frequency event that was experienced in Austria following a grid separation event on January 8th, 2021, and investigate how the controllers presented in the chapter would perform during the event. The outcome of this chapter illustrates clearly, which controllers are more suited for a strong interconnected system and estimates how large a BSS would have a significant effect on the stability of the grid. With the measured signal as the input data for the controllers, it could be shown that the novel event-based controller is capable of distinguishing a normal frequency oscillation and an actual frequency event.

In Chapter 6, a sensitivity analysis of the introduced controllers is carried out. The test grid that was developed and illustrated in Chapter 4 is used in these tests. An automated variation of the parameters of the different controllers is conducted and studied. A novel and interesting outcome of this analysis was, that a slight time delay in the activation of the BSS can have a beneficial effect on the system stability.

A summary of the findings of the work presented in the thesis is given Chapter 7 followed by recommendations for future work.

Chapter 2
Literature Review

2.1 Frequency Stability

A range of key characteristics of electrical power systems, and its components, which have evolved over many years are well established. Among these are those of the Synchronous Generators (SGs) and their inherent characteristics alongside with the refinement of operation and control of power systems. A key property of interest is the system strength of a power system which is a relative term that is used to describe the ability of a power system to maintain core characteristics, frequency, and voltage, close to the pre-defined limits as possible under all operating scenarios. It is a relative property as it depends on the location of interest of a power system, especially in the context of new loads and generation that are yet to be connected, as it is influenced by the installations already connected. The system strength of a conventional power system could be quantified using the following [25]:

- System impedance at a location of interest
- Ability to transfer power in steady state while maintaining supply voltage within limits
- Resilience in maintaining the frequency

Due to the increase of renewable energy sources with decoupled rotating masses such as permanent magnet synchronous generator type wind turbines or even no rotating masses as in the case of solar Photovoltaic (PV) systems, as shown in Figure 2.1, precise ways of defining the strength of a connection point has to be established.

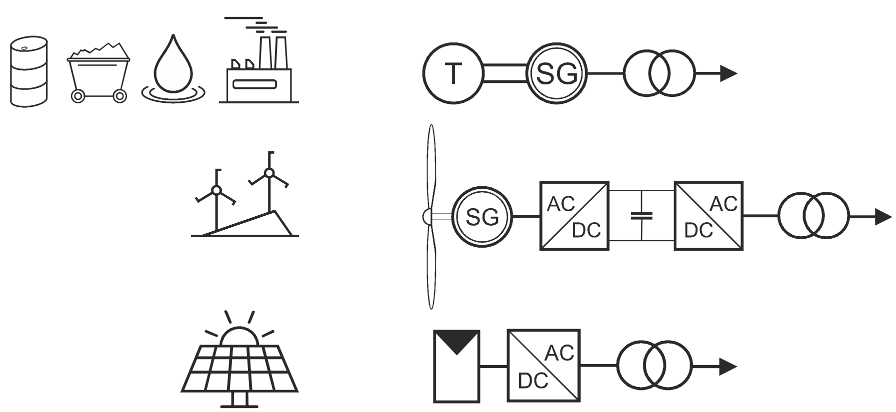

Figure 2.1: Connection of convectional generation, permanent magnet synchronous generator type wind turbine and solar PV system to the grid

The strength of a power system consists of many metrics. Commonly used key characteristics to assess general system strength are:

- The Short Circuit Ratio (SCR): With regard to a generator to be connected it relates the fault level at the connection point to the capacity of the generator where it strongly influences the ability of the generator to operate satisfactorily in steady state and following system disturbances. It is also possible to quantify the system strength employing the X/R ratio of the system impedance seen at the connection point. This is mostly relevant for transient analysis.
- Sensitivity of voltage changes due to changes in active and reactive power: The ability to transfer power from a generator to load centres relates with the sensitivity of the connection point voltage to changes in the generators active and reactive power.
- Rate of Change of Frequency (RoCoF): The resilience of the power system to contingency events and the stable operation under all operation scenarios are characterised by the Rate of Change of Frequency (RoCoF), the system inertia and the proportion of non-synchronous generation.

2.1.1 The role of Synchronous Generators in power system stability

Dynamic voltage stability depends on voltage sources that are equipped with extremely fast controllers or have a small impedance. For fast current changes, the relatively small sub transient reactance of SGs is the key component. The stiffness of a grid and therefore the small impedance could be defined by the short-circuit power of the system. With the increase of non-synchronous generation, this is no longer the case. While SGs are voltage sources with small internal reactances and therefore, support the grid inherently (grid forming), inverter-based generators act like constant current sources (grid following). Additionally, low level current controller of inverter-based generators limits the short-circuit current to a predefined value and voltage support is limited by the inverter sizing and is generally controlled separately in a high-level current controller.

Synchronous machines are not only perfectly suited for maintaining voltage stability but also frequency stability. A basic principle of electrical power systems is that demand must always be met with generation. When a load is connected to the grid, this demand needs to be immediately delivered. Power plants need to increase their power output according to the increased demand. This process takes some time to take effect, depending on the type of power plant. Valves need to be opened or the amount of fuel needs to be increased. During this time, the electrical power provided by the generator is not equal to the mechanical power derived from the turbine. Fortuitously, there is energy stored within the system - kinetic energy in all rotating generators and loads connected to the system. Without any counter action, taking this kinetic energy out of the system slows the rotational speed down and hence decreases the frequency. Likewise, if there is a surplus in power the generators will accelerate. The higher the inertia of the system, the higher is the capability to store and provide energy and therefore it is directly connected to the frequency gradient (RoCoF) following a change in the systems load/generation. This behaviour is defined by the swing equation of the machine, and it is not controllable. The governor of the generator will eventually measure the change in frequency and will increase the mechanical power output of the turbine. The smaller the RoCoF, the slower the prime mover must react to adjust the power output and keep the frequency within the acceptable band.

2.1.2 Electro-Mechanical Model of the Synchronous Generator

The equation of motion of a SG that relates the accelerating torque (T_a), mechanical torque (T_m) and the electrical torque (T_e) is according to [26] as follows:

$$T_a = T_m - T_e = J\frac{d\omega_m}{dt} \tag{2.1}$$

where J combined moment of inertia of generator and turbine in $kg \cdot m^2$
ω_m angular velocity of the rotor in mechanical rad/s
t time in s

Equation (2.1) can be transformed into per unit form giving

$$\overline{T}_m - \overline{T}_e = T_J\frac{dn}{dt} \tag{2.2}$$

The acceleration time constant T_J given in (2.3) is the time the machine takes to accelerate with rated torque ($T_{m,r}$) applied to rated rotational speed.

$$T_J = \frac{J \cdot \omega_{m0}}{T_{m,r}} = \frac{J \cdot \omega_{m0}^2}{S_r} = \frac{J \cdot \omega_0^2}{p^2 \cdot S_r} \tag{2.3}$$

where ω_{m0} rated angular velocity in mechanical rad/s
p number of pole pairs of the machine
S_r rated apparent power of the generator

Naturally, larger the acceleration time constant, the slower the machine changes speed due to changes between mechanical and electrical torques. It represents the ability of a rotating machine to store and release kinetic energy. In an interconnected system, this time constant is not only representative for how one generator behaves, but it can be used as a measure for the whole system.

The more commonly used inertia constant H can be calculated using the acceleration time constant. Most importantly, the inertia constant represents the stored kinetic energy (E_{kin}) at rated speed normalised using the rating of the machine:

$$E_{kin} = \frac{1}{2} \cdot J \cdot \omega_{0m}^2 \tag{2.4}$$

$$H = \frac{E_{kin}}{S_r} = \frac{1}{2} T_J = \frac{1}{2} \frac{J\omega_{0m}^2}{S_r} \tag{2.5}$$

The moment of inertia J can be re-expressed employing the inertia constant H. In this thesis, the inertia constant H is based on the totally installed apparent power. Other publications base the inertia constant on the system load.

$$H = \frac{E_{kin}}{S_r} = \frac{1}{2} T_J = \frac{1}{2} \frac{J\omega_{0m}^2}{S_r} \tag{2.6}$$

$$J = \frac{2H}{\omega_{m0}^2} S_r \tag{2.7}$$

Using this expression in the equation of motion in (2.1) yields

$$\frac{2H}{\omega_{m0}^2} S_r \frac{d\omega_m}{dt} = T_m - T_e \tag{2.8}$$

$$2H \frac{d}{dt} \left(\frac{\omega_m}{\omega_{0m}} \right) = \frac{T_m - T_e}{S_r / \omega_{0m}} \tag{2.9}$$

Using $T_{base} = S_r / \omega_{0m}$ as the base torque in per unit form, (2.9) can be written as:

$$2H \frac{d\bar{\omega}_r}{dt} = \bar{T}_m - \bar{T}_e \tag{2.10}$$

Figure 2.2 shows the connection of a large load to a single generator. In the initial period following the connection of the load, energy is extracted from the stored kinetic energy (shown by ①) until the governor increases the mechanical power (shown by ②). The frequency then stabilises, and the error remains. The process of stabilising the frequency is referred to as primary frequency control.

For simplicity, consider an unloaded generator where the electrical torque immediately changes to a new level, the mechanical torque stays constant.

$$T_a = 0 \tag{2.11}$$

$$J\frac{d\omega_m}{dt} = -T_e \rightarrow \frac{d\omega_m}{dt} = -\frac{T_e}{J} \tag{2.12}$$

The initial response is therefore solely dependent on the inertia of the generator or the interconnected system and the level of the load change. For interconnected systems, this means that only severe contingency events can cause a frequency gradient as illustrated in Figure 2.2. Accordingly, the RoCoF is the highest at the beginning of the contingency event and it gradually decreases when governor starts to react.

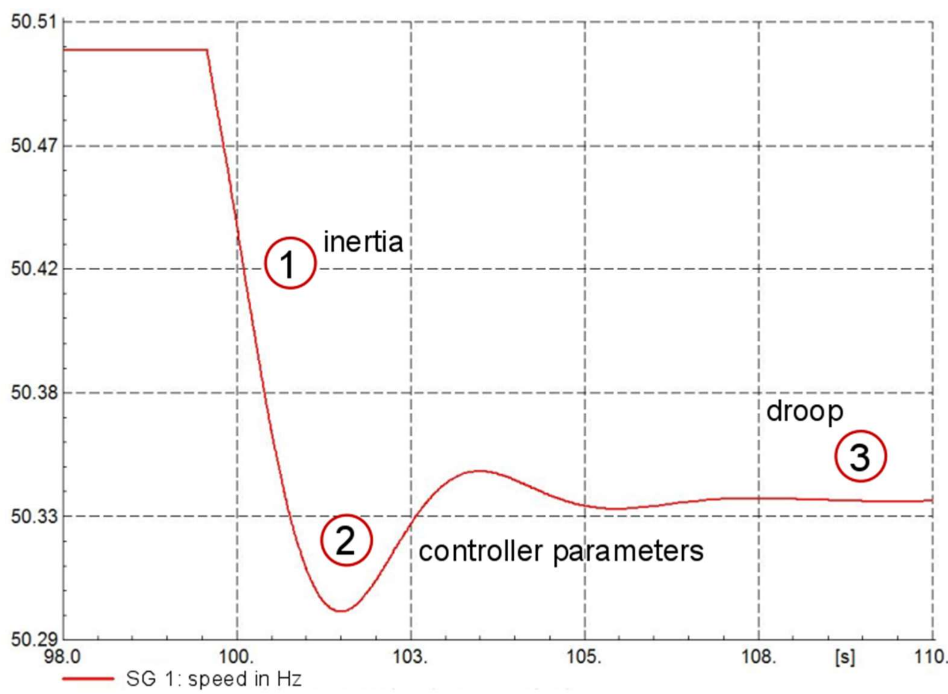

Figure 2.2: Demonstrative frequency drop after a severe contingency event

Although a run-of-river power plant has a high inertia due to large diameters and heavy components of the turbine, the slow rotational speed limits the stored energy drastically. Gas and steam turbines are not as heavily built as hydro turbines but operate at a much higher speed which generally leads to a much larger stored rotational energy. This can be seen in Figure 2.3, which depicts a comparison between different types of conventional generation. The figure was derived from data in [27], [28] and [29].

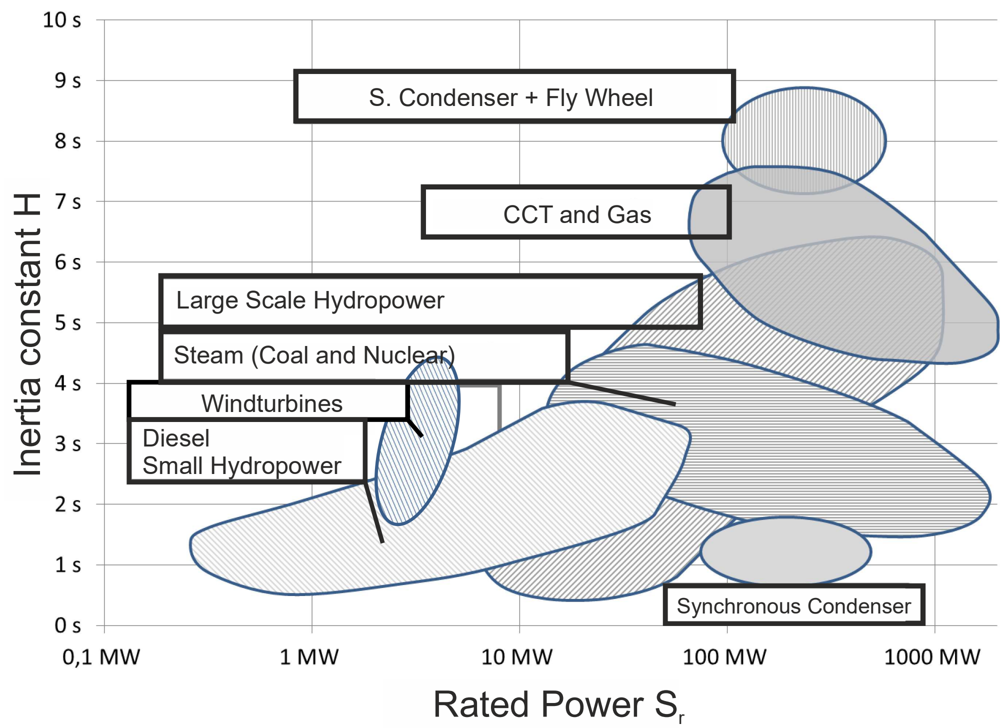

Figure 2.3: Graphical representation of different types of power plants and the respective range of inertia constant H [27]-[29]

Using (2.8), the stored kinetic energy, *E,* at a given time can be established. Following substitution of the mechanical speed with the electrical frequency in (2.8), it can be used to determine the absorbed or released energy between different frequencies as ΔE:

$$E = H \cdot S_r \frac{\omega_m^2}{\omega_{m0}^2} = H \cdot S_r \left(\frac{n(t)}{n_0}\right)^2 \tag{2.13}$$

$$\Delta E = H \cdot S_r \left(\left(\frac{n(t1)}{n_0}\right)^2 - \left(\frac{n(t2)}{n_0}\right)^2\right) \tag{2.14}$$

$$\Delta E = H \cdot S_r \left(\left(\frac{f(t1)}{f_0}\right)^2 - \left(\frac{f(t2)}{f_0}\right)^2\right) \tag{2.15}$$

For a given SG, (2.15) can be used to calculate the energy that is stored in the mechanical system of the generator. If a synchronous generator is replaced by a non-SG, this energy is missing and is causing higher RoCoF. A BSS that emulates a SG would also provide this amount.

2.1.3 Transformation of Power Systems

The replacement of SGs with non-synchronous generators leads to power systems where the strength of system is no longer sufficient. In some areas, the SCR is reduced to unacceptably low levels such that associated generators are not able to meet their performance standards. In other areas, the inertia of the system as a whole or that of a subsystem is no longer sufficient to withstand a major load event. This introduces the risk that generating systems may not remain connected to the power system in case of a major contingency in the power system.

While in large interconnected systems like Europe, RoCoF is generally not considered as problematic. However, problems intensify in areas with high wind and solar penetration levels that is further exacerbated by weak connection to the surrounding power system. In countries such as Ireland or weakly connected grids like the SA sub-grid have already demonstrated the effect of high levels of renewable energy generation on the grid stability. Problems in systems with insufficient amount of inertia of the above type will be more relevant in the future.

Following chapter will establish how inertia and other stabilising mechanisms can be provided by conventional means and subsequently by the introduction of storage systems with appropriate control schemes.

2.1.4 Frequency Contingency and Restoration Process

The power system frequency is subject to constant changes and fluctuations, based on the demand generation mismatch. The standard frequency for Central Europe (CE) is 50 Hz ±50 mHz. Small deviations from the standard frequency are normal and can occur due to differences between the forecast and actual demand or, for example, fluctuations in renewable generation. In case of a sudden and unplanned change in demand/generation the frequency changes more rapidly. Figure 2.4 depicts the limits specified by the European Network of Transmission System Operators for Electricity (ENTSO-E) for CE.

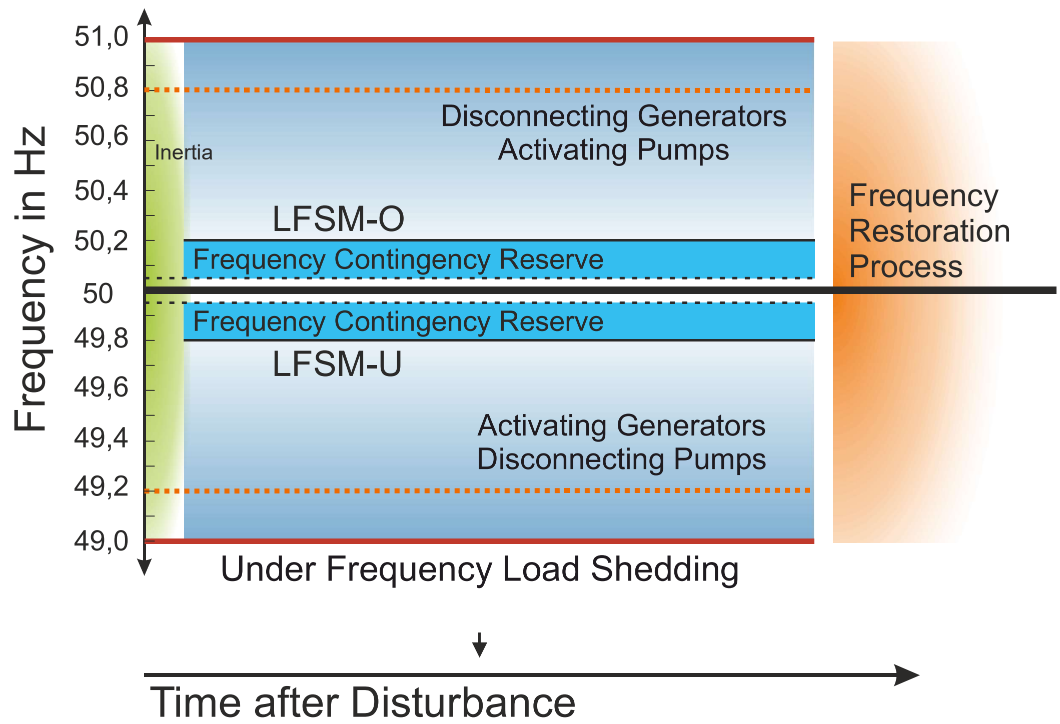

Figure 2.4: Limits and countermeasures for the frequency following a system disturbance according to the ENTSO-E for CE [30]

The frequency restoration process is implemented as follows: If the frequency stays within 49.8 Hz to 50.2 Hz, the FCR, also known as primary frequency control, stabilises the frequency and maintains it around the nominal frequency. Article 153 of [31] specifies a reference incident for Central Europe as 3000 MW in both positive and negative directions. With this reference incident level, the steady state frequency must be kept within the range of 49.8 Hz to 50.2 Hz. For a frequency deviation of ± 200 mHz the FCR is fully activated. It is also specified, that the full activation must be reached within 30 seconds and must be sustained for a minimum of 30 minutes. It is worthwhile noting that in Austria, Belgium, Netherlands, France, and Germany are starting to be organised as a market-based system with the goal to reduce costs associated with FCR.

In the case of a larger disturbance, the frequency excursion can be outside the ± 200 mHz range where additional measures are needed. This begins with the activation of the Limited Frequency Sensitive Mode for Under and Over frequency (LFSM-U or LFSM-O respectively) as illustrated in Figure 2.5 (with regard to LFSM-U).

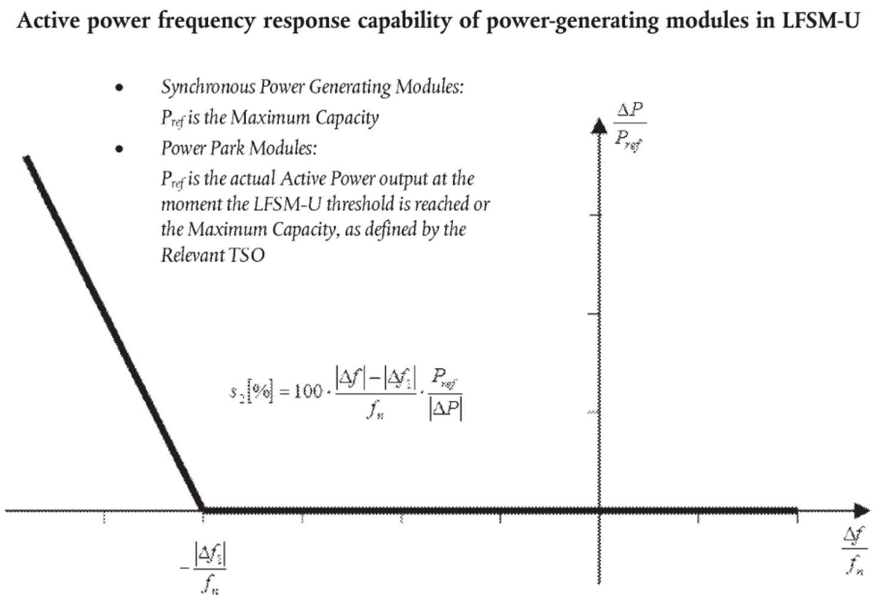

Figure 2.5: Required change in active power response capability in LFSM-U [32]

This mode puts all generation units of type C and D (generators above 50 MW rated power in CE) into a special mode that forces a change in power output proportional to the frequency deviation and with a predefined droop [16]. Figure 2.6 illustrates the activation times where the delay time t_1 and the activation time t_2 are specifiable by the Transmission System Operator (TSO), but the regulation gives limits for the maximum times. It is also specified that the response associated with t_1 must take place as fast as possible and not longer than 2 s. The time t_2 until the unit reaches the required output must not be longer than 30 s.

When the LFSM-U is activated, TSOs start to activate additional power plants that will be used for the frequency restoration process. Pumped-storage power plants switch from pumping mode into generation mode. Though these are additional measures, in case of a significant emergency, the frequency will deteriorate further. Once the frequency reaches 49 Hz, widespread automatic under frequency load shedding starts for predefined groups and intervals. Especially, thermal power plants and nuclear plants are very susceptible to low frequencies. To avoid damage to power plants, they can disconnect from the grid in a coordinated way when the frequency is at or below 47.5 Hz. The goal of stabilisation of the frequency is said to have failed at this point, and widespread blackout will be the result. If the frequency stabilises before reaching critical values, the TSO activates additional power plants, and the frequency is brought back to the nominal frequency with the frequency restoration process.

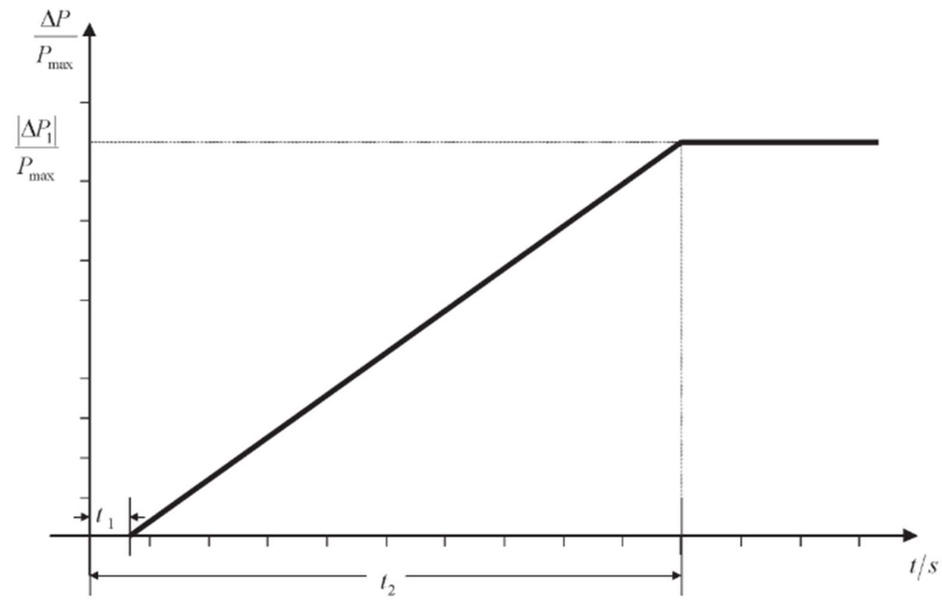

Figure 2.6: Activation times for generating units of type C and D for the LFSM active power change in both directions [32]

During a large-scale disturbance, time aspect is critical and hence is the inertia of the system. With high levels of system inertia, the RoCoF is smaller, and the contingency process usually has adequate time to react and increase or decrease the power output. In the case of system split, where the grid splits into zones with profoundly different generation to load ratios, or when certain parts of an interconnected grid with low levels of system inertia are disconnected, e.g. SA, RoCoFs can be too large to react appropriately. Thus, new systems are needed to assist in these situations.

For the Australian National Electricity Market (NEM), encompassing the southeast Australian grid, parameters from Table 2.1 apply for the mainland sates. The regulation in Australia separates between containment, stabilisation, and recovery and defines different frequency values for different conditions.

Table 2.1: NEM Mainland Frequency Operating Standards – interconnected system [33]

Condition	Containment	Stabilisation	Recovery
no contingency event or load event	49.75 to 50.25 Hz, 49.85 to 50.15 Hz 99% of the time	49.85 to 50.15 Hz within 5 minutes	
generation event or load event	49.5 to 50.5 Hz	49.85 to 50.15 Hz within 5 minutes	
network event	49 to 51 Hz	49.5 to 50.5 Hz within 1 minute	49.85 to 50.15 Hz within 5 minutes
separation event	49 to 51 Hz	49.5 to 50.5 Hz within 2 minutes	49.85 to 50.15 Hz within 10 minutes
multiple contingency event	47 to 52 Hz	49.5 to 50.5 Hz within 2 minutes	49.85 to 50.15 Hz within 10 minutes

2.2 Fast Frequency Response

The term Fast Frequency Response (FFR) is used in different ways to describe forms of fast reactions to the change in frequency after a large contingency. Many inverter-connected technologies, such as wind, solar PV, BSS, and other types of storage have the capability to deliver FFR [34].

2.2.1 North America

The North American Electric Reliability Corporation (NERC) defines FFR as “power injected to (or absorbed from) the grid in response to changes in measured or observed frequency during the arresting phase of a frequency excursion event to improve the frequency nadir or initial rate-of-change of frequency” [21]. This broadly defines FFR in terms of the activation time but not the way the response is to take place. Interestingly, the NERC includes conventional frequency response mechanisms such as synchronous machine inertial response and turbine-governor response besides fast-responding inverter-based generation associated with wind turbines and utility scale BSS, in the classification for FFR since they also fall into the arresting phase. This report also points out, that “fast” depends on the grid configuration where the FFR has to be achieved and should not be generalised.

2.2.2 Australia

In 2017, the AEMO defined FFR as “the delivery of a rapid active power increase or decrease by generation or load in a timeframe of two seconds or less, to correct a supply-demand imbalance and assist in managing power system frequency” [35]. Therefore, the Australian definition also specifies FFR via a time-based component, although this is specified more precisely here and is thus no longer applicable to different network topologies. Furthermore, the AEMO specifically excludes inertia as a FFR service with the reasoning that it would be detrimental to narrow FFR down to services that mimic the response of synchronous units. A reason for this argument could also be that the Australian National Electricity Rules (NER) introduced an inertia framework in 2017 that manages the levels of inertia within inertia sub-networks [17]. The AEMO also envisions that FFR is split into different services that are defined over the response time and frequency limits, most notably Contingency FFR and Emergency Response FFR. In 2021, the Australian Energy Market Commission (AEMC) introduced a draft rule determination concerning FFR [36]. This draft introduces a market framework for new fast acting frequency ancillary services to reduce overall costs and deal with ever decreasing inertia and incentivise technology development. FFR is again defined as a frequency ancillary service that reacts under 2 seconds.

2.2.3 Great Britain

The British National Grid, ESO, redefined the whole frequency response market to be able to deal with decreasing inertia levels. It started as Enhanced Frequency Response in 2016 [37] and moved on to Firm Frequency Response by 2019 [38] leading to its current form [39]. As depicted in Figure 2.7, the frequency response is now divided in to four categories.

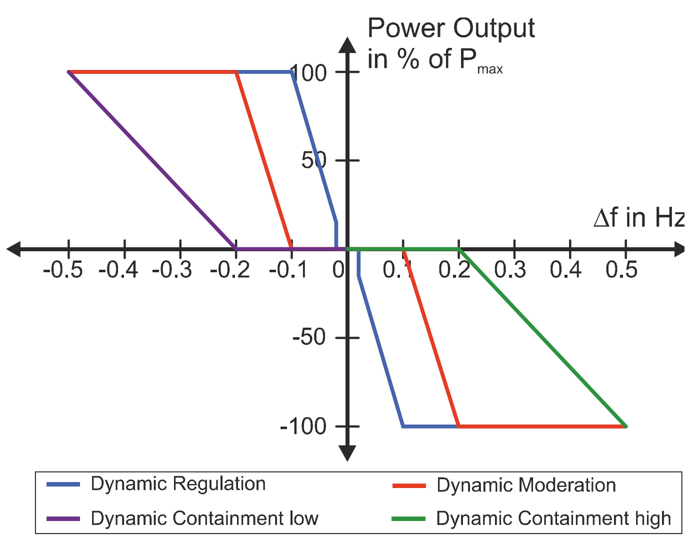

Figure 2.7: Activation thresholds of the proposed new frequency response services in Great Britain [39]

These new frequency response services are dynamic regulation, dynamic moderation, dynamic containment, and static containment. First stage of this approach will be the dynamic regulation, with a deadband of ±0.015 Hz and full activation taking place at ±0.1 Hz. Providers must be able to respond within 2 s and be able to reach ±100% output within 10 s. The providers of dynamic regulation must also be able to supply the needed output indefinitely. Dynamic moderation is an addition to support dynamic regulation when frequency deviations become excessive and also has a much faster activation time with a maximum delay time of 0.5s and a full output within 1 s. As detailed in the dynamic containment brochure by the National Grid ESO [40], dynamic containment replaces the FFR and is expected to be used infrequently for large frequency deviations, to keep the frequency within the limits of ± 0.5 Hz. The specification is illustrated as a symmetrical activation graph, starting at ±0.015 Hz with small delivery of up to 5% activation at ±0.2 Hz. After this point, the activation is directly proportional to the frequency deviation, reaching full delivery at ±0.5 Hz frequency deviation. The delivery time window is defined as follows: the delivery must be faster than 1 s but not faster than 0.5 s. The British approach is therefore like the Australian approach, splitting fast frequency services into an assisting contingency response and an emergency response in cases where deviations become exceedingly large. Due to the definition of the runtimes of these services, BSS or wind turbines are not able to meet the requirements for dynamic regulation.

2.2.4 Finland

As stated above in 2.2.2 and 2.2.3 for Australia and Great Britain respectively, Australia and GB are developing concrete market frameworks for the implementation of FFR. Based on the findings for the inertia problem in the Nordic synchronous system [41], Finland (Fingrid) implemented the so-called Fast Frequency Reserve in a market-based procurement system. Technical specifications are provided, and the FFR is defined by an activation time, a support duration, and a recovery time [42].

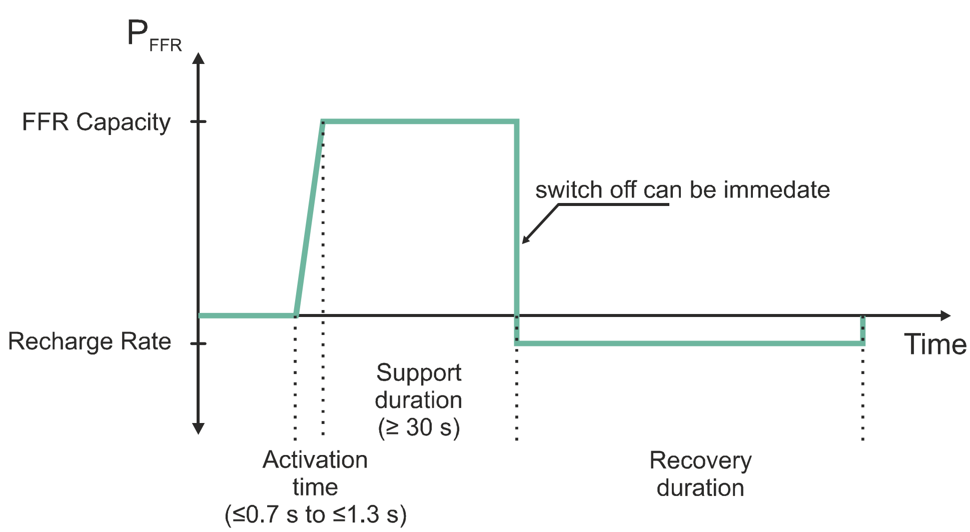

Figure 2.8: Fingrid 30 seconds support duration FFR [42]

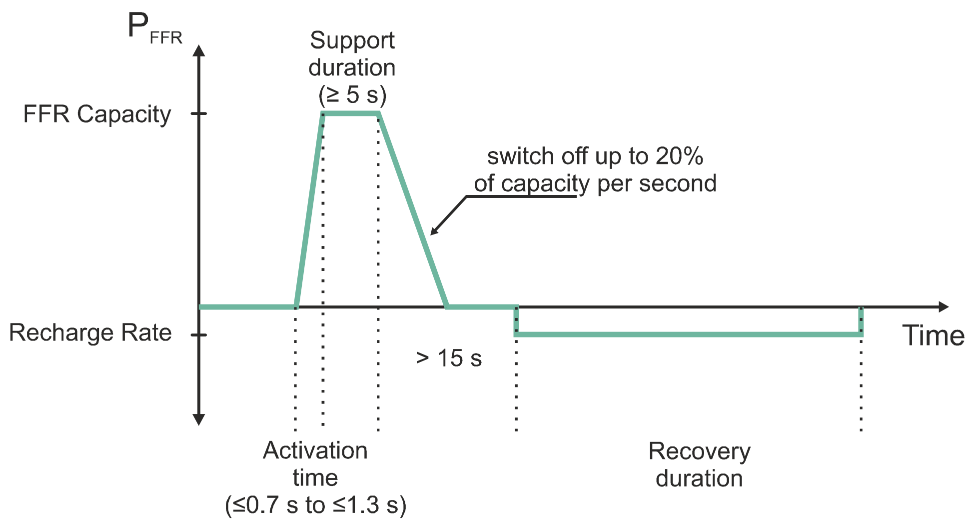

Figure 2.9: Fingrid 5 seconds support duration FFR [42]

Illustrated in Figure 2.8 and Figure 2.9, the guideline [42] distinguishes between 5 second and 30 second minimum support durations which also influence the maximum speed of deactivation. Three activation time thresholds are provided that depend on the frequency deviation with the slowest being ≤ 1.3 s at ≤ 49.70 Hz and the fastest ≤ 0.7 s at ≤ 49.50 Hz. In comparison with the other described regulations, Fingrid is providing the most detailed specifications as to what is defined as FFR.

2.2.5 Artificial Inertia (AI)

As widely researched [19], [43]–[49], manufacturer provided converter based systems have some type of storage included, it is possible to extract the energy in case of a major frequency deviation. Research even suggests that it is possible to use HVDC lines, using the energy stored in the DC cables, to provide AI [50]. These systems, in case of a disturbance, would help reduce RoCoF and provide more time for other Frequency Control Ancillary Service (FCAS) systems to react to the disturbance. In 2017, ENTSO-E published an extension document highlighting the possibility for TSOs to mandate AI from power park modules of types C and D [51]. In another example, HydroQuebec grid code goes a step further, mandating that wind farms of capacity greater than 10 MW to be equipped with a frequency control system and gives transmission providers the possibility to specify a minimum inertia constant for the connection of generating units.

2.2.6 Conclusion and Positioning within ENTSO-e Limits

As discussed above in 2.2 Fast Frequency Response, several grid operators and institutions are moving forward with FFR in their grids. Most commonly, it is defined as a rapid response within a 2 second timeframe.

In relation to this thesis, Fast Frequency Response is defined as follows: The rapid active power increase or decrease by a generator or a load in a frame of 2 s or less, to correct a supply-demand imbalance and assist in managing power system frequency within stipulated limits.

This definition leaves room to also include AI. Importantly, FFR services are envisioned to work in conjunction with conventional frequency control but not replace it.

Following the stabilisation of the system, the activated storage should gradually decrease the power output. This results in a slow decrease in frequency and gives FCAS sufficient time to react.

The goal of the systems introduced in this thesis, is to soften major frequency events with BSS and provide conventional mechanisms more time to react. Like the Australian and the British proposal, as illustrated graphically in Figure 2.10, this thesis also uses Contingency Fast Frequency Response (CFFR) and Emergency Fast Frequency Response (EFFR) in association with the responses in different frequency ranges. CFFR acts at the beginning of a disturbance and would be set to activate once the frequency deviates away from the range of FCR (49.8 Hz – 50.2). In the LFSM-U range, CFFR is supposed to support the grid until generators had enough time to start and increase the power output. If the frequency drops further, EFFR can be activated to avoid under frequency load shedding.

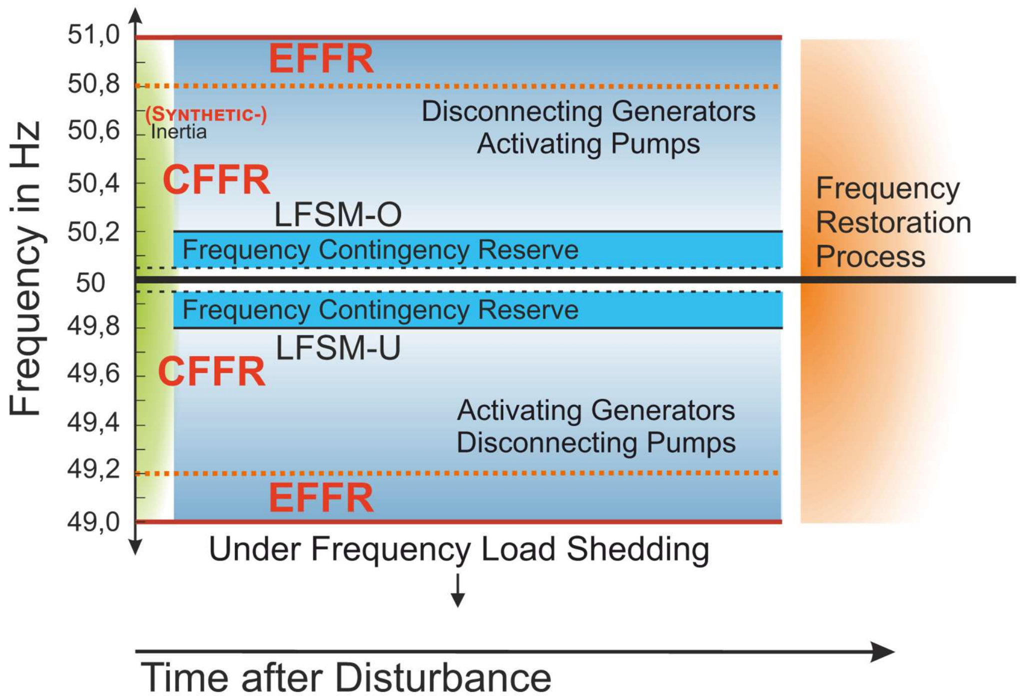

Figure 2.10: Limits and countermeasures for the frequency following a system disturbance according to the ENTSO-E including proposed FFR measures

It is acknowledged that grid-forming technologies are emerging which can help with RoCoF due to an integrated inertia emulating system. But these technologies are some distance away from being implemented on a large scale [52].

2.3 Activation Methods for Fast Frequency Response

A question that needs to be answered is when artificial inertia or FFR are needed and how they are activated. The inertia of rotating machines activates as a physical reaction to the change in grid frequency. The change of power output from inertia is continuous and is active for all frequency changes. This activation is thus not reliant on the external measurement of the frequency and detection of frequency changes. The rotating machines participate in the FFR process as a natural reaction to the change in grid frequency. This behaviour needs to be emulated in other generating interfaces where the rotating mass is masked from the grid through power electronic interfaces. It was already established that the frequency deviation and the rate of change of frequency are the defining parameters in the case of a frequency disturbance. These parameters can therefore be used to identify a frequency event. It is also possible, to use the operational states of the grid to define an upcoming frequency disturbance. For example, if a grid area is solely connected to the rest of the grid via one or two interconnectors, it is possible to estimate the size of the frequency disturbance if these interconnectors open.

The FFR needed can, therefore, be linked to the state of the breakers. As this is limited to a minimal number of cases, it is more important to develop a control scheme for general use which may be faster than conventional methods.

2.3.1 Direct Event Detection

As illustrated in Figure 2.11, the simplest method of activating an energy storage system in the context of FFR is to directly link it to a system operation state. For example, in a system with a limited number of interconnectors to a neighbouring grid, the storage system can be immediately activated when the interconnectors disconnect. The storage system would be connected to the state of breaker. When the breaker opens, the storage system can either release/absorb a predefined amount of real power or a variable amount depending on the last known loading status of the interconnector. Another example would be the unplanned disconnection of a large generator. Similar to the first previous example, the storage system would be activated with the opening of the circuit breaker. The main advantage of this activation method is that fast activation times are achievable. The activated storage should gradually decrease the power output. This results in a slow decrease in frequency and gives FCAS sufficient time to react.

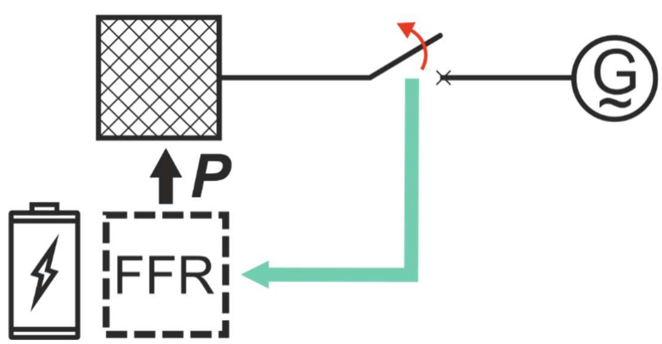

Figure 2.11: Direct Event Detection Method

Caution is necessary when activating the storage system, as a sudden power output change could cause oscillations in the system. Additionally, this method demands a communication link between the system operator and the storage system operator which may not be easily available or reliable.

2.3.2 Autonomous Activation – Event Based Activation

The autonomous event-based activation methods, as depicted in Figure 2.12 and Figure 2.13 react to a relevant frequency event based on measurements of the frequency. It is necessary to incorporate a waiting period to avoid an unnecessary and possibly damaging activation. Following the waiting period, the storage system can be activated based on severity of the frequency deviation. This activation is therefore inherently slower than the direct activation, but the storage system is able to react to all relevant frequency deviations and not only to the limited number of predefined events linked to the storage system. The frequency can be measured either at a centralised point and transmitted to the FFR device, depicted in Figure 2.12, or by each FFR device, depicted in Figure 2.13.

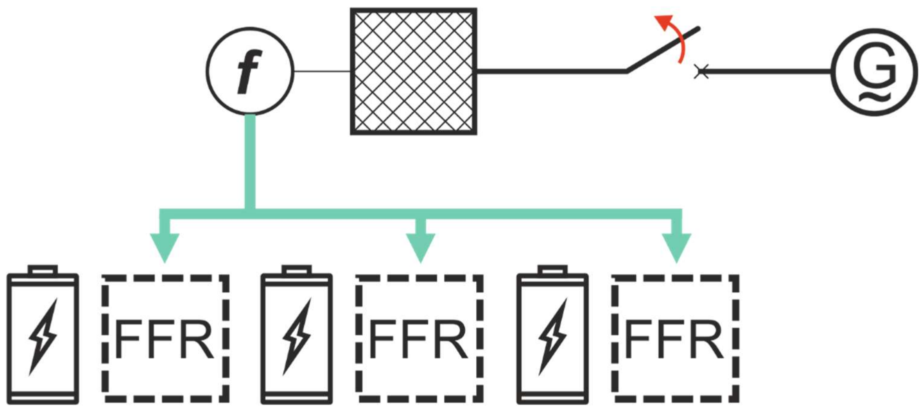

Figure 2.12: Autonomous and centralised frequency-measurement for FFR Devices

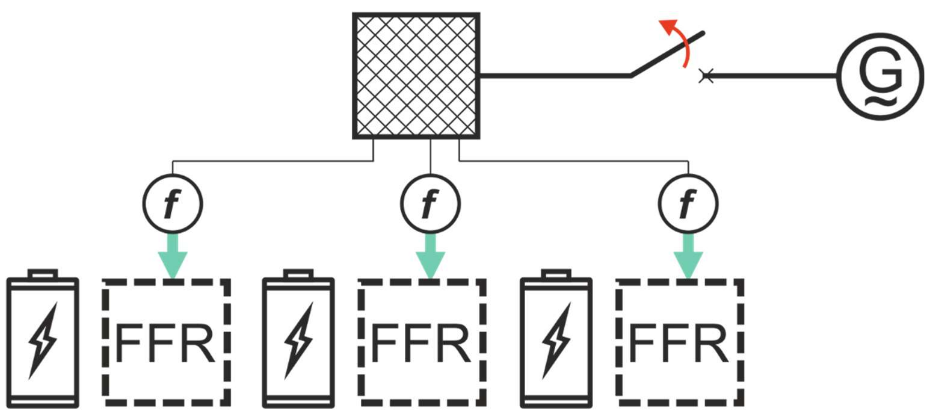

Figure 2.13: Autonomous and decentralised frequency-measurement for FFR devices

2.3.3 Autonomous Activation – Controller Based Reaction

Instead of activating the storage system employing the logic based on suitable events and that would provide a step-up response, appropriate controllers such as proportional controllers can be used to exhibit an optimal reaction to the disturbance. This can also introduce additional damping and an automatic adaption to changing circumstances.

2.4 Frequency measurement and Phase Locked Loop (PLL)

PLLs are used in converter-based generation to measure the frequency and to synchronise the voltage to the grid. This results in a great dependency on the characteristics of the whole system. A robust frequency measurement is especially necessary under abnormal grid conditions such as during faults where rapid changes of the frequency can lead to PLLs making incorrect measurements and regarding this aspect several publications indicate advances [53]–[57]. Besides a PLL, measurement of the frequency can be undertaken in a multitude of ways [58]. Most notably, the accuracy and speed of Phasor Measurement Units (PMUs) for Wide Area Measurements (WAMs) are widely known, where they can provide up to 100-240 samples per second. First described in 2005 [59], PMUs are now defined in an IEC/IEEE 60255-118-1 Standard that evolved over recent years and now provides specifications regarding the measurement of frequency and RoCoF, under steady-state and dynamic conditions [60].

RoCoF has been used to detect islanding associated with loss of mains relays that trip generating units to protect them. These RoCoF detection schemes are now being used in detecting major frequency events for the activation of FFR. Use and calculation of the RoCoF has several caveats. Depending on the measurement method used noisy measurements can lead to incorrect assessments. IEC/IEEE 60255-118-1 Standard requires P-class PMUs to have an accuracy of 0.4 Hz/s, which was changed from 0.01 Hz/s in the first iteration of the standard [61]. RoCoF calculation needs several cycles to calculate the values, as there is a trade-off between fast and precise readings. To obtain robust readings, up to 500 ms filtering windows are being used. The ENTSO-E states that as a minimum requirement for using RoCoF as protection criteria for generators and loads, the measurement window must not be longer than 180-240 ms or otherwise the performance of the needed application is negatively impacted [62]. [61] found several problems after testing the proposed RoCoF calculation methods defined in the Standard. One major issue with RoCoF calculation is caused by phase steps that is strongly affected by the window size where longer window frames can avoid miscalculation to a greater extend. These issues have different impacts depending on the size of the FFR topology as summarised by [22] and described in Table 2.2. For example, using smaller units can mitigate the effect of false triggering of one unit but makes detection more expensive since every unit needs to be equipped with proper frequency measuring technology.

Table 2.2: Advantages and disadvantages of different topologies and detection mechanisms [22]

Number and Capacity	Local RoCoF measurement	Direct event detection
Few, large resources	Advantage: Cheaper topology	Advantage: Low risk of false triggering
	Disadvantages: High risk of false triggering	Disadvantages: Only applies for specific events; Moderate cost for communications
Many, small resources	Advantage: Reduces consequences of false triggering	Advantage: Low risk of false triggering
	Disadvantages: Expensive detection	Disadvantages: Expensive communication

2.5 Devices capable of providing FFR and Artificial Inertia

Many technologies can deliver a fast change in power output which are discussed in the following sub sections.

2.5.1 Battery Storage systems

There is a wide variety of energy storage systems and a wide area of potential applications [63], [64].

Out of the several available flexibility measures [2][3], energy storage technologies are particularly promising response options because of their unique ability to decouple power generation and load over time [4]. In addition to shaving and load levelling [5][65][66], BSS can be used for transient and steady state voltage control [67], [6] and frequency control for example in the European grid [68] and many more.

A comprehensive overview of storage technologies can be found in [69], [70] and as depicted in Figure 2.14, energy storage systems cover a wide range of capacities and power rates [71]. It also shows that Li-Ion battery is the technology that best covers the necessary area for a FFR application.

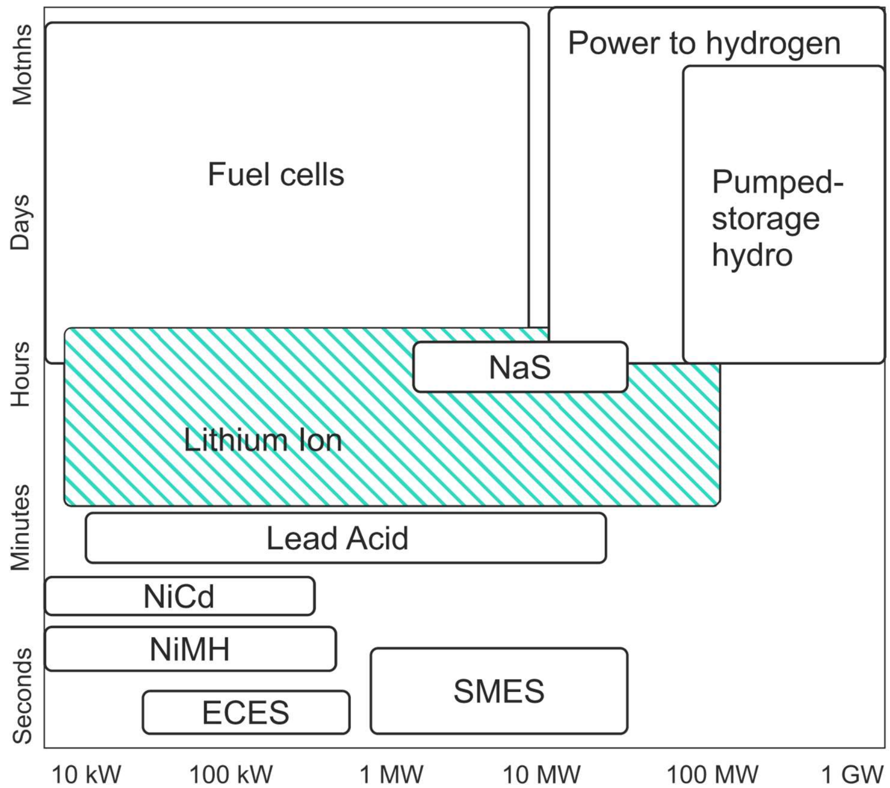

Figure 2.14: Overview of different storage types for discharge time vs power rate [71]

Battery research is gaining increased popularity because of the public interest in electrical vehicles. Even tough research focuses on increasing power density, weight and costs [72], the advances can be used for large scale battery systems where size does not matter. Li-Ion batteries have many features such as high specific energy, zero maintenance, low toxicity, and fast charging abilities.

Given the limited battery storage sizes in the past, mainly the application in distribution grids as well as in micro grids are well researched [73], [74]. However, large-scale battery storage systems already exist, for example, South Australia [75][7], California [76] and in Quinghai [77]. As illustrated in Figure 2.15, 3.3 GW of newly installed battery storage systems have been recorded globally in 2018 and 3.1 GW in 2019 [78].

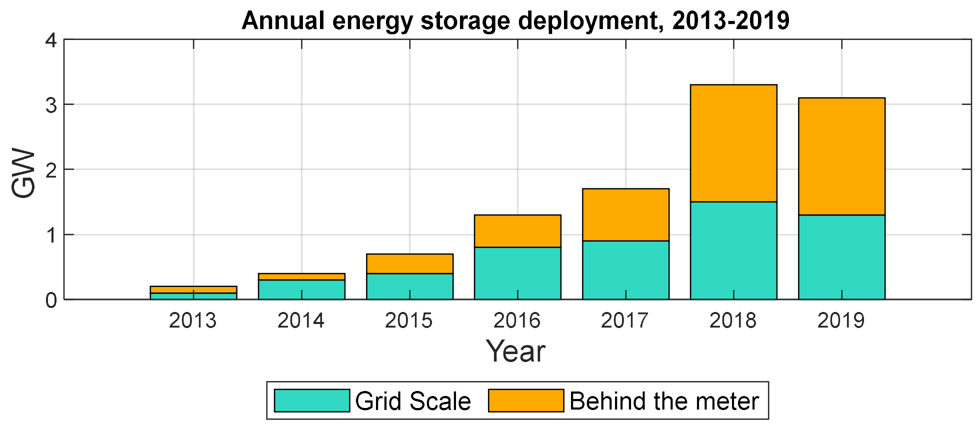

Figure 2.15: Yearly globally newly installed BSS in GW [78]

Table 2.3 shows an overview of large-scale battery systems that already exist and the service that they provide.

Table 2.3: Overview of utility scale battery systems and the provided services

Size	Location	Service Provided
100 MW / 129 MWh + 50 MW / 64.5 MWh [75]	South Australia	Frequency regulation capacity firming
100 MW / 400 MWh [76]	California	RES shifting
90 MW / 120 MWh [79]	Germany	Frequency regulation
50 MW / 100 MWh [77]	China	RES shifting
35 MW / 232 MWh [80]	Italy	Grid Investment deferral Reduced RE curtailment
250 MW / 250 MWh (planning stage) [81]	Germany	Grid booster

Li-Ion technology is becoming increasingly widespread [82], [83] and has become the most widely used storage technology. With the rise of electric cars, which mainly rely on nickel-manganese-cobalt battery technology, this technology is increasingly used in large battery storage systems for energy grids. The increased research efforts in this area with regard to higher storage densities, lower weight and lower costs will also lead to improvements in the utility sector in the future. In addition to the technical advances, new developments have also had an impact on the costs of battery storage, which have fallen rapidly in recent years [84]. As can be seen in Figure 2.16, a further drop in prices is expected in the future, ranging from 20% to 67% by 2030, depending on the scenario considered.

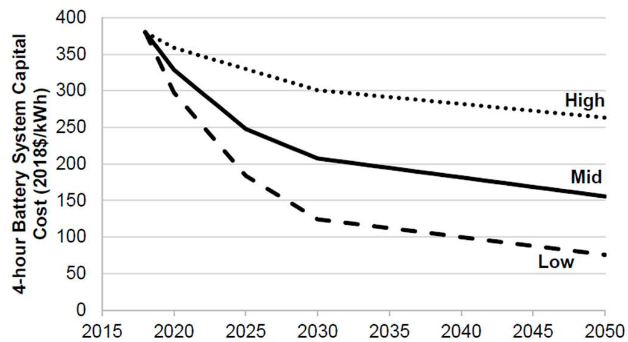

Figure 2.16: Price development of 4-hour Li-Ion BSS in comparison to the prices in 2018

Expected costs can be calculated with [85] using data from 2020. Table 2.4 summarises the cost for lithium-ion iron phosphate batteries for different operating times under full load. The time data correspond to 2/4/6 hours of operation at nominal power.

Table 2.4: Installation costs for a 100 MW Li-Ion iron phosphate battery storage system with cost items and for different storage sizes [85]

		100 MW storage		
Parameter	**Unit**	**2 h**	**4 h**	**6 h**
Storage Block	€/kWh	137.76	135.30	134.48
Storage Balance of System	€/kWh	33.62	31.16	30.34
Power Equipment	€/kW	51.66	51.66	51.66
Controls and Communication	€/kW	1.64	1.64	1.64
System Integration (Storage with Inverter)	€/kWh	39.36	36.08	34.44
Engineering, Procurement and Construction	€/kWh	47.56	43.46	41.82
Project Development	€/kWh	57.40	51.66	50.02
Grid Integration	€/kW	16.40	16.40	16.40
Total BSS installation cost	€/kW	700.28	1263.62	1820.40
	€/kWh	**350.14**	**315.70**	**303.40**

A BSS with 100 MW and 200 MWh of storage would therefore cost **€ 70 million** and as stated above, a price decline is to be expected in the next few years, which could reduce the installation costs to **€ 50 million** by 2030.

2.5.2 Wind turbines

Emulated inertia response and FFR from wind turbines is achieved by actively operating the generator. Kinetic energy stored in the turbine and the generator is used to react to frequency changes, and in case of an under-frequency event, slowing the wind turbine down. Subsequently, the wind turbine needs time to recover this spent energy. This recovery is dependent on the wind speed. Unfortunately, several stochastic variables influence the outcome of such a system [1] . Appropriate control strategies have been developed and they can have a positive effect on grid frequency but the energy that is available is limited and thus their usefulness [19], [86]–[91].

2.5.3 Solar PV

Artificial inertia and FFR by Solar PV can be provided in two ways. The first is to change active power set-points proportional to the frequency gradient during a frequency event. Lowering the power output can be done easily but to increase the output, it is necessary to curtail the maximum power during normal operation so that in case of a drop in frequency there is still headroom. The second possibility is to use larger sized capacitors in the DC link as additional energy storage [92] .

2.6 Conclusion

This chapter covered frequency stability and how FFR can be introduced beside conventional frequency stability mechanisms such as FCR. FFR is becoming accepted within grid codes of several countries but the definition of what FFR is supposed to be doing varies between the countries. As described in Chapter 1 under motivation for the research presented in this thesis, past studies concerning FFR do not compare different types of controllers. This, and the difference between grid codes and the approaches manufacturer take (for example summarised in [21]) indicate that there is a clear lack of understanding on the characteristics of the different approaches.

Following the comparison of different grid codes and FFR applications, it was decided to clearly define FFR in the context of this thesis as the control of rapid active power by a generator or load in a time frame of two seconds or less, to correct a supply-demand imbalance and assist in managing power system frequency. The difference between activation methods and technologies that can provide FFR were highlighted. Between wind power plants, solar PV and BSS, the latter has the advantage of proving the widest range of freedom because of the large and independent energy storage. Wind turbines rely on the energy stored in the mechanical system and incorporating larger DC capacitors in solar PV needs to be accompanied by a larger converter or to curtail the power output during normal operation to be able to increase the power output for FFR.

Chapter 3

Fast Frequency Response Using Battery Systems

This chapter investigates BSS in relation to FFR as they offer the widest range of freedom. BSS are used because the stored energy is relatively much larger than what can be extracted from wind turbine systems or from enhanced solar PV systems. The insights developed based on the literature review of Chapter 2 are used in this chapter to develop and compare different types of FFR controllers for a Li-Ion BSS.

With regard to traditional FFR and the utility practice, the widely employed FFR controller has an output which is proportional to the frequency deviation and has a deadband to avoid activations for small frequency deviations. The activation range and the width of the deadband can vary depending on the use-case, regulation or manufacturer. This is exemplified in Figure 3.1.

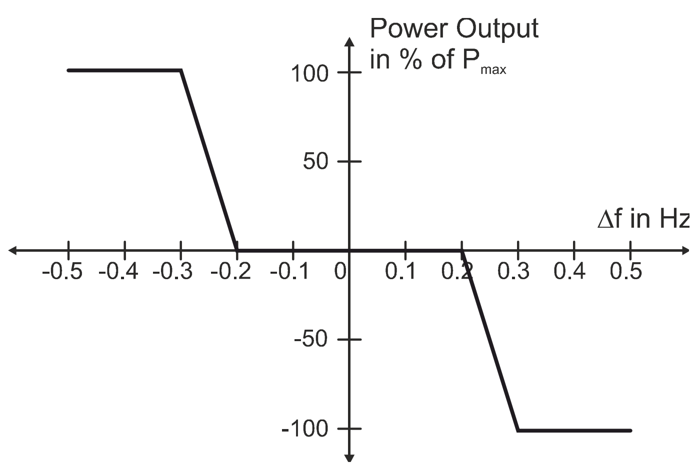

Figure 3.1: Example of a frequency deviation proportional controller with a deadband

This activation method is used by industry applications that already exist and by the British regulation regarding FFR.

Another activation method is an event-based approach that triggers a certain amount of reserve after a frequency threshold is reached. The Finish regulator approached FFR with this type of event-based activation. Following a certain support duration, the FFR device is allowed to shut off, either in ramp form as illustrated in Fig. 22, or instantaneously.

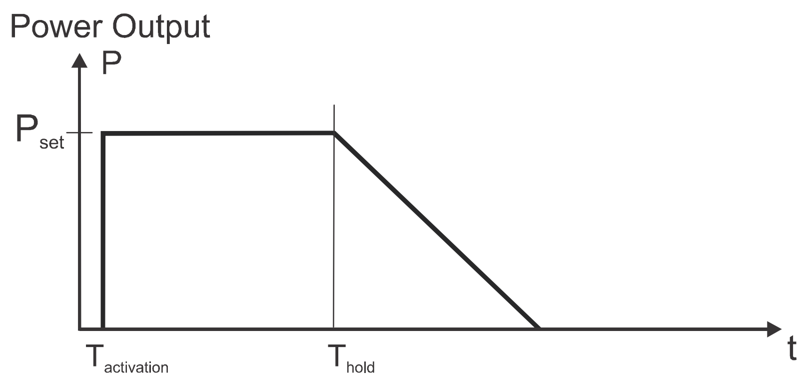

Figure 3.2: Example of event-based activation of FFR devices

3.1 Battery and Controller Modelling

3.1.1 Battery Model

A multitude of battery models exist which differ depending on the application and the associated details required [93]–[96].

It is concluded in [96] that connected with the manner in which the power is controlled the ac behaviour of the battery storage system on the grid side is independent of the State of Charge (SOC) and the temperature of the battery cells as long as the dc voltage does not fall below the low voltage limit. Hence, the aging and temperature effects are not considered in the simulation model used.

As depicted in Figure 3.3, DIgSILENT PowerFactory provides a basic model for a BSS.

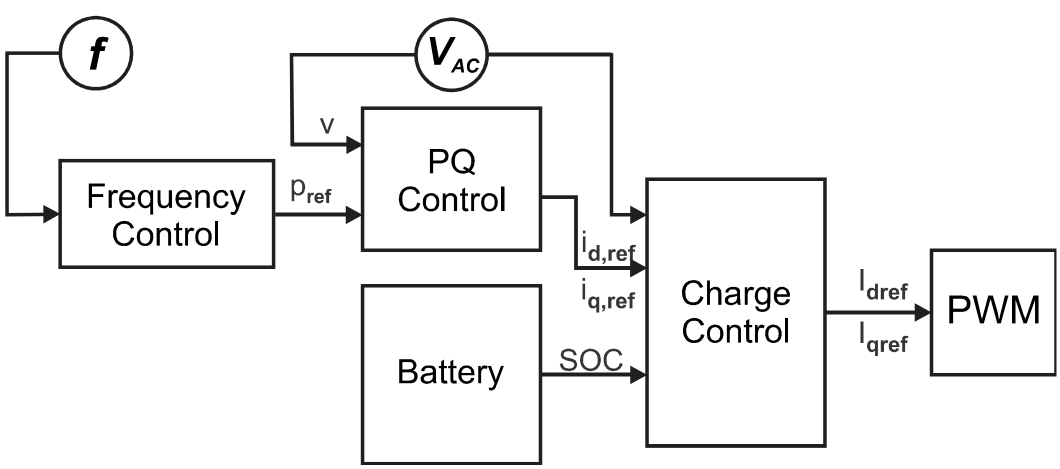

Figure 3.3: Schematic of the control frame of the Battery Storage System

Employing the associated terminology “frame” and “slots”, several slots simulate the behaviour of the BSS. In these slots, the actual models, similar to the model for the battery behaviour or the frequency controller, are inserted. The frequency control slot occupies the developed frequency controllers and has an output signal p_{ref} as the active power set-point. The PQ controller uses this set-point and calculates the current i_d. The PQ controller also calculates the reference signal i_q for voltage/reactive power control. The block “Battery” consists of the simplified electrical model that provides the state of charge (SOC) of the battery as an output. A generic PQ controller was used to calculate the currents in the dq-axis The controller is shown as block diagram in Fig. 24. The parameters given in Table 6 were used in the PQ controller.

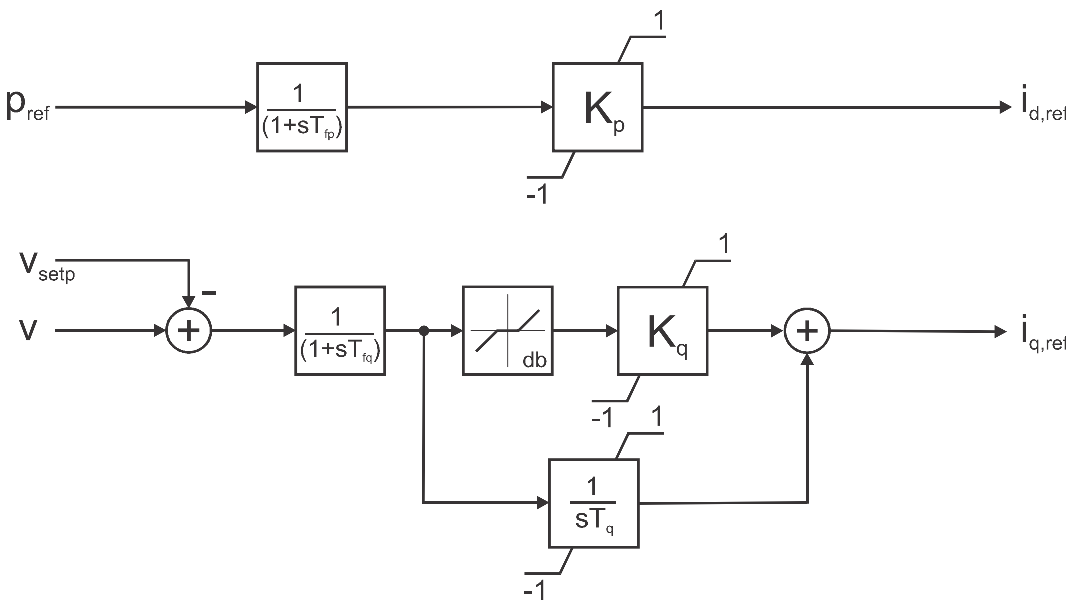

Figure 3.4: Block diagram of the PQ controller

For the simulation, following parameters were used:

Table 3.1: Parameters of the PQ controller

Parameter	Description	Value
T_{fp}	Filter time constant, active path	0.05 s
T_{fq}	Filter time constant, reactive path	0.01 s
K_p	Proportional gain, active path	1
K_q	Proportional gain, reactive path	2
db	Deadband to avoid activation for small voltage deviations	0.1 pu
$1/T_q$	Integrator gain	1

The charge control block calculates the final outputs. For this, several boundaries need to be considered. The state of charge needs to be considered in the simulation because the BSS can only consume active power if the battery is not fully loaded and provide active power if the battery is not empty. The reactive power output of the BSS is not limited by the battery capacity, but the apparent power S of the converter is constrained and therefore the reactive power is:

$$Q = \sqrt{S^2 - P^2} \tag{3.1}$$

The combined active and reactive power cannot be bigger than the apparent rated power. The charge control model includes the charging of the BSS in case it completely discharges during operation. However, in the work presented in this thesis, this feature was removed as it is not relevant for initial observations of the frequency.

3.1.2 Battery Controller Models

In the initial investigations, two controllers were utilised: a standard droop activated controller (C1) and AI controllers (C2.1 and C2.2). Based on the insights gained by the application of the controllers C1 and C2, two novel controllers C3 and C4 were also subsequently designed. The newly developed controller (C3) is based on an event-based concept which injects/absorbs a defined level of active power following the detection of a major frequency deviation, and the second controller (C4) uses a rolling average set-point to reduce the output power of the storage system gradually over a given period. Both these controllers employ a mechanism that prevents the battery storage system from counteracting the frequency restoration.

The general approach to test controllers is by applying a step function and analyse the reaction of the controller. With regard to actual electricity grids, in practice, frequency deviations do not occur in the above manner, and hence a ramp function with varying gradients and maximum deviations were used instead.

3.1.2.1 C1 - Proportional Controller

The block diagram of the proportional controller tested is shown in Fig. 25 of which the parameters are given in Table 7. Naturally, a storage system that utilises this type of controller has a permanent output depending on the deviation of the actual frequency from the nominal grid frequency and as long this deviation is larger than the included deadband. This leads to the storage system completely depleting or charging fully after a certain time. The time this process takes is dependent on the frequency deviation (and thus the power output), the capacity of the storage system and the state of charge before the event. When the battery is full or empty, the storage system shuts down and causes another rapid change in frequency.

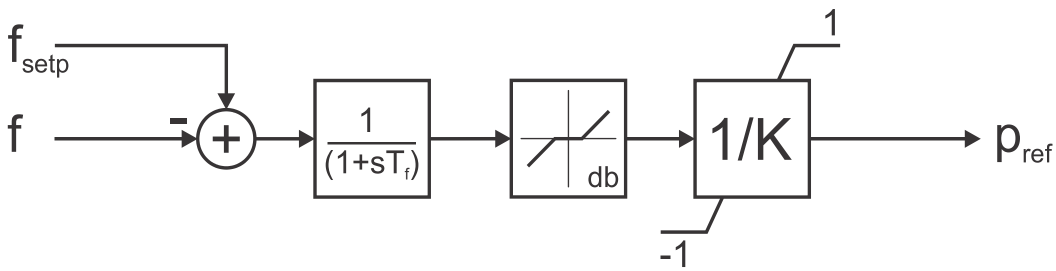

Figure 3.5: Block diagram of the proportional controller C1

Table 3.2: Parameters of the proportional controller C1

Parameter	Description	Value
T_f	Filter time constant	0
1/K	Proportional gain	25
db	Deadband to avoid activation for small deviations in pu	0.001

With this gain, the maximum power output is reached for a frequency deviation of 0.04 pu. The frequency drop to 0.92 pu in Figure 3.6 has a maximum frequency deviation of 0.08 pu, thus the output of 1 pu is reached sooner.

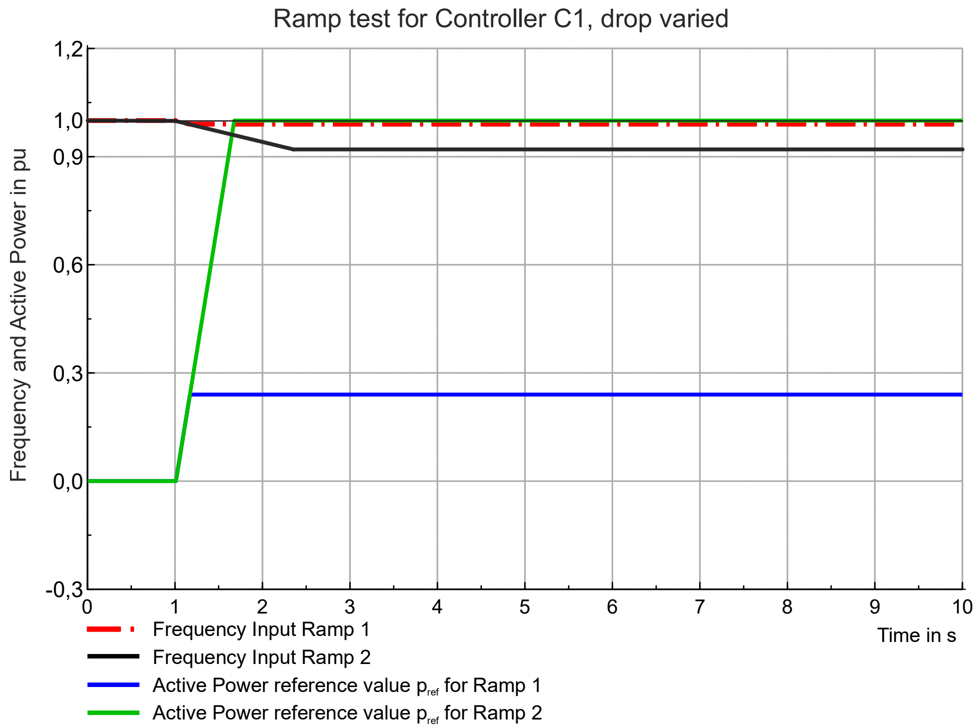

Figure 3.6: Output of the proportional controller C1 for a frequency drop with a ramp of 0.06 pu/s

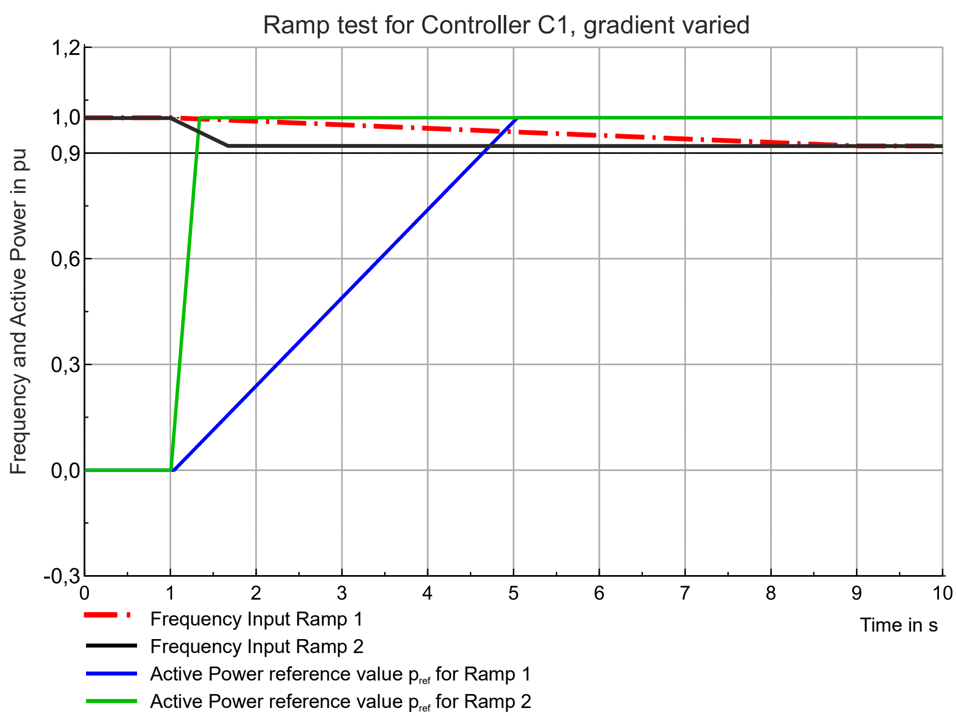

Figure 3.7: Output of the proportional controller C1 for a frequency drop with a ramp of 0.92 pu/s

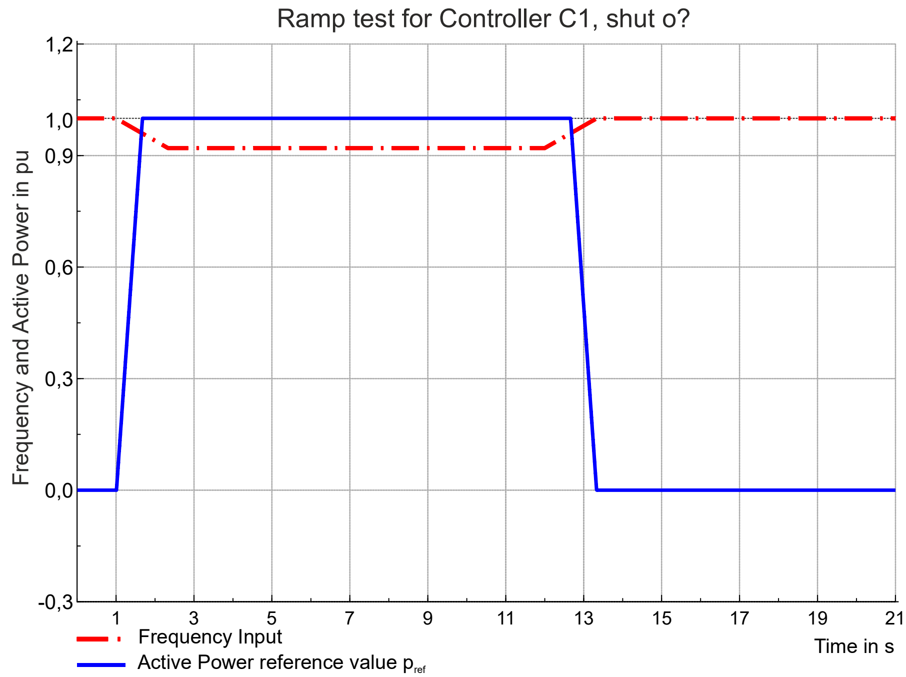

Figure 3.8: Shutting down of the proportional controller C1 output from a change to 0.92 pu back to 1 pu

The controller C1 was tested with real frequency measurements to analyse the feasibility for power plants participating in FCR. Data from a PMU located at the Graz University of Technology Austria was gathered and is used to illustrate the variations in the Frequency for the CE system. In Figure 3.9, the deviations from the nominal frequency of 50 Hz are illustrated for the whole month of January 2019.

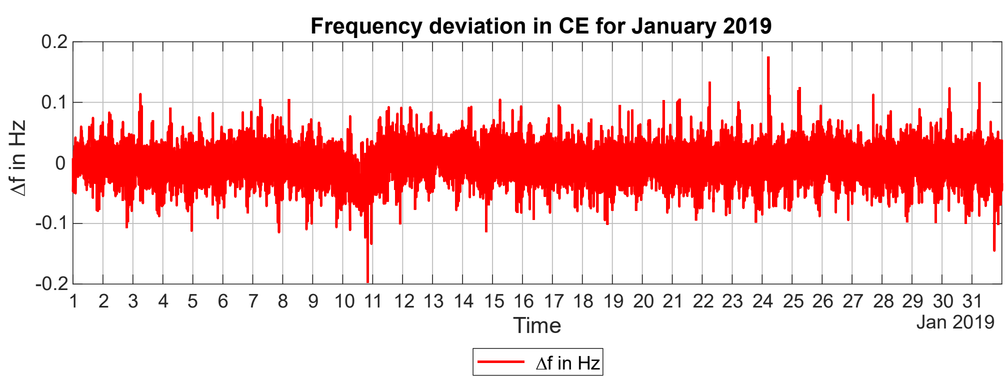

Figure 3.9: Measured frequency deviations for January 2019

This data was used to determine the required active power output of a virtual BSS plant in the frequency containment process and equipped with an FCR controller based on the design parameters outlined in [9]. Specifically, it is stated, that a power plant, or group of power plants which participate in FCR, active power output by means of a proportional governor should lead to a maximum power output for 200 mHz frequency deviation within 30 seconds. The gain must therefore be 1/K = 5. Since a BSS can change the power output extremely fast, the above stated timeframe for activation can be neglected. The active power output was calculated in pu (on the basis of $P_{r,BSS}$) for discrete time steps (Δt = 200 ms) of the measured signal using the controller C1 as depicted in Figure 3.5. With the step width, the total energy usage can be calculated. Since Austria, Belgium, Netherlands, France and Germany are organised as a market-based system regarding FCR, the four-hour time blocks in which the FCR is divided throughout a day were considered. Units that have been allocated a period must be capable of meeting the FCR requirement for that entire period. Figure 3.10 shows the results established based on the aforementioned approach. The calculated energy commences from zero at the start of every time block.

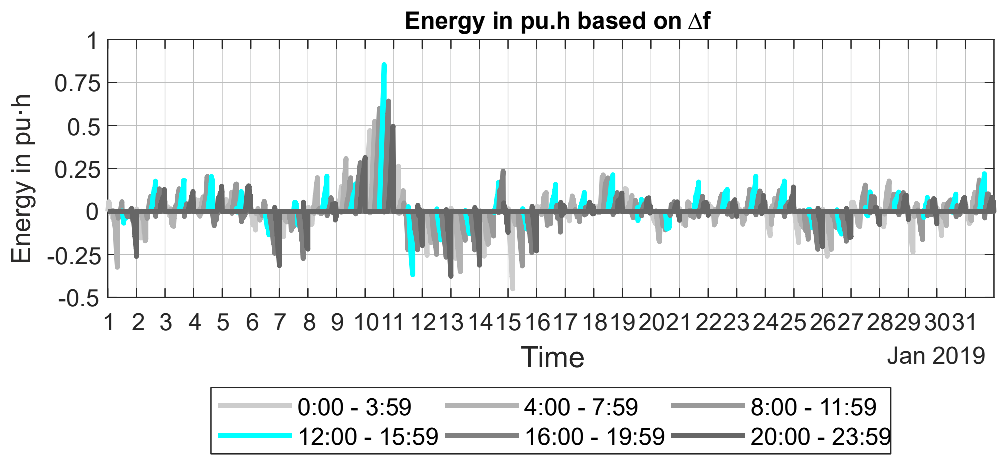

Figure 3.10: Energy usage during each 4-hour FCR window

The needed energy varies strongly in both directions. The maximum energy was required on January 10th during the 12:00 to 15:59 with 0.8547 pu·h. Considering these results, several observations can be drawn. Firstly, in order to be prepared for all eventualities, the BSS needs to be charged to 50% before the timeslot starts. Taking the maximum energy values for this month into account leads to a storage capacity of 1.71 pu·h. For example, a BSS with 100 MW rated active power needs a storage capacity of 171 MWh. Secondly, the BSS needs time to recharge, which makes continuous operation difficult to achieve. From a power output perspective, using BSS for FCR is entirely possible, but the high and unpredictable energy requirements make it nearly impossible to replace conventional power plants on their own for a continuous period, despite having the advantage of very fast activation times for a BSS. The most feasible solution to use BSS for FCR is in conjunction with a slow acting power plant, where the

BSS activates quickly to comply with activation times, which is slowly replaced with the FCR function of the power plant.

3.1.2.2 C2.1 - Artificial Inertia Controller

The Artificial Inertia Controller emulates the electro-mechanical behaviour of a conventional synchronous generator connected to the grid. This controller provides power to the grid during frequency changes and therefore reduces the RoCoF. The artificial inertia controller has no impact on the steady-state frequency deviation.

$$\Delta p = -T_J \cdot \omega \cdot \frac{d\omega}{dt} \tag{3.2}$$

The parametrisation of the controller can be achieved by setting limits which the controller should achieve by providing maximum power output Δp. The only variable parameter in (3.2) is the acceleration time constant T_j. As an example, the controller should be fully activated when the frequency deteriorates with a RoCoF of above -3 Hz/s which equates to -0.06 pu/s. Assuming a steady state frequency of 1 pu. the gain T_J can be calculated:

$$T_J = -\frac{\Delta p}{\omega \cdot \frac{d\omega}{dt}} \tag{3.3}$$

$$T_J = -\frac{1\ \mathrm{pu}}{1\ pu \cdot \frac{-0.06\ pu}{1\ s}} \tag{3.4}$$

$$T_J = 16.667\ s \tag{3.5}$$

Figure 3.11 shows the block diagram of the artificial inertia controller.

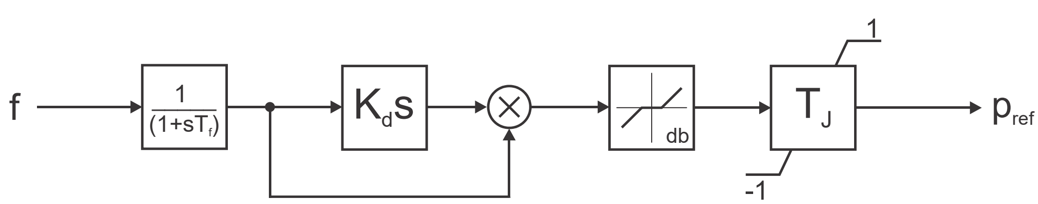

Figure 3.11: Block diagram of the Artificial Inertia Controller C2.1

Table 3.3 lists the parameter values that were used in the controller tests.

Table 3.3: Parameters of the Artificial Inertia Controller C2.1

Parameter	Description	Value
T_f	Filter time constant in s	0
K_d	Differentiator gain	-1
db	Deadband to avoid activation for small RoCoF in pu	0.001
T_J	Proportional gain; equivalent to acceleration time constant in s	17

In Figure 3.12 and Figure 3.13, the filter was made inactive to illustrate the basic control principle. shows the response of the controller to a ramp with a gradient of 0.06 pu/s. Ramp 1 illustrates a drop to 0.99 pu, and Ramp 2 a drop to 0.92 pu. The first observation is, that the output is only active if the input is changing. The second important observation is that the output decreases with decreasing frequency. The gain could be adjusted so that a decreasing frequency would not lead to this behaviour.

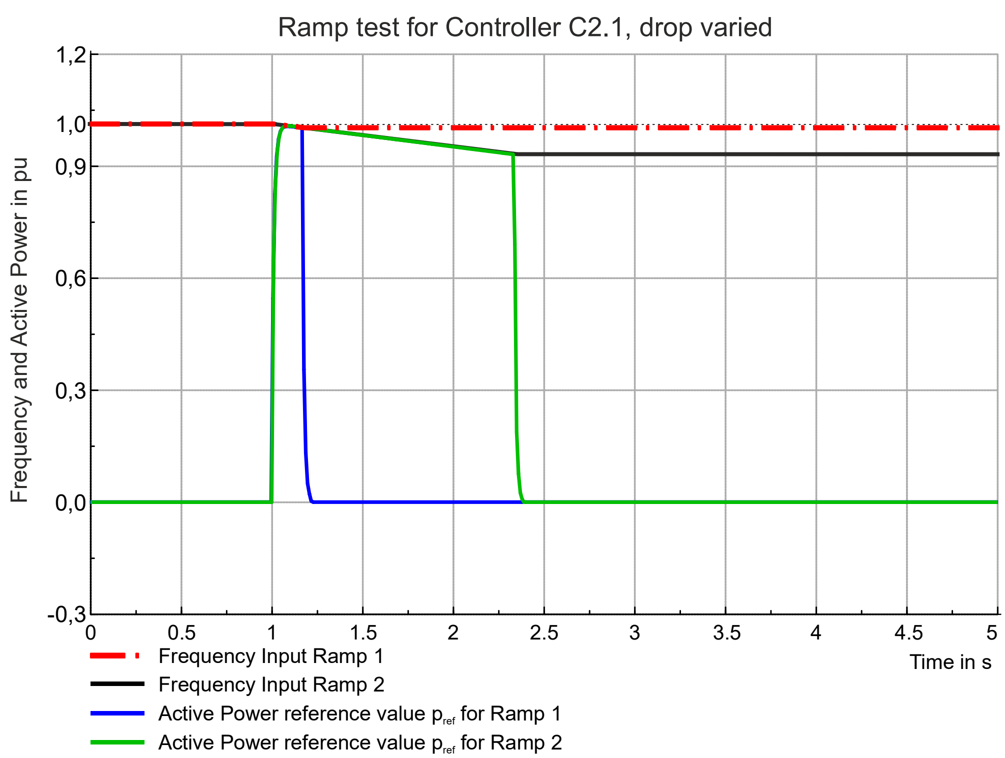

Figure 3.12: Output of Controller C2.1 for a frequency drop with a ramp of 0.06 pu/s

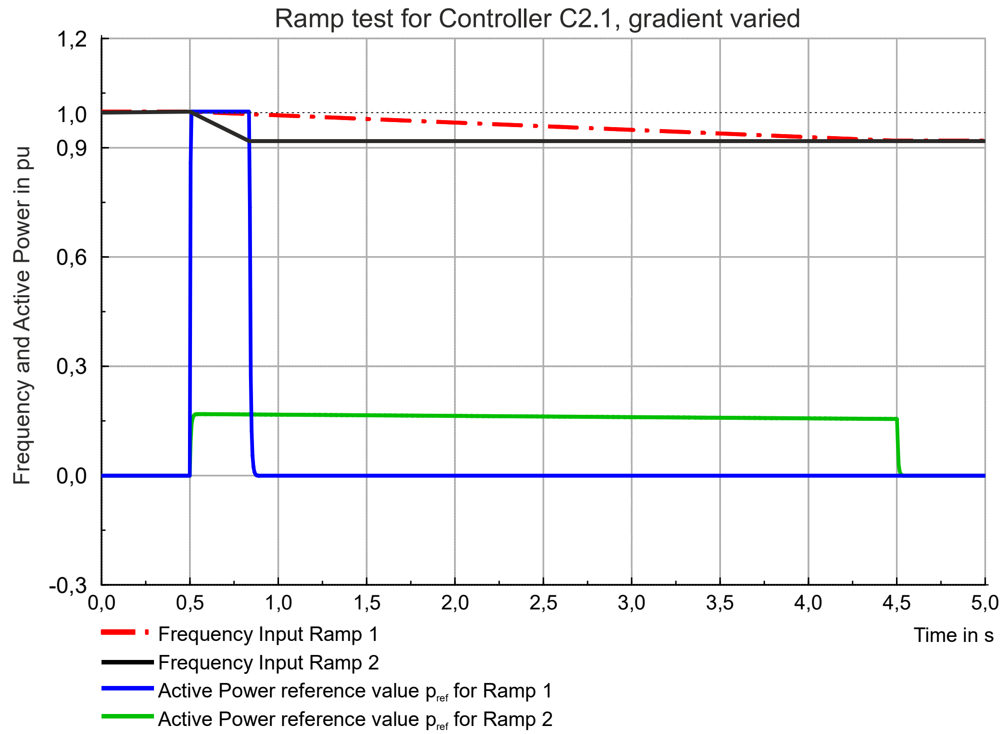

Figure 3.13: Gradient variation test for the Artificial Inertia Controller C2.1 and a drop to 0.92 pu

Figure 3.14 shows the effect of the filter time constant on the output. For illustration purposes, a frequency drop with a ramp of 0.06 pu/s to a new frequency of 0.92 pu was simulated. The filter time constant was set to 0 s, 0.1 s, 0.5 s, and 1 s respectively. The output decreases with increased filter time and the controller leads to increasing levels of BSS remaining energy output at the end of the frequency drop process. Larger the filter time constant, the longer it takes for the controller to settle down.

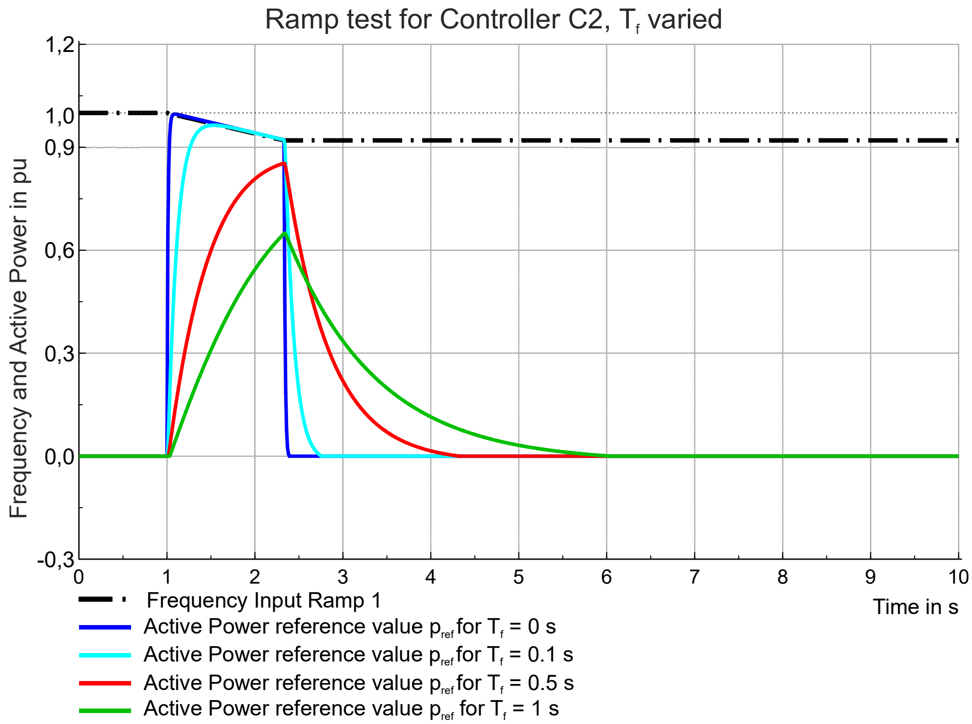

Figure 3.14: Output of Controller C2.1 for with ramp 0.06 pu/s and for different filter time constants

3.1.2.3 C2.2 – Altered Artificial Inertia Controller

Based on (3.2), it is evident that as the frequency reduces, the active power output decreases, and vice-versa with increasing frequency, provided the ROCOF stays constant. This behaviour is natural in synchronous generators but can be avoided by not using the system frequency ω as a multiplier as described in (3.6).

$$\Delta p = -T_J \cdot \frac{d\omega}{dt} \tag{3.6}$$

Figure 3.15 illustrates how this altered AI controller is realised.

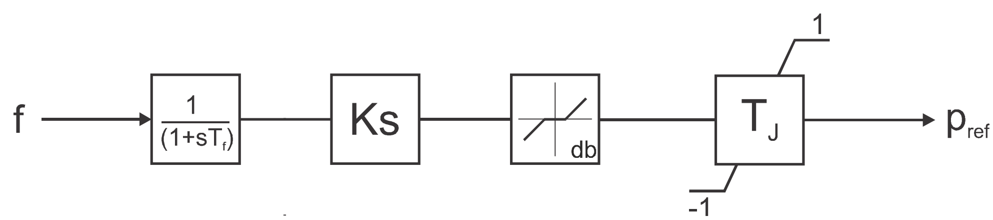

Figure 3.15: Altered artificial inertia controller

As can be seen in Figure 3.16, the power output does not degrade with the decreasing frequency which is a more suitable behaviour. The advantage of omitting the frequency as a multiplier is most relevant in situations where the frequency decreases. A decreasing power output during a falling frequency is the opposite of what is necessary in this situation, where an increase in power output is necessary to keep the frequency stable.

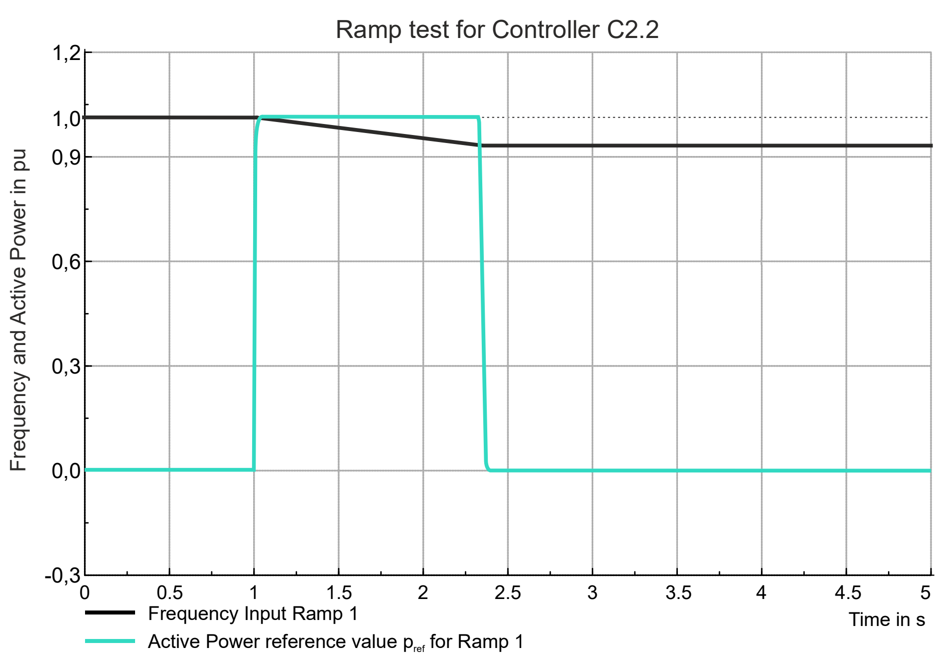

Figure 3.16: Output of Controller C2.2 for a frequency drop with a ramp of 0.06 pu/s

3.1.2.4 C3 - Event Detection Controller

This controller is based on the event detection principle. An event can be detected by the frequency deviation or by RoCoF and as explained above, false triggering can be a problem. Following objectives were taken into account when designing the controller:

- Robust event detection
- Inclusion of parameterisation options to comply with different jurisdictional regulations
- Automatic adjustment of the output based on the severity of the event
- Frequency restoration should not be detected as an event

Figure 3.17 shows the block diagram of the event detection controller developed. The controller can be divided in three main parts that are indicated with different colours. The first is the red block that is used to detect an event employing RoCoF as the measure. The blue block is the verification of the frequency deviation and gain calculation, and the green block ensures that an activation only happens in the correct direction.

Starting with the red block, the recognition is first made by determining the rate of change of the frequency. If this change is above a threshold setting, a logic signal ‘true’ is triggered. This is realised with a deadband that is the input to the signal generator which converts the analogue input into a binary signal with 0 for an input value of zero and 1 for all non-zero values. A minimum activation time is included to be able to comply with regulations such as the Finish grid code that includes activation times from 5 to 30 seconds. Otherwise, the logic signal stays ‘true’ until the frequency is settled.

In the blue block, the logic signal of the red block activates two processes. An integrator is enabled which integrates the frequency deviation from the time of triggering. To make sure that the calculation starts from zero, this integrator is reset whenever the output is deactivated. The input signal (the frequency deviation) must be multiplied by -1 to gain a positive power output signal for negative frequency deviations. Using an integrator here compensates for possible oscillations in the frequency. Especially following a fault, the frequency can experience severe oscillations. Furthermore, the logic signal ‘true’ releases a holding element with a delay. This hold element stores the output of the integrator at the time of triggering together with the delay. Thus, a certain time is spent in capturing the event and avoids a false activation. If there is no frequency deviation during this time, the battery storage is not activated as the output of the integrator is zero. Such false activations can take place if only the RoCoF is considered as input variable. As explained above, phase jumps which can occur due to brief voltage dips in the grid can be interpreted as high RoCoF and can lead to false triggering.

Once the logic signal returns to zero, the gradient is limited to avoid an additional frequency dip. This is realised in the green block. To achieve this, the output needs to be separated into a negative path for a frequency deviation greater than the nominal frequency and a positive path for a frequency deviation smaller than nominal frequency. This is necessary as the output rises with a positive slope and falls back to zero with a negative gradient. The opposite occurs for a negative output. A single gradient limiter that limits the negative gradient for the reduction of a positive output signal would, in turn, reduce the initial gradient of the negative output in case of a positive frequency deviation. The split ensures a reduction of only the deactivation gradients without limiting the initial activation gradient.

Table 3.4: Parameters of the event detection controller C3

Parameter	Description	Value
T_f	Filter time constant in s	0
K_d	Differentiator gain	-1
db	Dead to avoid activation for small RoCoF in pu	0.012
T_i	Integrator gain	0.004
T_{Delay}	Sampling time in s	0.5
T_{hold}	Minimum active time in s	2
k_1	Negative gradient limiter; positive path in pu/s	-0.1
k_2	Positive gradient limiter; negative path pu/s	0.1

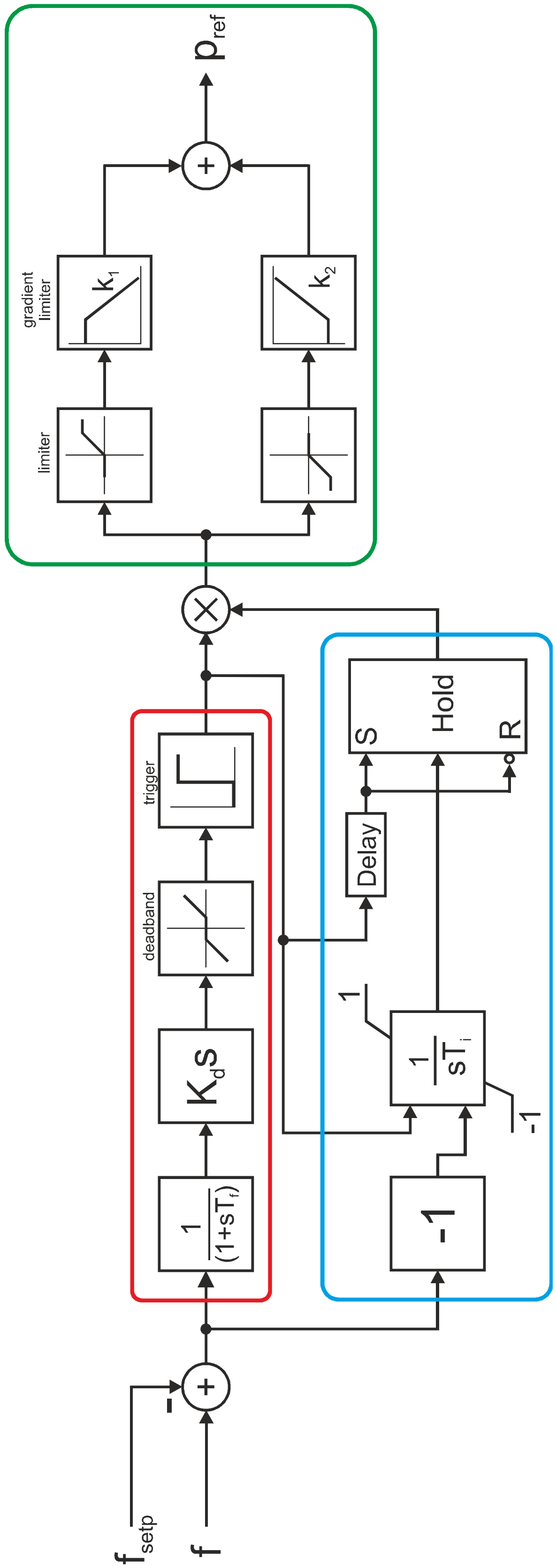

Figure 3.17: Block diagram of the event detection controller C3

In summary, the controller activates a constant output that is proportional to the integrated frequency deviation over a predefined sampling time T_{delay} and holds it for the time T_{hold}. This can be seen in Figure 3.18 at the power output for Ramp 2. The controller holds the output at 1 pu longer than the duration of the ramp. After this, the controller output gradually decreases over time. The length of T_{hold} is defined by a minimum activation period but can be extended if the frequency is still changing following this period. The response to Ramp 1 yields a power output as long as there is a change in frequency detected and then starts to slope down. The duration of Ramp 1 is here longer the defined holding time. The behaviour of this controller is predictable and easily customised for different grids and operational states. False activation is avoided by giving combined attention to both RoCoF and the frequency deviation. The holding time can be adjusted to suit the time that participating generators require to start and/or ramp up the power output to the grid. At the end of the active period, the output of the controller is reduced with a limited gradient to avoid additional frequency disturbances that occur when shutting off the BSS instantaneously.

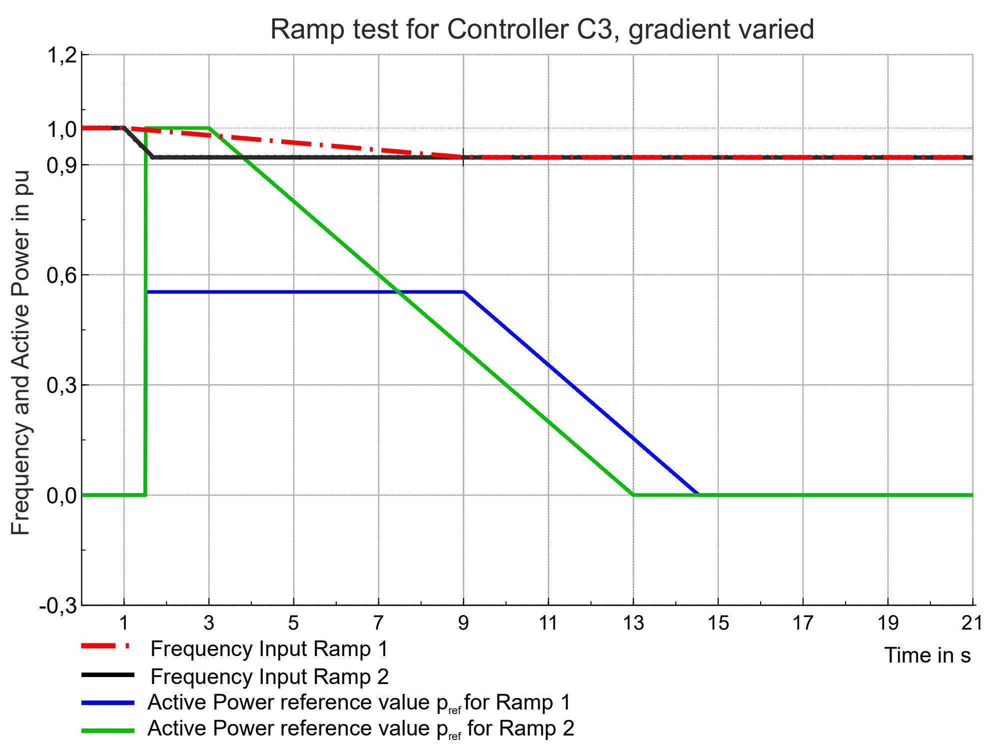

Figure 3.18: Gradient variation test for the event detection controller C3 and a drop to 0.92 pu

The results depicted in Figure 3.19 show that both gradients result in the same output of the controller. The reason is that the change of frequency is the same during the assessment of the event.

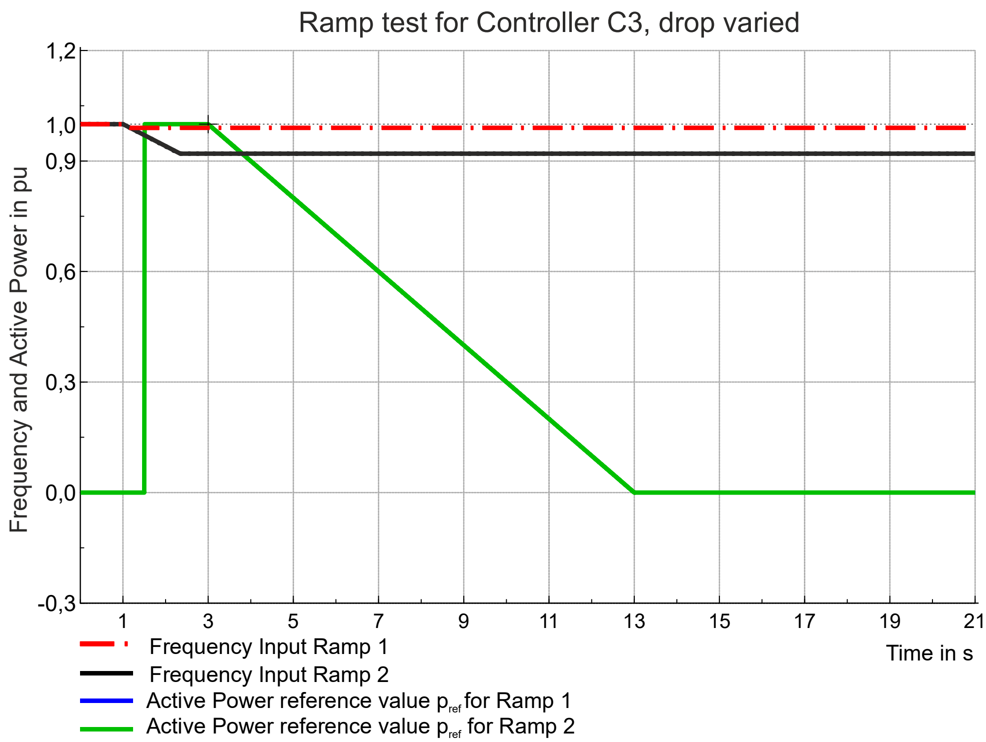

Figure 3.19: Drop variation with a gradient of 0.06 pu/s for the event detection controller C3

3.1.2.5 C4 – Rolling Average Set Point Controller

The Rolling Average (RAVG) Set-Point Controller is an evolution of the proportional controller. As described in Section 3.1.2.1, the proportional controller remains active as long as there is a frequency deviation from the nominal frequency. If the frequency restoration process takes too long, the BSS discharges fully or charges completely and such sudden shut off of the power output can cause additional frequency disturbances. A system needs to be in place to reduce the power output of the storage system automatically and gradually to avoid a sudden shutdown. Additionally, higher power output is more critical at the beginning of the disturbance. These aspects were solved by introducing a rolling average mechanism that averages the input following a defined holding period which is subsequently used as the set-point for the controller.

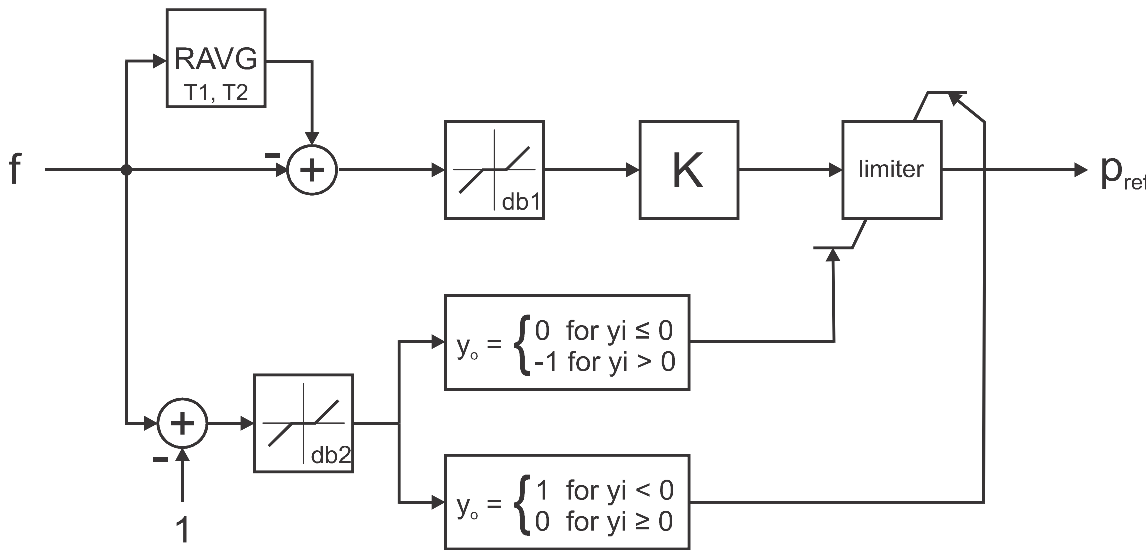

Figure 3.20: Block diagram of the Rolling Average Set-Point Controller C4

Table 3.5 gives the values the parameters of the controller C4 used in the simulations.

Table 3.5: Parameters of the event detection controller C4

Parameter	Description	Value
T1	Waiting period before sampling window is activated in s	0
T2	Sampling window length in s	10
db1	Deadband to avoid activation for small frequency deviations in pu	0.0001
db2	Deadband to set activation thresholds in pu	0.002
K	Proportional gain	50

Figure 3.21 shows the controller output when different slopes for frequency variations are applied. The maximum power output is reached when the frequency reaches a frequency deviation of 0.02 Hz.

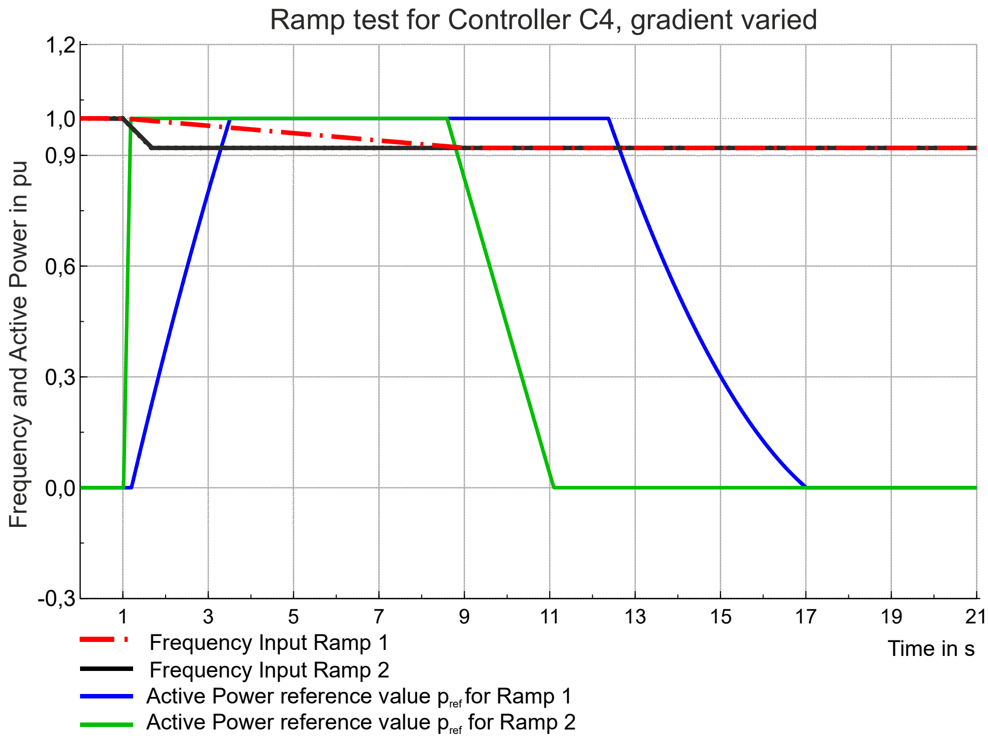

Figure 3.21: Gradient variation test for the RAVG controller C4 and a drop to 0.92 pu

During the frequency restoration process, the set-point would remain at the new steady-state frequency, and the controller would, therefore, counteract the restoration process. This problem was solved by implementing a system that limits the controller to a positive output for under-frequency and a negative output for frequency above the nominal frequency. This behaviour is illustrated in Figure 3.22. In the controller, this is solved by adjusting the limits of the output. When the frequency is below the nominal frequency, the controller can only have a positive output and when the frequency is above the nominal frequency, the limits are changed so that the controller can only have a negative output. Due to the variable set-point, an additional deadband was introduced. With the second deadband, an area can be defined where there is no output at all. For the usage as CFFR, this applies to frequencies in the normal operation bandwidth of ± 200 mHz (see Figure 2.10).

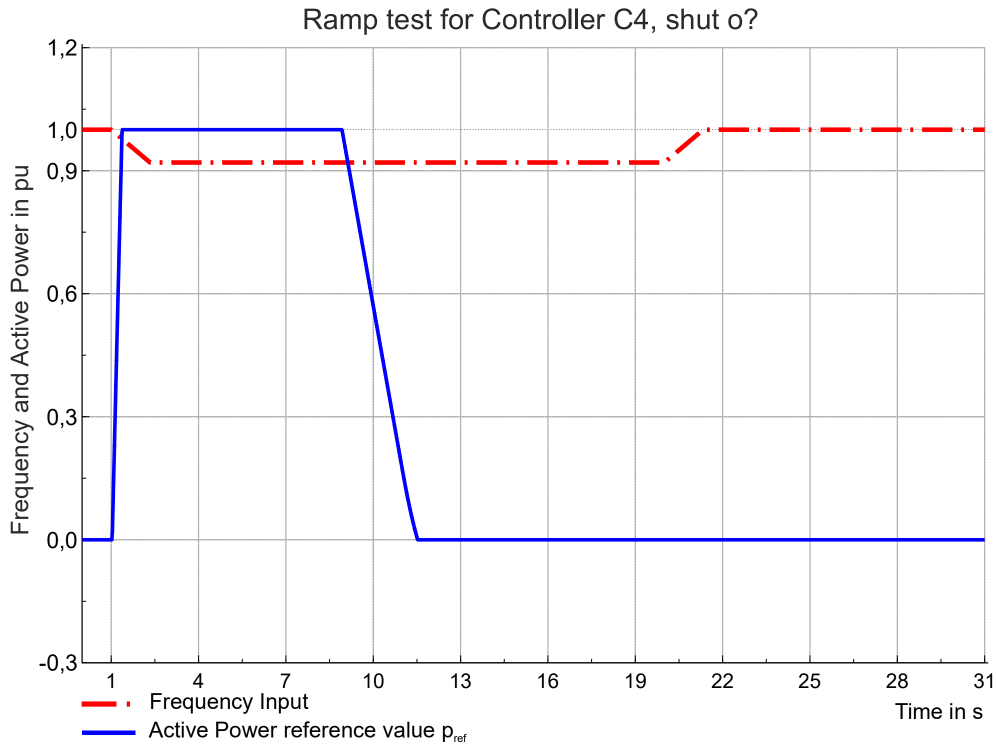

Figure 3.22: Locking of the output during the restoration process

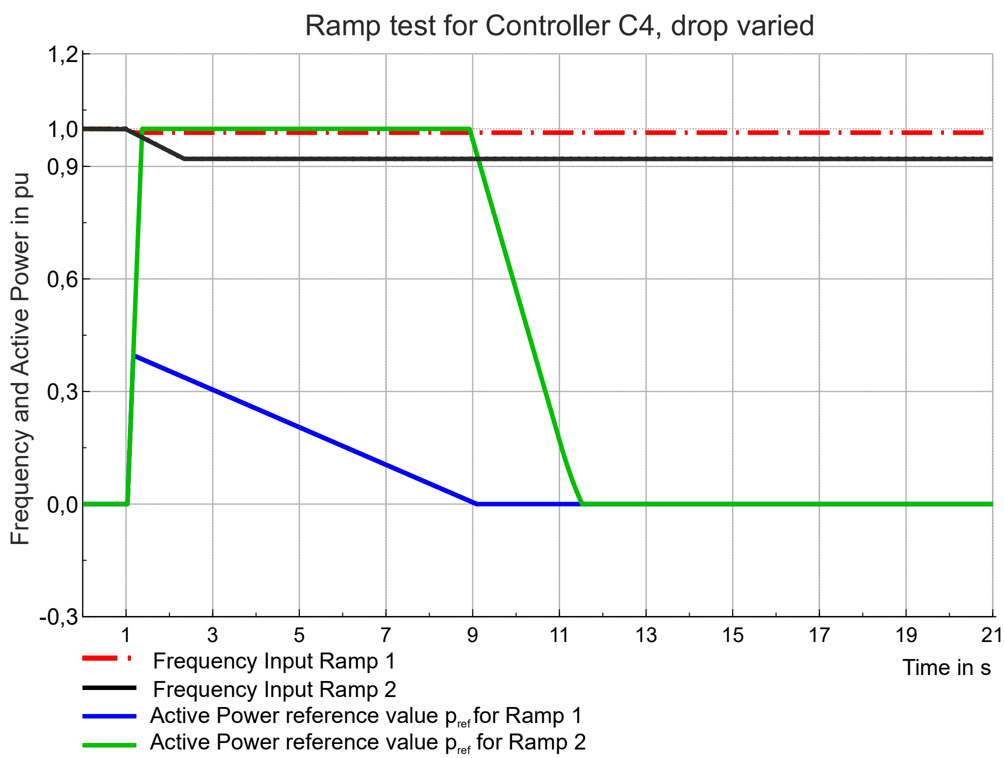

Figure 3.23: Frequency drop variation with a gradient of 0.06 pu/s for the RAVG Controller C4

3.2 Conclusion

In this chapter, four controllers that can be employed for fast frequency response were introduced together with detailed simulation outcomes. For each controller, the behaviour was shown with a gradient variation and a drop variation test. It was shown that a standard proportional controller has several downsides. Even though some manufacturers propose BSS with a proportional controller to participate in FCR, the application is limited by the capacity of the storage system. FCR market regulation demands that a participating generation unit must be able to participate in FCR during the whole time slot. There are exemptions for this rule in Austria but only if the BSS is operated in cooperation with a power plant that covers the long-term output. This highlights the fact that BSS are not suitable for FCR operation but should rather be used as FFR devices. Using a proportional controller for FFR has the disadvantage that it does not include a shut off. The BSS would have a power output if there is a frequency deviation outside the deadband. This would lead to the battery shutting off suddenly, when the BSS is either full or empty – depending on the direction of power.

An artificial inertia controller (C2) was also included in this chapter as the definition of FFR in this thesis includes forms of artificial inertia. A modification was introduced to decouple the output of the controller from the frequency so that the output is solely dependent on the RoCoF. The advantage of this controller is that it limits the RoCoF. The downside is that it has no effect on the arresting stationary frequency.

The event detection controller C3 was developed from ground up. The goal was to automatically detect relevant frequency events and activate according to the severity of the disturbance. It can be argued that a full activation might be more appropriate if there is a significant event detected. This argument holds some significance as long as there is only a small number of FFR devices installed. With a higher degree of implementation, fully activating all FFR devices would lead to an overcompensation, unwanted oscillations and not the ideal outcome. Therefore, developing and testing a controller that can react accordingly was conducted. The controller also includes a sloping shut-off period to not negatively affect the frequency restoration process.

A simple improvement to the proportional controller was made in the proposed controller C4 (Rolling Average (RAVG) Set Point Controller). With an included rolling average set-point change, the BSS automatically reduces the power output after a predefined period. Resulting from the of set-point changes, the frequency recovery would lead to deviation between set-point and the actual frequency. To avoid activation during the restoration process, a mechanism was introduced to only provide a positive power output while the frequency is below nominal frequency and vice-versa for frequency above the nominal frequency.

Chapter 4

Network Simulation Model, Scenarios and Frequency Response observed using different Controllers

The first objective of the chapter is to model a grid featuring high levels of renewable energy generation and featuring a weak connection to the main grid, so that a disconnection from the main grid is a possible scenario that can be investigated. A grid like this would exhibit high RoCoF and is in danger of a widespread blackout following the disconnection from the main grid during times of peak import or export. The established grid is then used to test the established controllers from Chapter 3 and analyse the effectiveness of FFR using a battery system.

4.1 Description of the simulation model

A weak grid characterised by relatively reduced inertia was developed using the modified IEEE 9-bus test system [97] as shown in Figure 4.1 which portrays the characteristics of the South Australian network in 2020. This simulated grid features aggregated generating resources: gas fired synchronous generators (G1, G2 and G3), wind farm (WT1) and solar farm (S1). The gas fired generators are divided as follows: aggregated G1 and G2 represent generators that run efficiently at near maximum capacity and do not participate in primary frequency control. Aggregated gas fired generator G1 serves as the slack generator. Aggregated gas fired generator G3 represents the generators in the network that do participate in primary frequency control. The wind farms are assumed to consist of permanent magnet synchronous generator type wind turbines. Additionally, it is assumed that 10% of all gas fired generators participate in FCR. The loads (Ld1- Ld3) are implemented as static (constant impedance) loads. Different scenarios were simulated including a scenario representing a connection to the main grid represented by G4, and several cases featuring different levels of renewable energy penetration. A BSS is introduced after the initial modelling of the scenarios to study the effect of FRR in the described network.

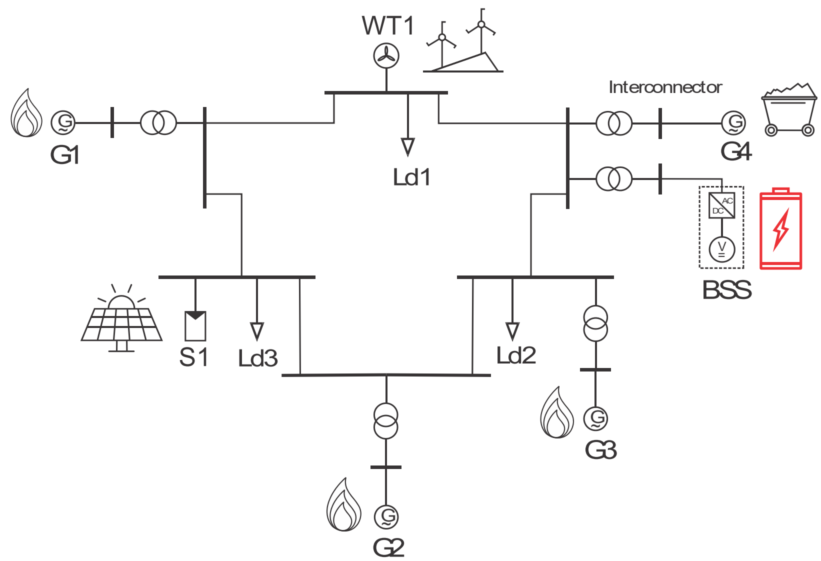

Figure 4.1 : Simulated grid featured by reduced inertia

4.2 Generation Scenarios of the Network

Figure 4.2 and Table 4.1 depict the four different scenarios that were considered. The scenarios differ in terms of amount of renewable energy generation.

Scenario 1 (S1) corresponds to the base case where the network represented by Figure 4.1 together with the interconnector intact and corresponds to normal operational state (similar to the normal operation of the SA network). The effect of the missing interconnector is simulated in Scenario 2-4 (S2-S4). These scenarios represent the network after a disturbance (e.g., a fault or overloading) causes the interconnector to disconnect and therefore separate the illustrated subsystem from the main grid. Figure 4.2 illustrates Scenarios 1-4. The depicted generation is proportional to the generated active power *P* from each form of generation. Table 4.1 provides the corresponding values for the inertia constant *H*, the rated power S_n and the active power *P* set-point of the generators in the network. The inertia constant *H* is based on S_n of the generator.

A BSS is then introduced for FFR using the controllers presented in Chapter 3. The load and generation of the presented system is using scaled values of the actual SA grid. Considering this, the size of the installed BSS was chosen to be in relation to be approximately the relation between the Hornsdale Power Reserve after the completion of the first stage in 2017 and the average loading of the SA sub-grid. The rating of the BSS was chosen to evaluate how this existing BSS can already affect the frequency stability in an optimal way.

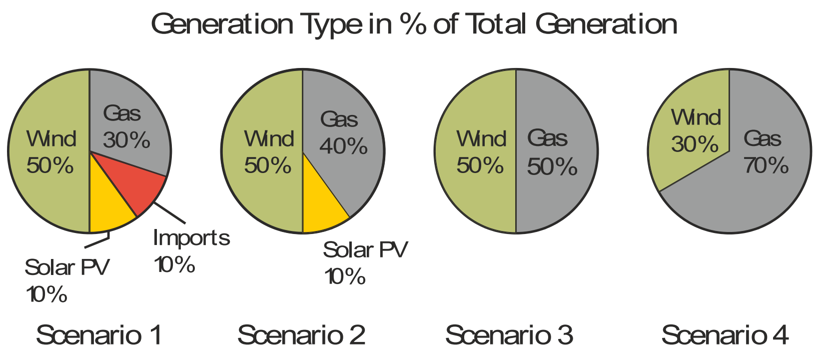

Figure 4.2: Simulated Generation Scenarios

Table 4.1: Generator parameters (inertia constant H, rated power S_n and active power setpoint P) considered under the different scenarios

		S1		S2		S3		S4	
	H (s)	S_n (MVA)	P (MW)	S_n (MVA)	P (MW)	S_n (MVA)	P (MW)	S_n (MVA)	P (MW)
G1	4	75	50	125	110	175	160	275	260
G2	4	105	80	105	80	105	80	105	80
G3	4.5	60	10	60	10	60	10	60	10
G4	40	500	60	0	0	0	0	0	0
SF	/	50	50	50	50	0	0	0	0
WT	/	312.5	250	312.5	250	312.5	250	187	150
Total Load	/	/	500	/	500	/	500	/	500
E_{kin} in MWs		20990		1190		1390		1790	

A load event was defined to test the capabilities of the controllers being considered. The worst-case scenario is the disconnection of the interconnector, which supplies 10% of the demand of the network being simulated. Therefore, the reference event is equal to the maximum capacity of the interconnector so that the behaviour of the grid frequency in the network can be investigated following a sudden disconnection from the main grid. Scenario 1 is included to serve as a comparison for the following cases (S2-S4) and to highlight the effect a disturbance of the same size would have on the frequency with an intact connection to the main grid. To achieve this, the grid was simulated with the same load during all scenarios. Since the interconnector is getting disconnected during the disturbance, there is no need to consider it before the disturbance.

4.3 Frequency Response of the network without Battery Storage System

The system response for the four different scenarios (S1 – S4) without the BSS is depicted in Figure 4.3. The black curve is the system response for a 10% generation loss (50 MW) in the network that is connected to the main grid. Due to the high system inertia, the frequency decline is slow, and the maximum frequency deviation is Δf = 0.6 Hz. The highest RoCoF is associated with the scenario S2. Scenario S2 features the highest amount of renewable energy generation and hence has the least amount of system inertia. The frequency reaches a nadir of 48.74 Hz resulting in a maximum frequency deviation of Δf = 1.26 Hz. The new steady state frequency for Scenarios S2-S4 is 49.16 Hz. The other curves refer to scenario 2 to 4 with no connection to the main grid (islanded operation). The steady state frequency deviation corresponds to the power frequency characteristic of the sub system, which is determined by the individual droop settings of the governors and amounts to 59.52 MW/Hz.

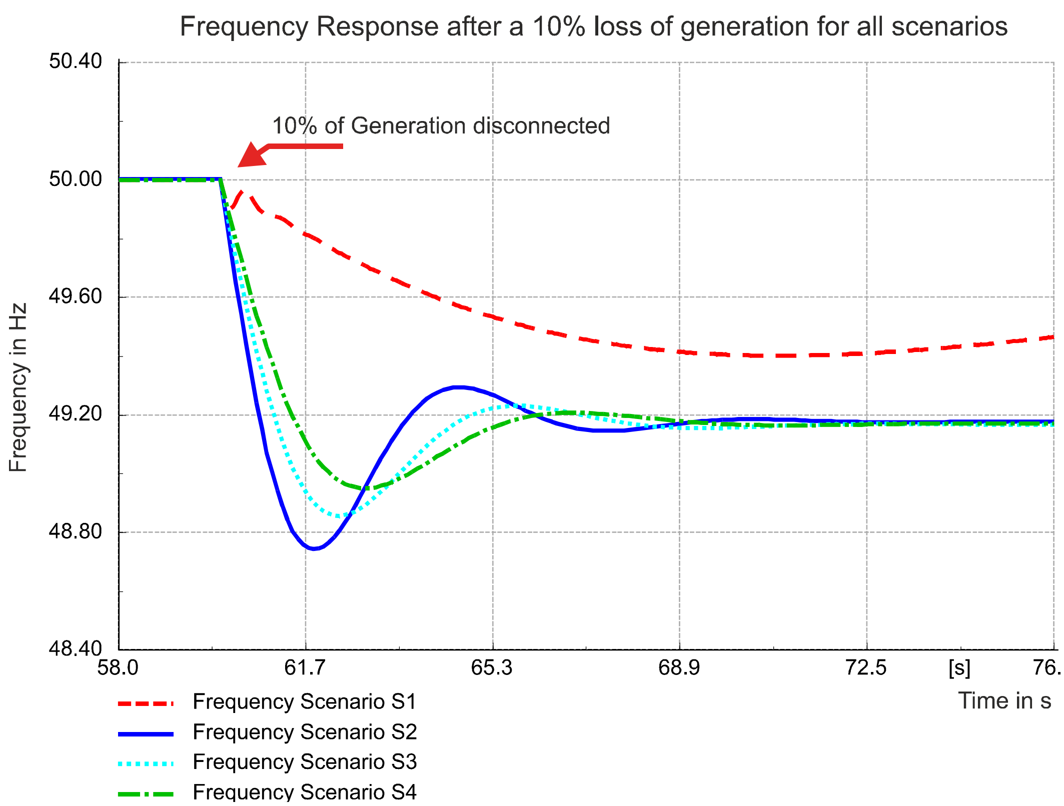

Figure 4.3: Frequency Response of the test system for the considered scenarios without the battery system

4.4 Frequency Response of the Network with Different Battery Controllers under Scenario 2

Figure 4.4 illustrates the impact of the introduced controllers on the frequency in the subsystem following the disconnection of the interconnector. All scenarios detailed in Section 4.3 were used to validate the results. Because Scenario 2 is the most severe in terms of RoCoF and maximum frequency nadir, this scenario is used to illustrate the effectiveness and the behaviour of the BSS.

It is evident that all controllers have a positive effect on the frequency nadir. Controllers C1 and C4 are seen to yield near identical results as they are fundamentally proportional controllers. The artificial inertia Controller C2 does not affect the permanent frequency deviation because it only delivers power during a change in frequency. The performance of controller C3 is slightly worse than controllers C1 and C2 because of the measurement and evaluation time needed to assess the event. Corresponding to these frequency curves are the power outputs depicted in Figure 4.5.

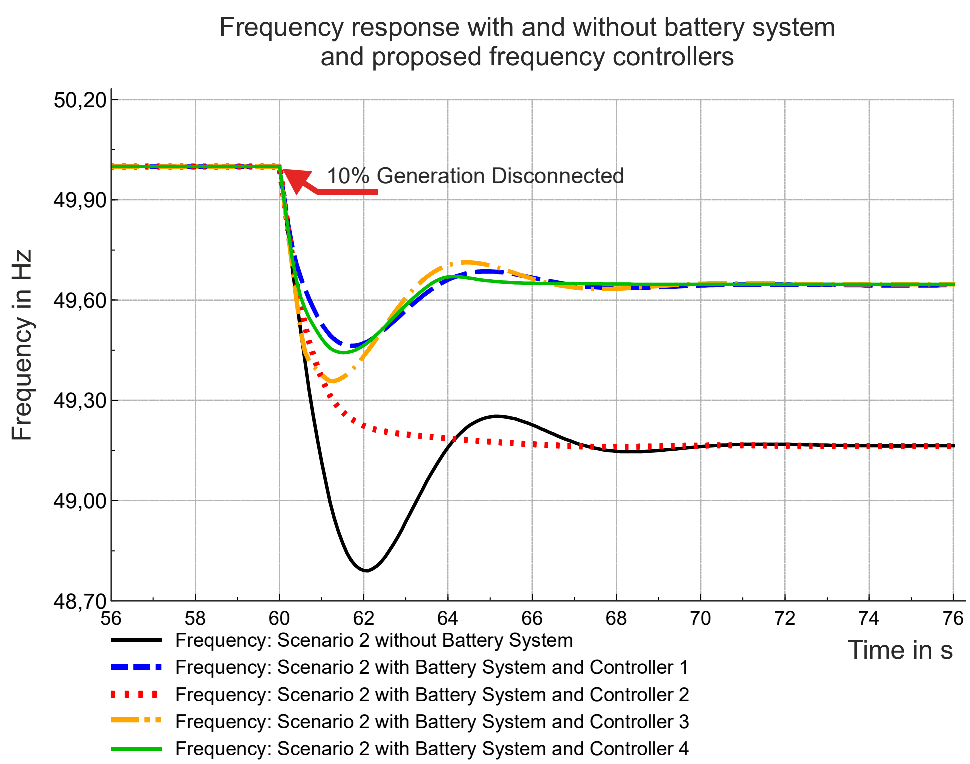

Figure 4.4: Frequency response with and without battery system and proposed frequency controllers for a loss of 10% generation

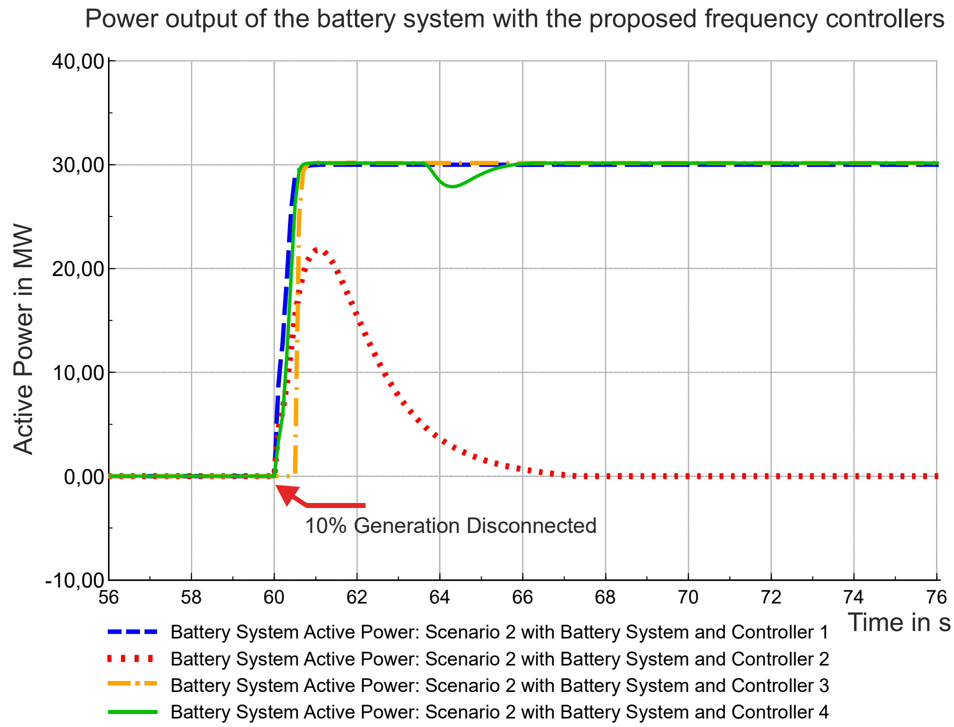

Figure 4.5: Power output of the battery system with the proposed frequency controllers

The time variation of the frequency and the power output are shown in Figure 4.6 and Figure 4.7 respectively. The major differences between the controllers are the ways how the battery storage system reduces its power output. The results show that the controllers behave in the way described in Section 3.1.2. The battery system with controller C3 can deliver a fast and predictable power output that is easily customisable for different grids. Controller C1 runs until the battery is empty (which could lead to its sudden shutdown and thus additional stress on the system) or until the frequency is restored. Controller C4 has the same advantages as Controller C3 but utilises standard control theory functions which gives the controller the capability to react to changing circumstances where C3 would follow the programmed curve. This gives controller C4 the ability to either reduce the power output alongside the frequency restoration or in a controlled way after a predefined time. With the controllers C3 and C4 it is possible to reduce the impact of a high RoCoF due to large amounts of renewable energy generation in the system and give conventional generators more time to react to the change in frequency with less energy consumption compared to Controller C1. While only one event was simulated, several frequency disturbances can occur in succession. For situations of that type, a manual adjustment of the power output of, possibly several, storage systems, is not achievable. An automated system, such as the proposed controllers C3 and C4, that adjusts to the situation is therefore favourable.

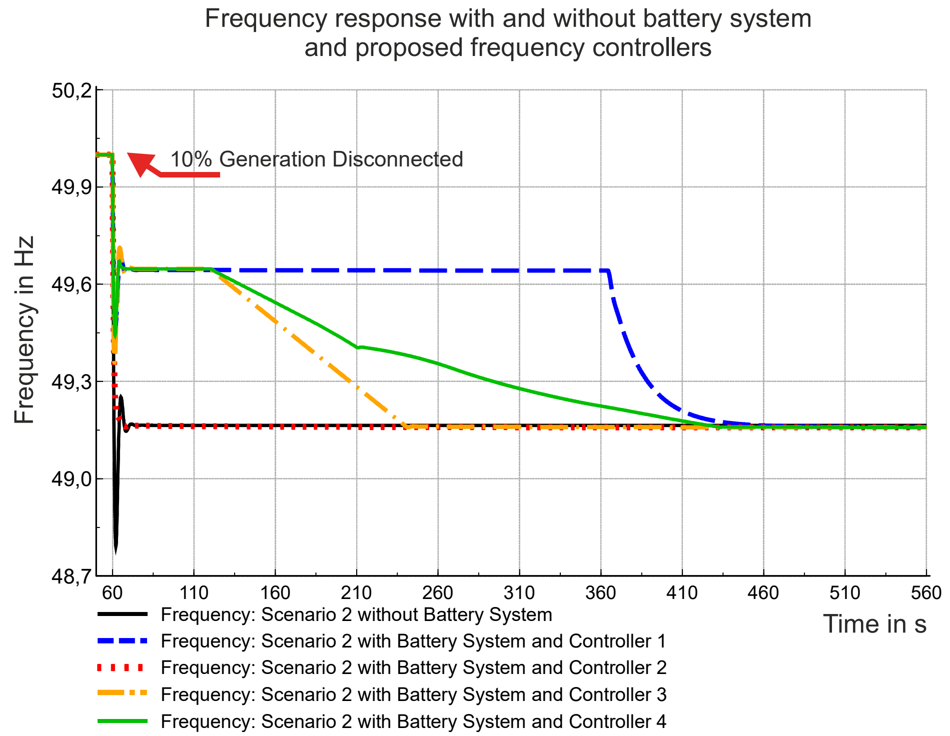

Figure 4.6: Frequency response with and without battery system and proposed frequency controllers; overview

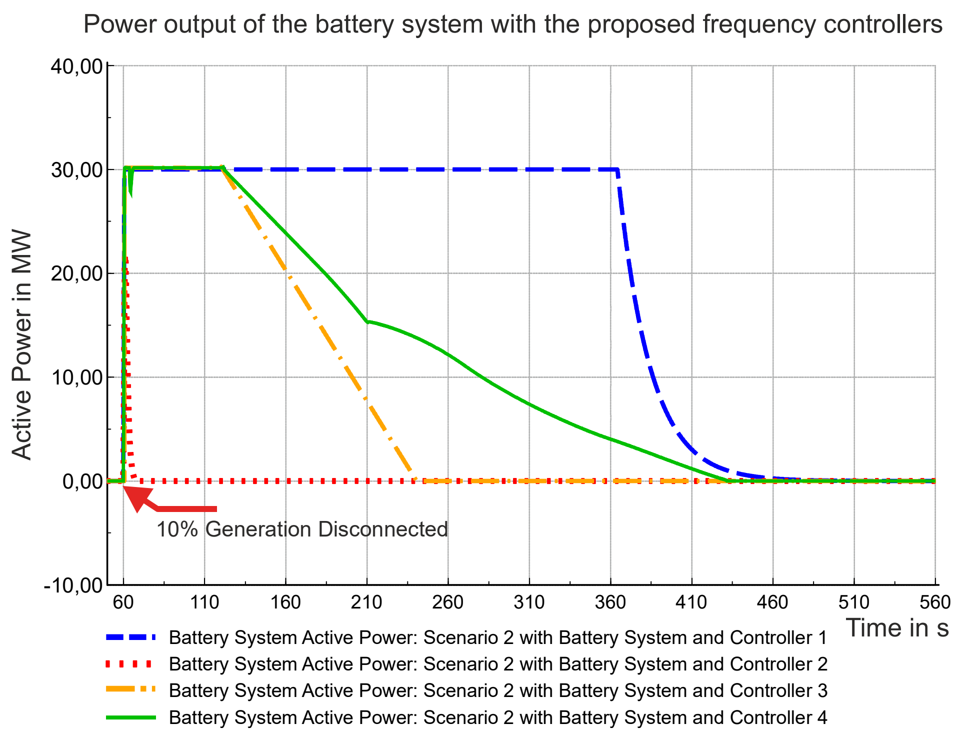

Figure 4.7: Power output of the battery system with the proposed frequency controllers; overview

4.5 Conclusion

The addition of a BSS can help mitigate the negative impacts of high rates of change of frequency following a significant grid disturbance linked to ever-increasing levels of inverter-based renewable energy sources. It could be shown that all investigated controllers have a positive impact on the frequency drop following a major disturbance. The work also highlighted the fact that a simple proportional controller can be modified to reduce the illustrated drawbacks. With the controllers C3 and C4 it is possible to reduce the impact of high RoCoF associated with large amounts of renewable energy generation in the system and give conventional generators more time to react to the change in frequency. In the process of carrying out the simulations, it became apparent that there is a high degree of influence of the controller parameters on their effectiveness. For example, simulations showed that the artificial inertia controller works better with an increased delay and aspect which will be further investigated in Chapter 6.

Chapter 5
Real Life Frequency Disturbance as Simulation Input

The aim of the chapter is to utilise a real frequency event that was experienced in Austria following a grid separation event on January 8th, 2021, and how the controllers presented in Chapter 3 associated with BSS would perform during the event. It is however recognised that the system frequency that is input to the controllers is simply what was observed following the actual network event and not the actual frequency that would be observed had the BSS was in operation. The controllers that have been used were C2, C3 and C4. To analyse the effect of a possible future scenario, where many BSS with FFR controllers might be present, the European grid was simplified, and the disturbance simulated. The size of the BSS was varied to showcase the impact of different installation stages.

5.1 Description of the Frequency Event

On January 8th, 2021, a grid separation event occurred within the ENTSO-E, splitting the Continental European grid into a North-West area and a South-West area. During this time, Austria was part of the North-West area that experienced a frequency drop. A PMU situated at TU Graz measured the event with a measurement interval of 200 ms. Figure 5.1 depicts the measured frequency in Austria during the disturbance.

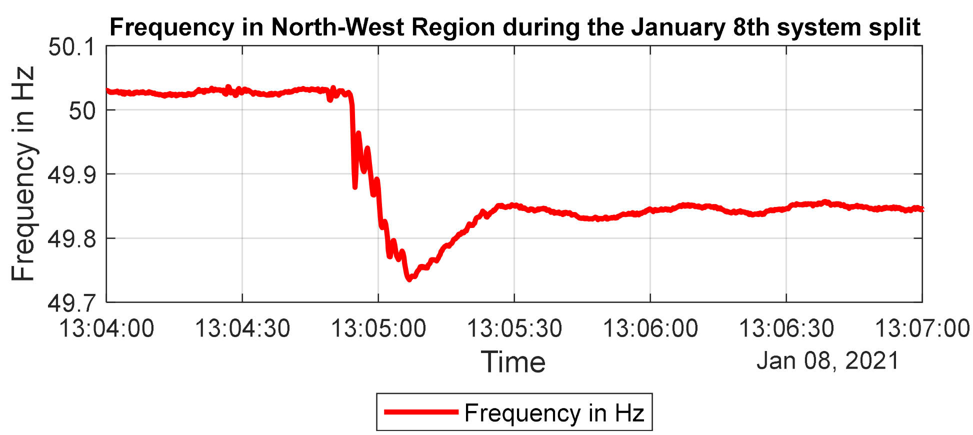

Figure 5.1: Measured Frequency during the January 8th, 2021, system split disturbance in Austria

During this event, the frequency dropped to a nadir of 49.74 Hz and reached a steady state frequency of 49.84 Hz. According to an ENTSO-E report on the event ,1.7 GW of loads had to be interrupted according to a load shedding scheme in France and Italy. Additionally, 420 MW of FCR was activated during this period [98]. The initial RoCoF after 0.5 seconds was -0.226 Hz/s.

5.2 Methodology Employed to Examine the Behaviour of Controllers Associated with BSS using a Measured Signal

The measured frequency was utilised as an input to the controllers to investigate the reaction of a BSS while the different controllers are active. The simulation setup includes the controllers only without the BSS as depicted in Figure 5.2 where measurement file represents the recorded network frequency in the form of an ASCII file.

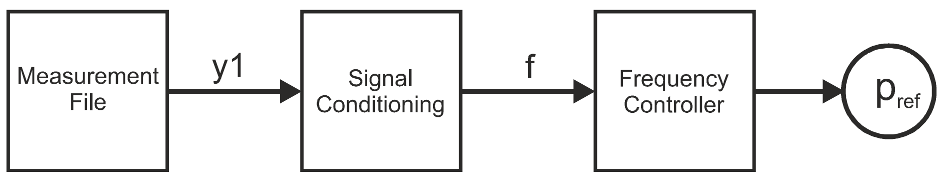

Figure 5.2: Simulation setup for the usage of a measurement file as input for the frequency controller

The signal conditioning module provides a starting value for the frequency at f(t=0) = 1 pu so that the program can initialise the simulation with a starting value. After the simulation is started, the measured signal is the output of the signal conditioning block

(f(t>0) = y1). The output f is the frequency that is used as an input for the frequency controllers. The final output p_{ref} is the active power reference for the PQ controller and BSS as described in Section 3.1.1 covering the Battery Model that can be implemented for frequency management.

In the simulations undertaken, the active power reference value was integrated to establish an estimate of the energy usage. Since the power output is a pu quantity, the resulting energy will be shown in pu·h which can be converted to establish the actual energy using the rated power S_r of the BSS.

The input data includes approximately 60 seconds of measurements before the actual event occurred.

Employing this form of simulation yields the results of a small BSS that would have been connected during the event. A single small BSS would not have a measurable effect on the frequency response of the European grid. Therefore, the results of this setup show only the reaction of the BSS.

5.3 Results for the Controllers using a Measured Input Signal

5.3.1 Results for Controller C1

As a result of the short active time, the results associated with controller C1 (Section 3.1.2.1) would essentially be the same as with controller C4 (Section 3.1.2.5) and hence the detailed results are presented in Section 5.3.4 that covers the controller C4. The active time of the BSS is the time where the BSS has a non-zero power output.

5.3.2 Results for Controller C2

The improved controller C2.2 (Section 3.1.2.3) was used in this investigation and will be called. The advantage of supplying artificial inertia with a BSS, is that it's possible to emulate a much higher acceleration time constant. For this simulation, the values in Table 5.1 were applied to the controller using a T_J of 250 s. Higher values for T_J also work better with generally lower RoCoF in the European system, otherwise the output would be negligible.

Table 5.1: Parameters of the controller C2 used during the simulation with measurements

Parameter	Description	Value
T_f	Filter time constant in s	0.5
K_d	Differentiator gain	-1
db	Deadband to avoid activation for small RoCoF in s	0.001
T_J	Proportional gain; equivalent to acc. time constant in s	250

Figure 5.3 shows the response of the artificial inertia controller C2.2 and the frequency during the first 100 seconds after the separation event. It is clearly visible that the highest output (P_{ref}) occurs during the first downswing of the frequency. Most importantly, caused by the oscillations in the frequency, the controller is seen to demonstrate a damping effect. The small oscillations in frequency at the end of the frequency containment process are too small and as a result the controller does not demand any power output. Figure 5.4 illustrates the corresponding energy associated with the BSS. During the controller active period, the supplied energy by BSS is seen to be positive thus leading to the conclusion that the BSS has a positive impact on the RoCoF.

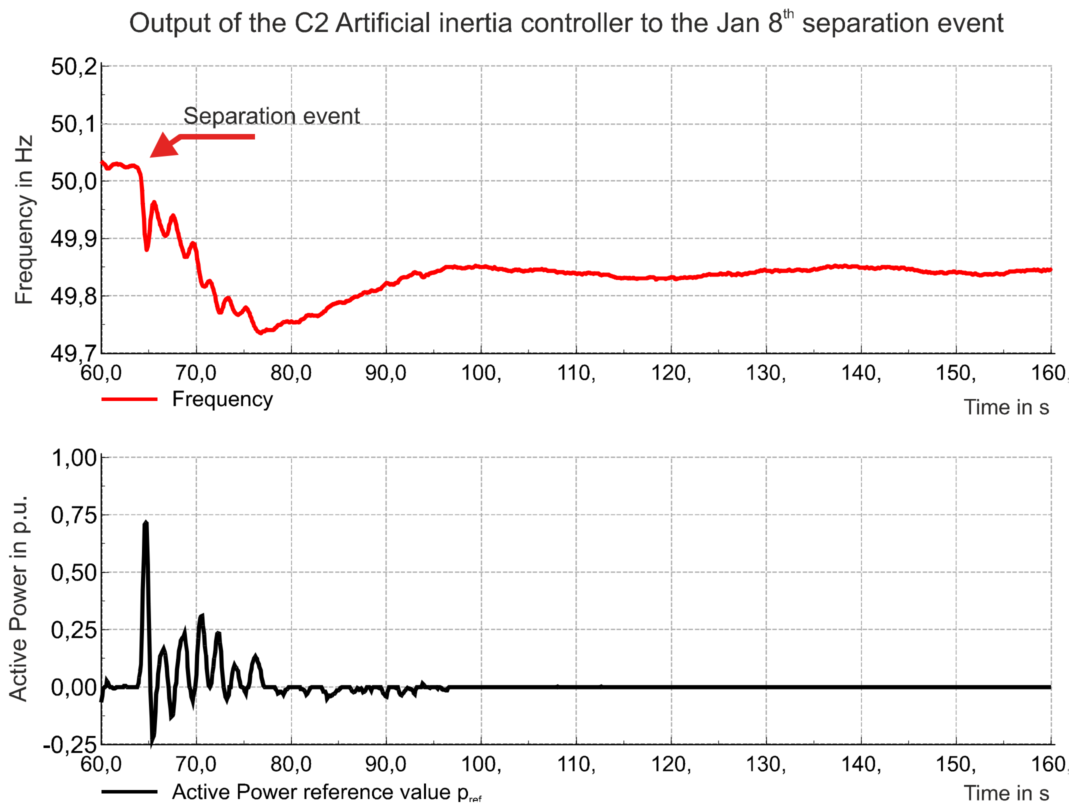

Figure 5.3: Active power signal of the artificial inertia controller for the January 8th separation event

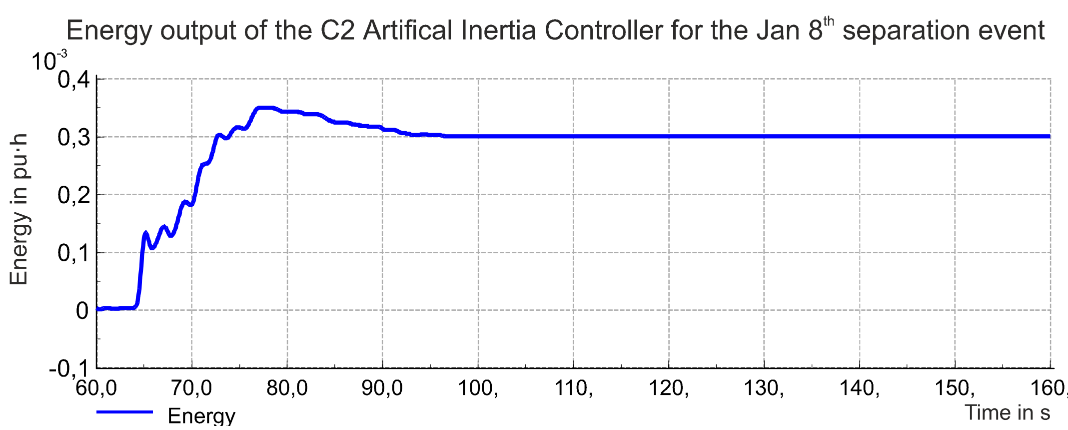

Figure 5.4: Energy output of the C2 Artificial Inertia controller for the January 8th separation event

5.3.3 Results of Controller C3

The parameters of the controller C3 were adjusted to account for the lower RoCoF values and higher frequency nadirs generally observed in the European grid. As a result of the lower RoCoF, the sampling window was increased to 1 s. Table 5.2 gives the parameters of controller C3 used in the simulations undertaken.

Table 5.2: Parameters of the controller C3 used during the simulation for the January 8th separation event

Parameter	Description	Value
T_f	Filter time constant in s	0
K_d	Differentiator gain	-30
db	Deadband to avoid activation for small RoCoF in pu	0.0012
T_i	Integrator gain	0.002
T_{Delay}	Sampling time in s	1
T_{hold}	Minimum active time in s	60
k_1	Negative gradient limiter; positive path in pu/s	-0.1
k_2	Positive gradient limiter; negative path in pu/s	0.1

The results shown in Figure 5.5 indicate that the frequency oscillations observed before the commencement of the actual event does not cause a false activation. The active time was set to hold the power output for 60 s and a drooped shut down period with 0.1 pu/s can be seen at 124 s.

The RoCoF in the first second is much more severe than the total RoCoF over the period until the frequency nadir. This leads to a power output of 0.467 pu until the shut off. The energy output is shown in Figure 5.6. A constant power output naturally leads to a constantly rising energy output.

The key positive effect of the event-based controller is the fast activation of additional active power through the estimation of the severity of the event right at the beginning of the frequency change. This would help to decrease the RoCoF and the maximum frequency deviation.

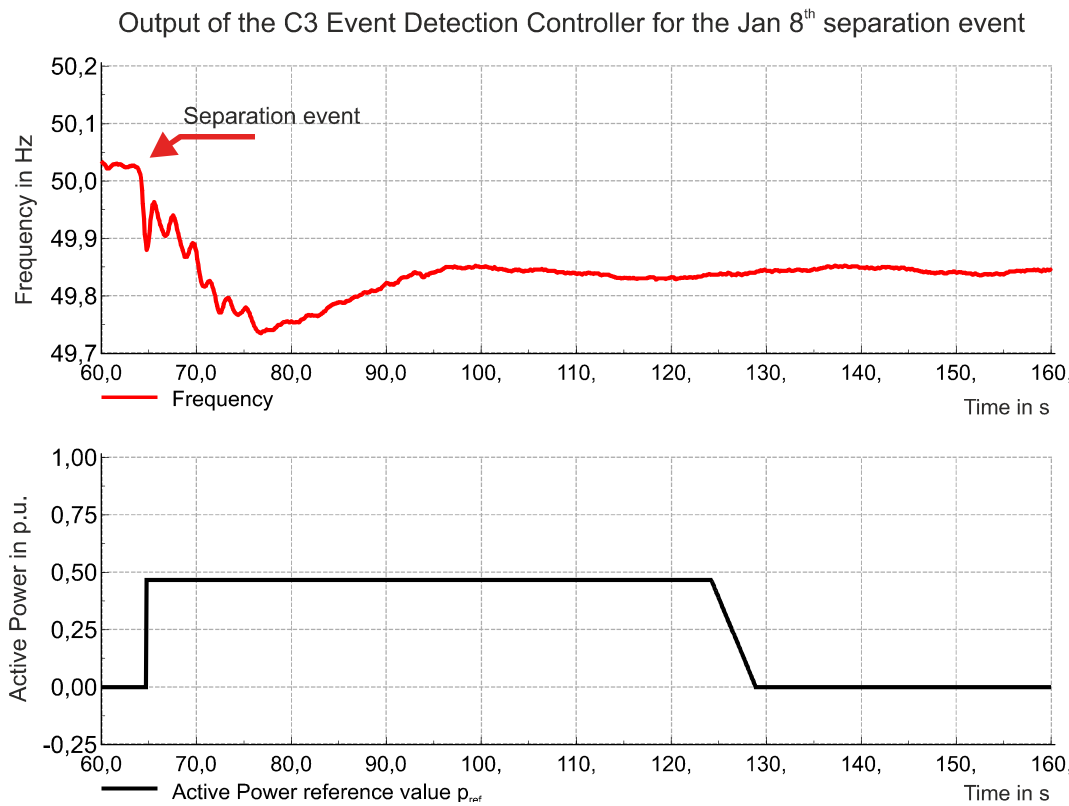

Figure 5.5: Active power signal of the C3 event detection controller for the January 8th separation event

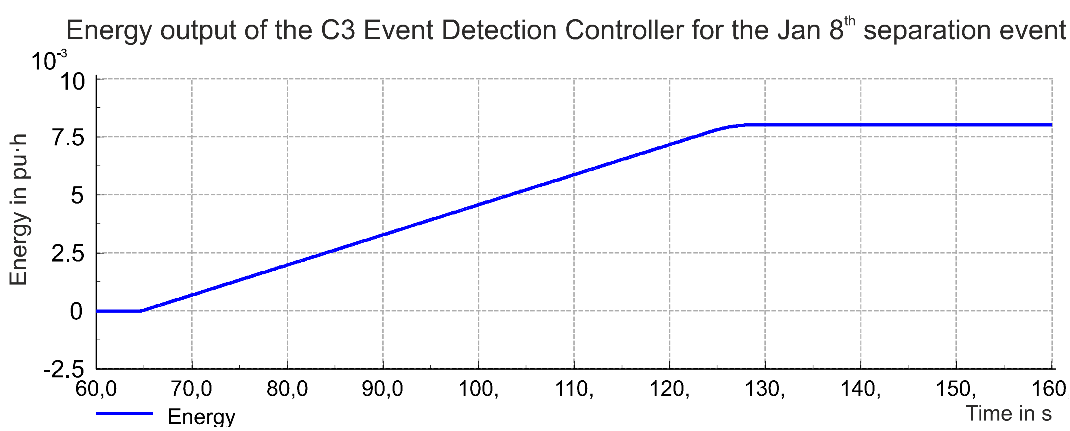

Figure 5.6 Energy output of the C3 Event Detection controller for the January 8th separation event

5.3.4 Results of Controller C4

The simulations with this controller were carried out with two different settings for the gain. A gain with K = 50 leads to a maximum power output at a 1 Hz frequency deviation as it was used for the simulations in Section 4.4. The setting of K = 500 leads to a maximum power output with a 0.1 Hz frequency deviation as pictured in Figure 3.1. The output for both starts when the frequency reaches 49.8 Hz. The other parameters are summarised in Table 5.3

Table 5.3: Parameters of the event detection controller C4 during the simulation for the January 8th separation event

Parameter	Description	Value
T1	Waiting period before sample window in s	90
T2	Sample window length in s	120
db1	Deadband to avoid activation for small frequency deviations in pu	0.0001
db2	Deadband to set activation limits to ±200 mHz in pu	0.004
K	Proportional gain	50 500

Figure 5.7 shows the results for both simulations. The full curve represents the results with a gain of K = 500 and the dashed line shows the result for K = 50. Because the frequency does not drop far below the threshold of 49.8 Hz, the power output with an area of operation to 49 Hz is nearly negligible. The simulation with K = 500 results in an output that can have an effect on the frequency. Compared with the event-based detection, the output occurs much later, during a time were FCR was already starting to stabilise the frequency. The active time was below the holding period, therefore was the automatic output reduction not necessary.

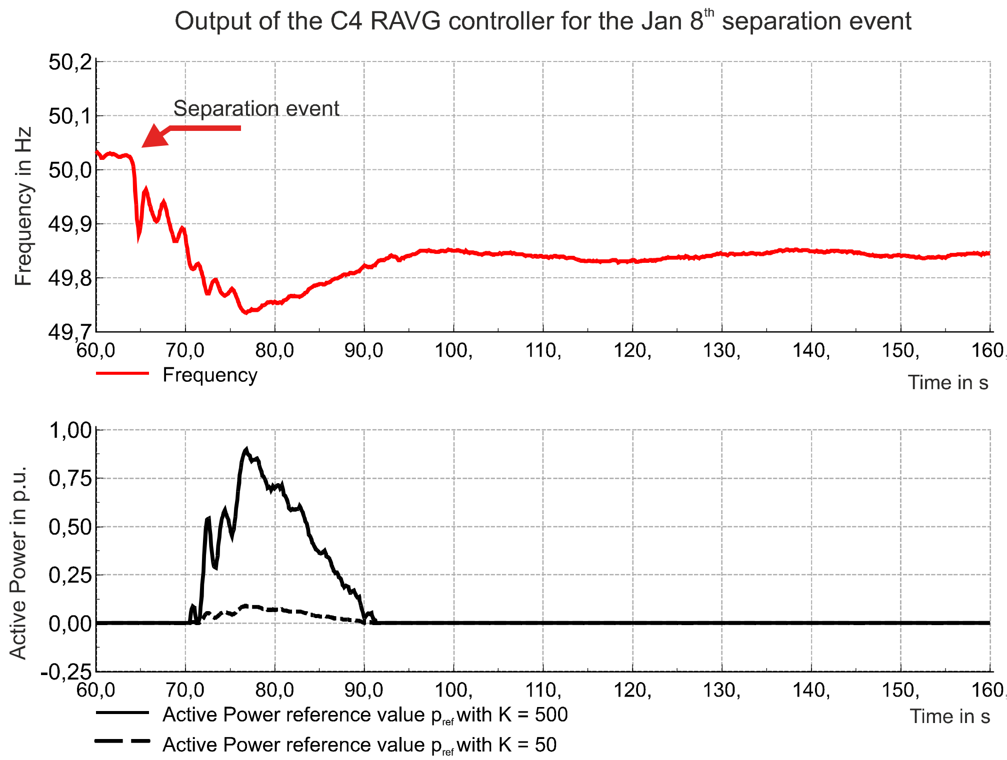

Figure 5.7: Active power signal of the C4 RAVG controller for the January 8th separation event

The energy consumption during the event is depicted in Figure 5.8 for both gains. Because the power output of the BSS is much higher for a gain of K = 500, the energy demand is also higher.

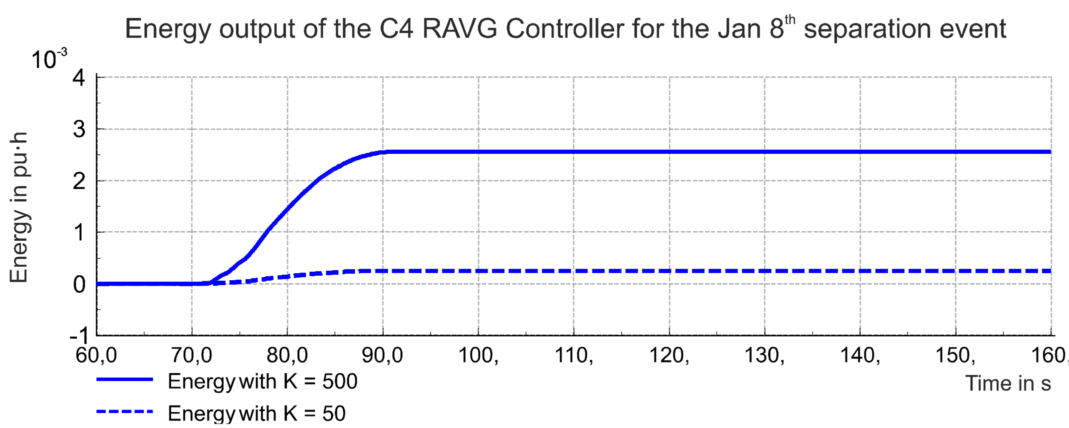

Figure 5.8: Energy output of the C4 RAVG controller for the January 8th separation event

5.4 Methodology Employed to Examine the Behaviour of Controllers Associated with BSS using a Simulation Model for the Disturbance

To examine the effect, the BSS would have had on the disturbance, the affected grid was modelled in DIgSILENT PowerFactory employing a simplified single busbar approach. Two SGs, two loads and one BSS were used during the simulation. The total load before the disturbance was 326 GW. The disturbance caused total of 5650 MW of missing generation in the north-western region. The acceleration time constant H was identified as H = 4.5 s (rated to rated apparent power of the generator S_{gn}).

The simulation model consists of one unresponsive generator and one generator participating in FCR. The generator participating in FCR is equipped with a governor. The modelling of the grid was approached by first estimating a value for the acceleration time constant and then improving the value towards a comparable response during the first second. The second step was to adjust the governor parameters. The parameters utilised for this where the controller time constant and the droop.

The loads were split in a base load and a load representing the combined load shedding in Italy, France, Great Britain, and Denmark. These combined loads of 2300 MW were gradually reduced over a period of three seconds, starting at two seconds after the disturbance.

The modelled frequency response of the disturbance in comparison with the measured signal is illustrated in Figure 5.9. The approximation with the described generator setup and the included load shedding compares very well with the measured signal. Oscillations are not present since it is a simplified setup with an aggregated load shedding instead of induvial loads that would disconnect rapidly.

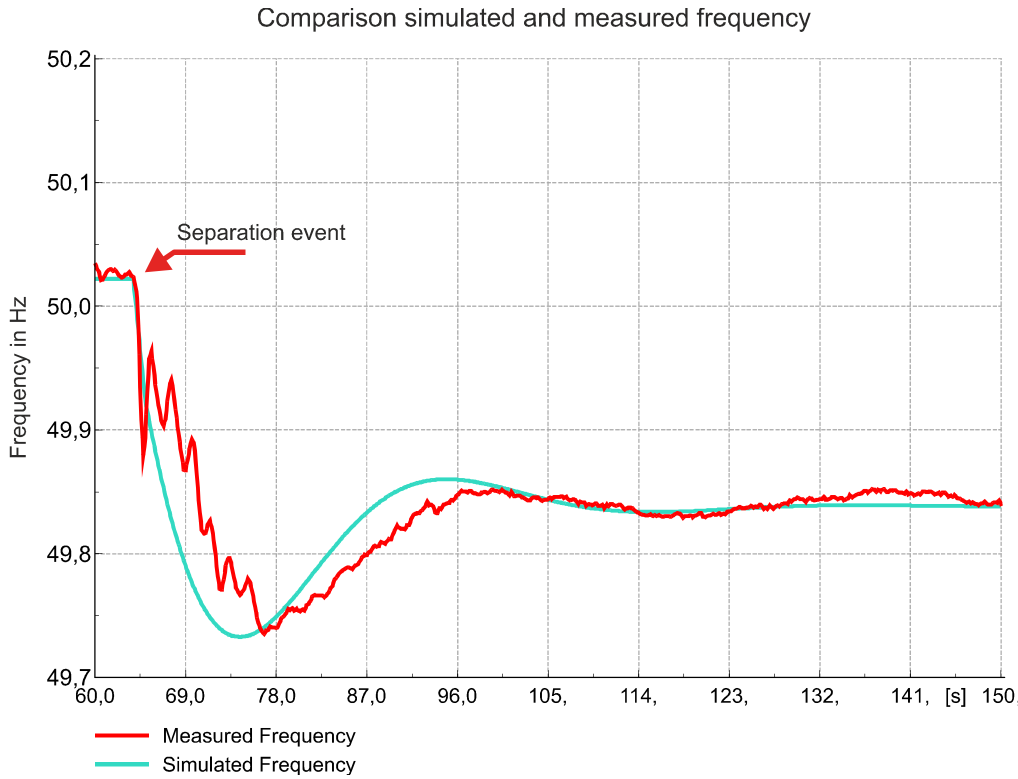

Figure 5.9: Modelled and measured frequency response

The battery size was varied with the intention to simulate three different stages of BSS adoption in the system. Based on the findings in Chapter 2, a BSS with a rated power of 100 MW has been installed in grids and analysis can be found based on this size. For first development stage it was assumed that five BSS will be installed. This results in a totally installed power of 500 MVA. The second stage is a widespread adoption of, for example 25 large, BSS installed throughout the whole system. This yields a totally installed power of 2500 MVA. The last stage is possible scenario where BSS are widely used and 5000 MVA of BSS are present in the system. Another valid future scenario that small BSS (S_n < 10 MW) will be installed throughout the system and participate in FFR. To summarise:

- First stage: 500 MW of installed BSS, referred to as BSS1
- Second stage: 2500 MW of installed BSS, referred to as BSS2
- Third stage: 5000 MW of installed BSS, referred to as BSS3

The same controllers as in Section 5.3 were considered during the simulations. Furthermore, the same controller settings were employed. These controllers are the Artificial Inertia Controller C2 (Section 3.1.2.3), the Event Detection Controller C3 (Section 3.1.2.4) and the Rolling Average Set Point Controller C4 (Section 3.1.2.5).

5.5 Results for the controllers using the simulated disturbance

The results feature the frequency response and the power output of the BSS for each controller and for the three stages of installed BSS.

5.5.1 Results for Controller C2

The resulting frequency response utilising the Artificial Inertia Controller C2 is depicted in Figure 5.10. The effects on the frequency are small for all considered implementation scenarios. The reason for that, is that the frequency is not deteriorating with a high RoCoF. The initial RoCoF during this simulated disturbance was 0.0827 Hz/s. To achieve a higher participation, a higher gain would be necessary but could cause unwanted oscillations. The power output depicted in Figure 5.11 shows that the BSS is not utilised to the full extend.

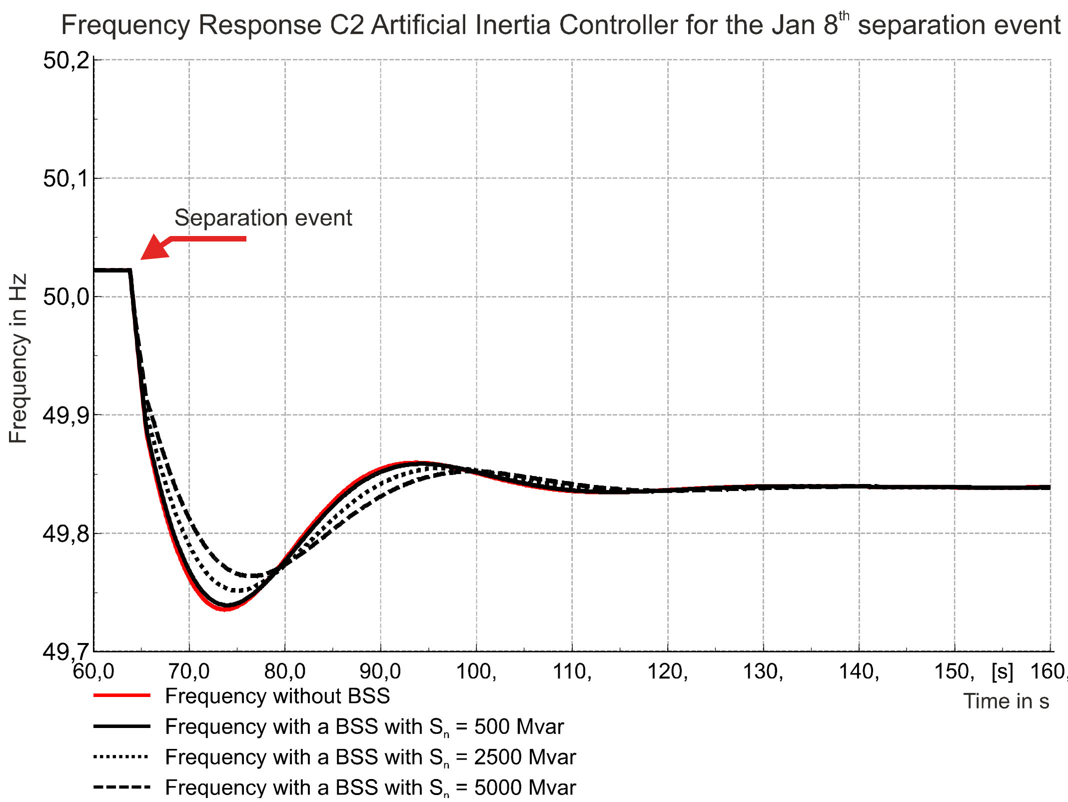

Figure 5.10: Variation of the frequency response over time for the three scenarios

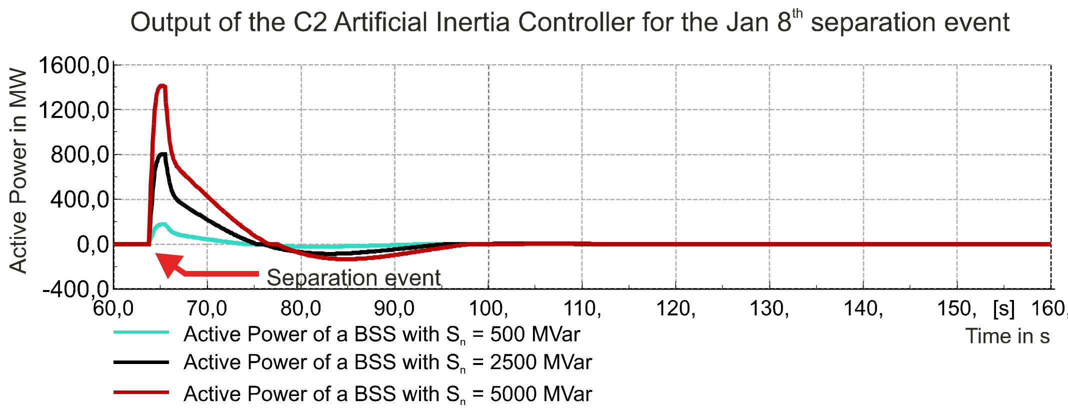

Figure 5.11: Variation of the power output of the BSS over time for the three scenarios

5.5.2 Results for Controller C3

The event was correctly assessed by the controller and a power output of 40% of the nominal power was activated after the sampling time of one second. The frequency response is shown in Figure 5.12. The controller is active for 60 seconds before the output gradually decreases. The controller starts to decrease the power output after 60 seconds of active time. The deactivation is drawn out to limit the impact on the frequency. It can be argued that a higher activation is possible with different controller settings to assess the event. This holds value if there is not a widespread installation of BSS with an Event Detection Controller. It is important to consider, that since the power output is calculated and employed at the beginning of the disturbance, an overactivation is a possibility. BSS3 nearly manages to bring the frequency back to the nominal frequency before the controlled shut-down process begins.

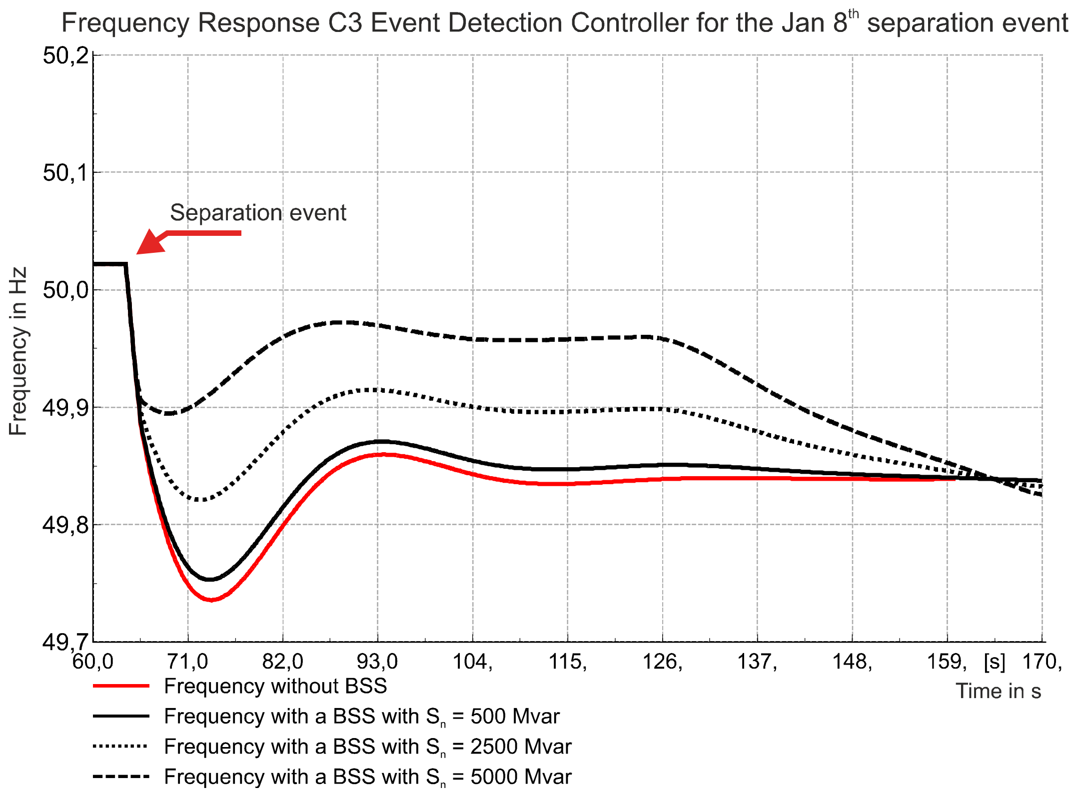

Figure 5.12: Variation of the frequency response over time for the three scenarios

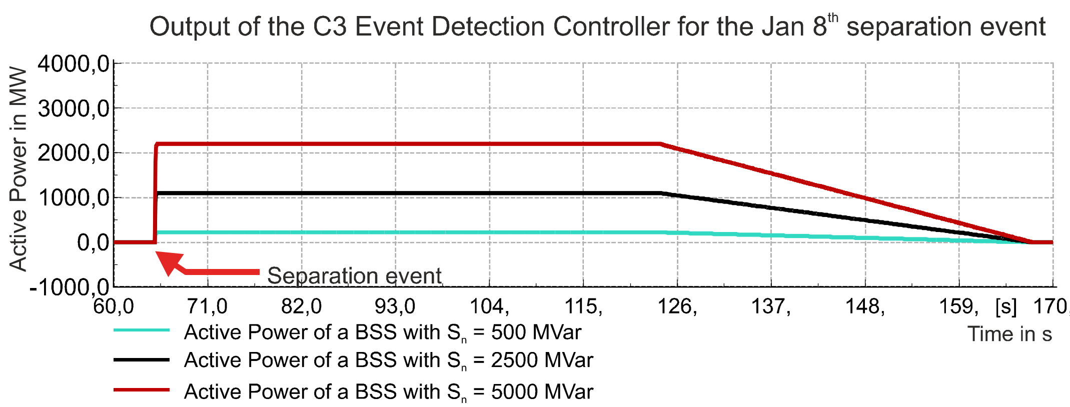

Figure 5.13: Variation of the power output of the BSS over time for the three scenarios

5.5.3 Results for Controller C4

As stated in Section 5.3.4, the controller with the intended limits for FFR and a gain of K = 50 (which yields a maximum power output at Δf = 1 Hz) has a limited effectiveness. This observation can be confirmed with the results from this simulation. In Figure 5.14, the frequency responses for the three tested scenarios are shown. It is evident, that the effect on the frequency of even the largest installation stage is marginal. Because the controller is set up with the intended activation limits from Figure 2.10, the controller is only active below 49.8 Hz. The corresponding power output is shown in Figure 5.15. BSS1 utilises the most of the available power capabilities. The difference between BSS2 and BSS3 is minimal, especially considering that BSS3 has twice the power capabilities than BSS2.

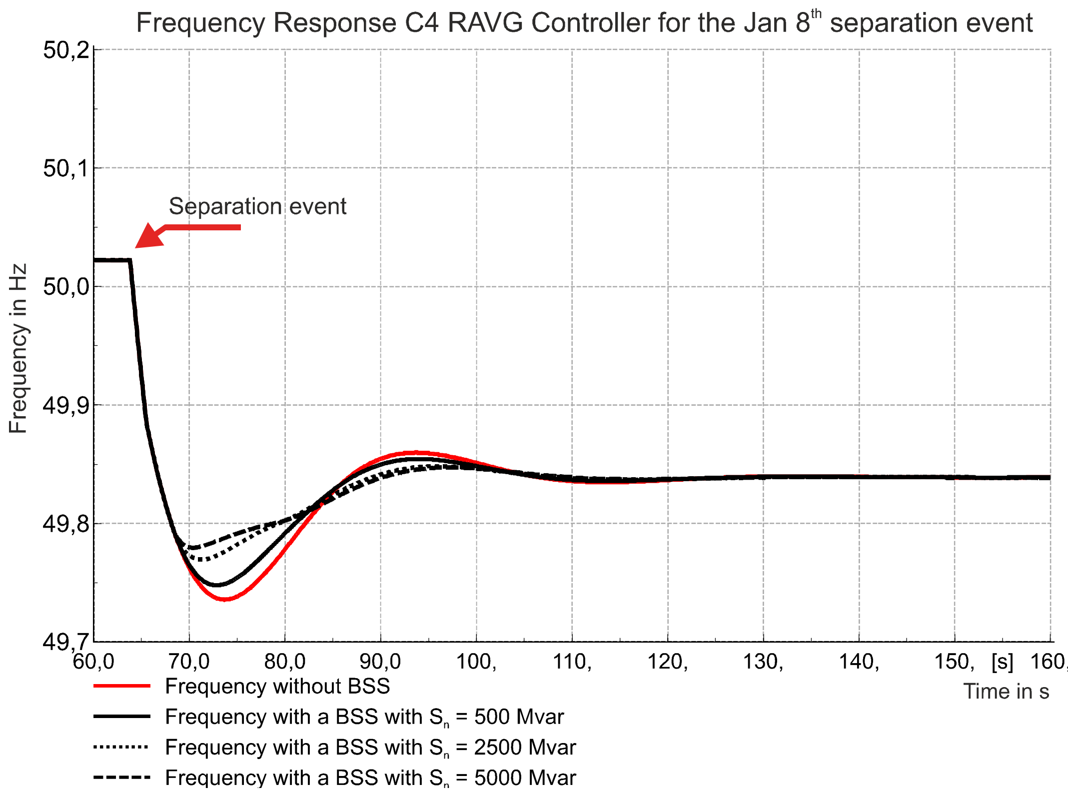

Figure 5.14: Variation of the frequency response over time for the three scenarios

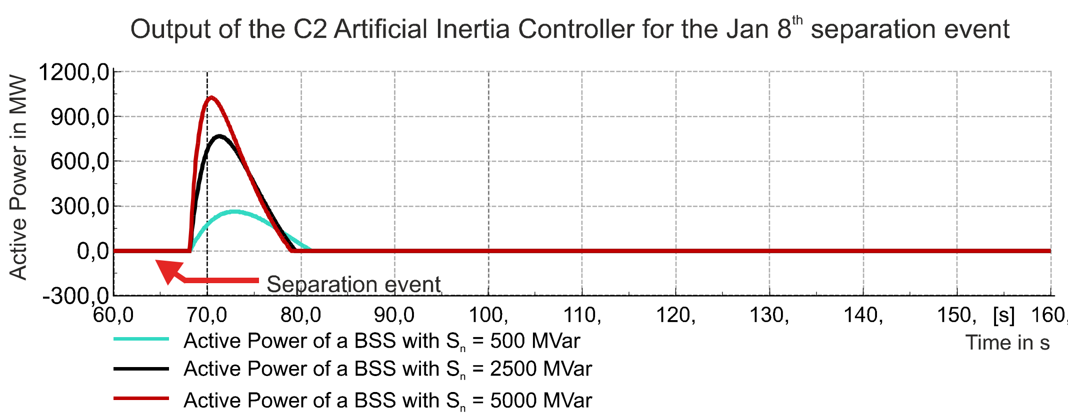

Figure 5.15: Variation of the power output of the BSS over time for the three scenarios

From this observation can be concluded, that for Controller 4, the thresholds for FFR are not suitable for a large interconnected system with higher levels of inertia and a strong FCR response that is capable of handling large disturbances. The aim of the controller could be optimised to avoid the disconnection of loads at 49.8 Hz. The threshold for activation can be lowered to 49.95 Hz, so that the BSS activates at the same threshold as the FCR. Additionally, the gain can be increased to achieve a full activation for smaller frequency deviations. Figure 5.16 illustrates the results for the controller C4 using these improved settings. The improvement is clearly visible when compared to the results depicted in Figure 5.14. BSS1 reduced the frequency nadir to 49.774 Hz. BSS2 and BSS3 were able to reduce the frequency nadir to 49.871 Hz and 49.9 Hz respectively.

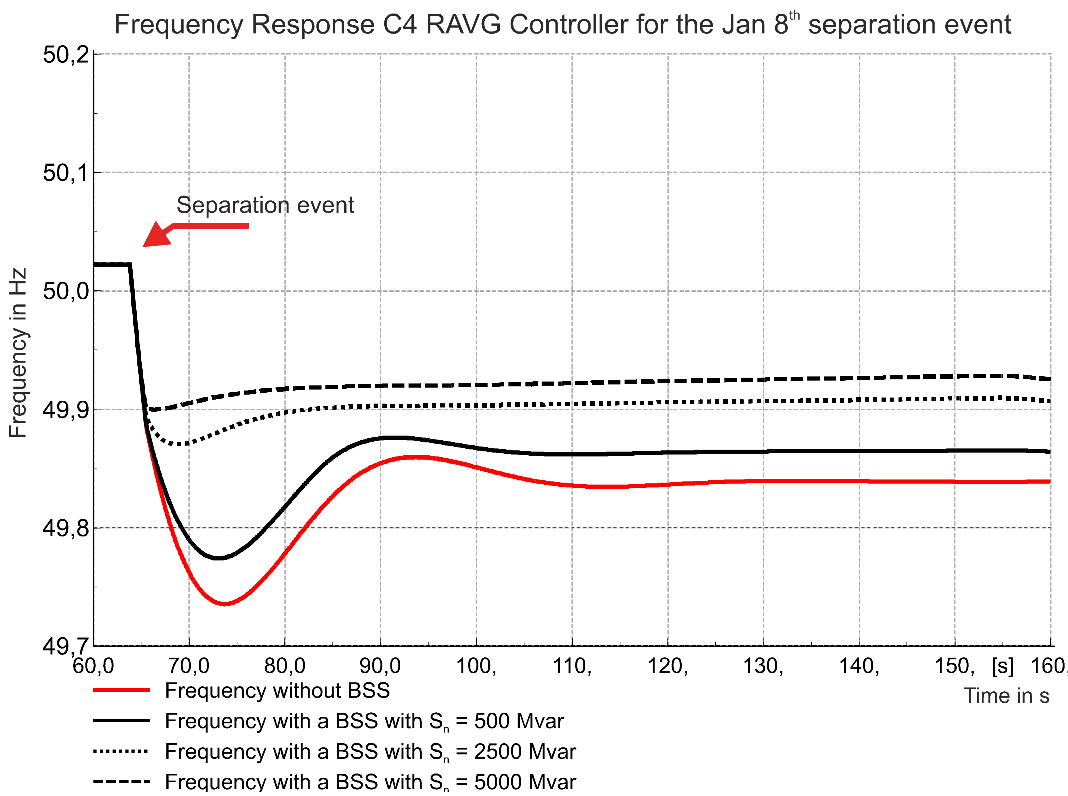

Figure 5.16: Variation of the frequency response over time for the three scenarios

Regarding the power output shown in Figure 5.17 can be said, that the increase in rated power between BSS2 and BSS3 is not utilised. The effects on the frequency are only minimally different and BSS2 peaks with 1994 MW whereas BSS3 peaks with 2521 MW. The output of BSS1 reaches the active power limit of 500 MW.

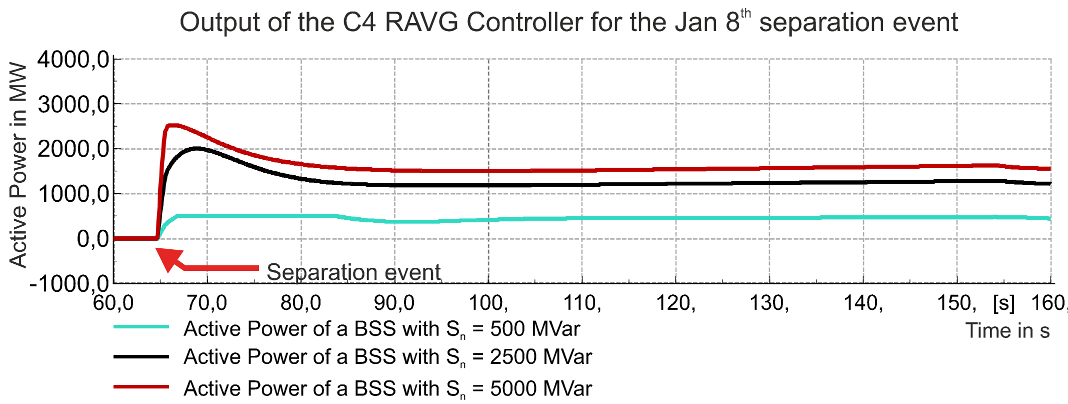

Figure 5.17: Variation of the power output of the BSS over time for the three scenarios

5.5.4 Comparison of Results

To compare the controllers, the results for BSS2 (S_n = 2500 Mvar) were considered. The best result was achieved using the Rolling Average Set Point Controller C4 with the optimised settings. This was followed by the Event Detection Controller C3 and then the Controller C4 with the originally intended limits for FFR. The least impact had the Artificial Inertia Controller C2. Controller C4 also manages to provide additional damping whereas C3 only provides a constant power output during that time.

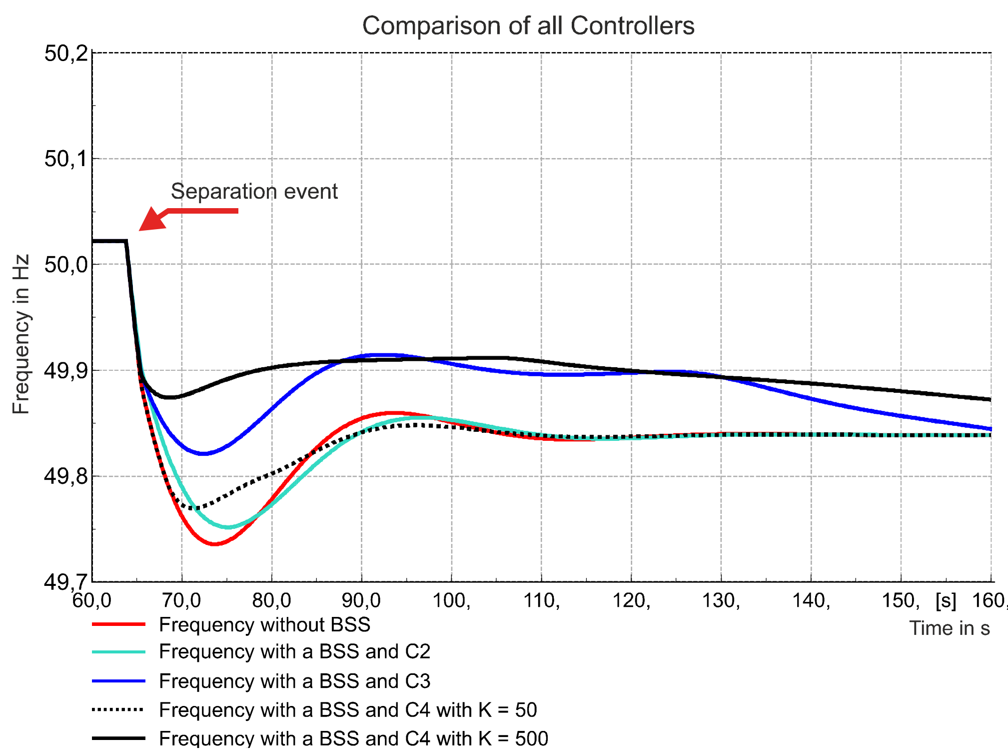

Figure 5.18: Variation of the frequency response over time for the controllers

The energy used during the disturbance is depicted in Figure 5.19. The highest impact controllers also used the highest amount of energy. Generally, only a fraction of the available energy storage was used for all controllers. The controllers C2 and C4, with not optimised settings, used a very low amount of energy but C4 achieved better results concerning the frequency deviation. From the energy consumption can be concluded that a possible implementation strategy could be to use the implementation of these two controllers for converter-based generators and the addition of a small storage capacity. Controllers C3 and C4 with optimised settings can then be used in dedicated BSS that are installed for the purpose of providing grid services. The most important factor is parametrisation of the controller and generally the installed power.

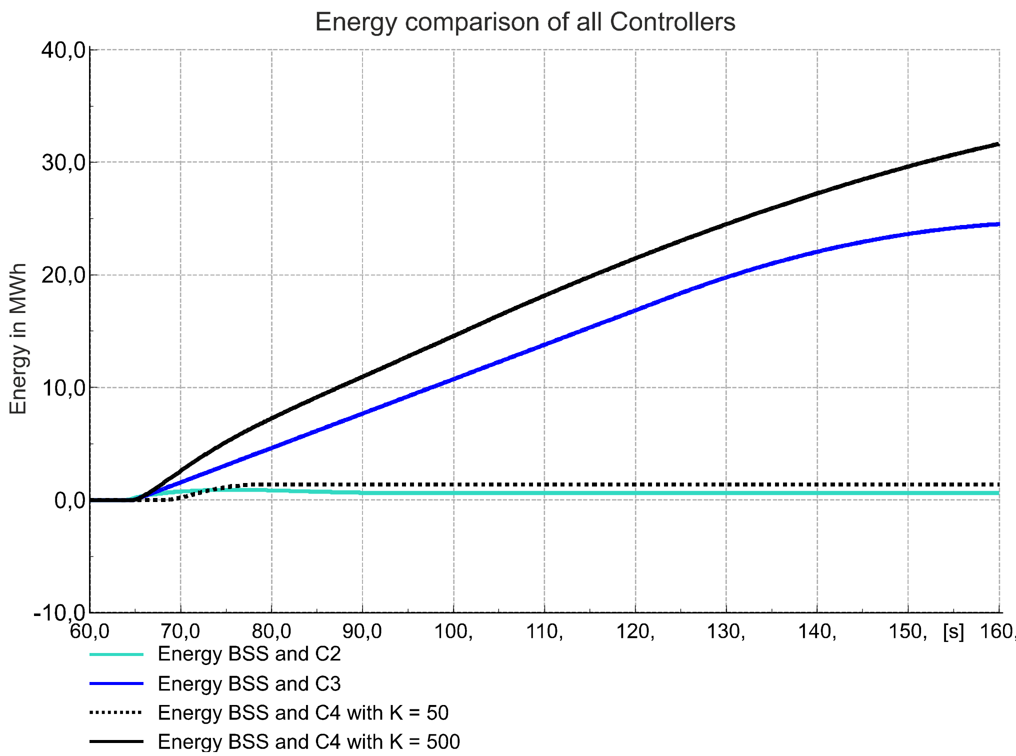

Figure 5.19: Variation of the energy over time

5.6 Conclusion

This chapter demonstrated how a BSS with the proposed frequency controllers would have reacted in a grid with higher levels of inertia than in the test case showcased in Section 4.2 and for a real measured disturbance. Two approaches were used to analyse the European grid separation event from January 8th, 2021. The first approach was to use a measured signal from the event and use it as an input for the proposed controllers. This was an investigation into how the reaction of a BSS would have been, had it been connected to the grid at the time of the event. The upside to this approach is that the controllers can be tested with a real signal that also includes oscillations. The downside is that the effect on the frequency cannot be determined. A key finding was that the controllers work for a real-life measurement of the frequency.

The second approach was to model the separation event in DIgSILENT PowerFactory and use the controllers with varying sizes of BSS to study the efficacy of the different controllers and study the impact of varying installation stages.

Overall, the results indicate that, Controller C3 and C4 are suitable to assist in the event of a disturbance in the Central European Grid. Controller C2 had only a minimal effect on the frequency. Because of the definition of FFR and the resulting activation thresholds, the Rolling Average Set-Point controller C4 activates too late. To fully utilise the BSS with controller C4 under these conditions, the intended threshold for activation must be lowered to achieve a beneficial effect on the frequency. The event-based controller is able to activate earlier because it is estimating the event right at the beginning of the frequency change. Another important aspect is that the reaction of the controllers can be seen where the measured frequency experiences oscillations. In this regard, the event-based controller can distinguish the actual event in comparison to noise.

Finally, the largest tested BSS size did not significantly influence the outcome when compared to an intermediately sized BSS.

Chapter 6

Network and Battery Energy Storage System Performance Sensitivity to Controller Parameter Variations

It is important to examine the sensitivity of the network and battery energy storage system performance in relation to frequency to parameters of the controllers implemented. With DIgSILENT PowerFactory it is possible to run external scripts and automate the various steps in the simulation. The simulation setup described in Chapter 4 is used for this purpose where the scenario with 50% penetration of renewable energy (Scenario 2) was chosen in the study as it has the studied disturbance has the most severe effect on the frequency during this scenario. Controllers considered during this parameter study were the Artificial Inertia Controller C2.2, the Event Detection Controller C3 and the Rolling Average Set-Point Controller C4.

6.1 Artificial Inertia Controller C2.2

The filter time constant of the artificial inertia controller C2.2 was varied in the range 0 s to 4.99 s in 0.01 s steps resulting in 500 simulations. The parameters of the controller given in Table 6.1 apply to the simulations.

Table 6.1: Parameters of the artificial inertia controller C2.2 for the filter time variation

Parameter	Description	Value
T_f	Filter time constant in s	**0 to 4.99**
K_d	Differentiator gain	-1
db	Deadband to avoid activation for small RoCoF, in pu	0.002
T_J	Proportional gain; equivalent to acc. time constant	120

Figure 6.1 and Figure 6.2 illustrate the frequency variation with time observed with smaller time constants in red and the larger time constants in cyan. The result with the lowest frequency nadir is shown in black. It is evident that the smallest fastest filter time constant does not yield the best result in terms of limiting the nadir. The best result was achieved in the range of 1.3 s ≤ T_f ≤ 1.61 s. This leads to the conclusion that a faster controller is not necessarily better. This can be explained using how governors of power

plants with SGs react. These governors contain a proportional controller with a droop characteristic that needs a frequency deviation to change the power output. If the BSS activates very quickly with a large power output when the measured frequency deviation is lower, a small power output will be outcome with the synchronous generator. A slightly delayed power output of the BSS enables governors of synchronous generators to pick up a higher frequency deviation at first with the BSS coming in to play with a delay leads to a better overall result. A higher filter time constant is also suboptimal because it dampens the output too heavily. As evident from Figure 6.1, the results for smaller filter time constants are better compared to those with larger filter time constants but very fast filter times yield a delayed and lower frequency nadir then values around T_f = 1.3 s.

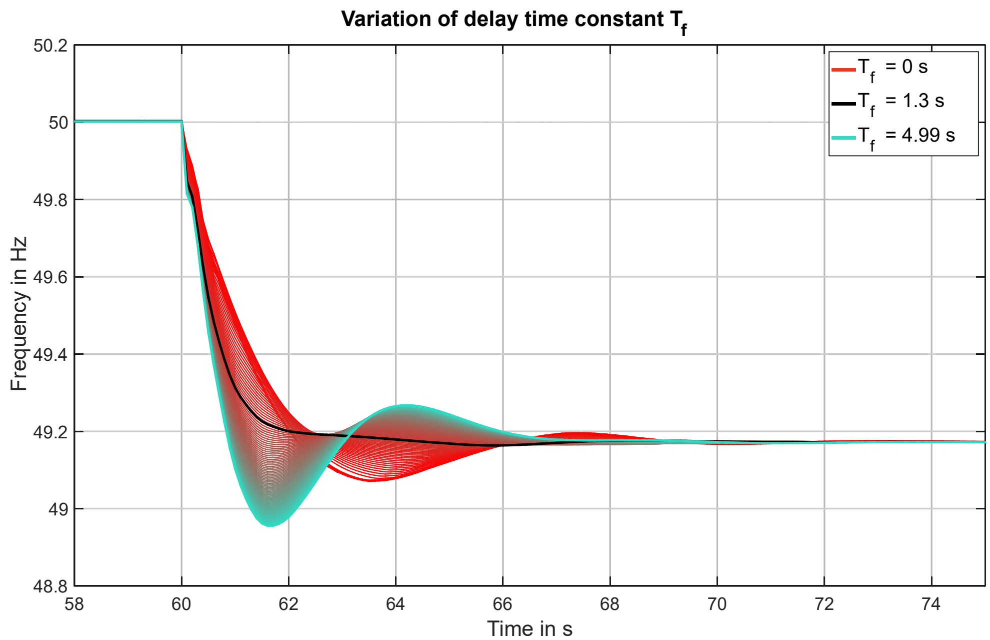

Figure 6.1: Variation of the frequency response of the system with time

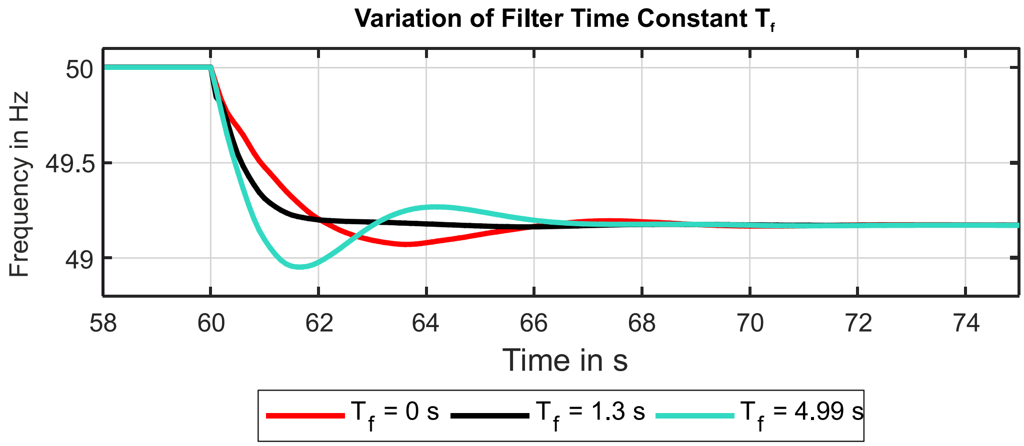

Figure 6.2: Variation of the frequency response of the system with time

In relation to power output of BSS, it is visible that the best result in terms of frequency nadir does not correlate with the case of highest power output as seen from Figure 6.3.

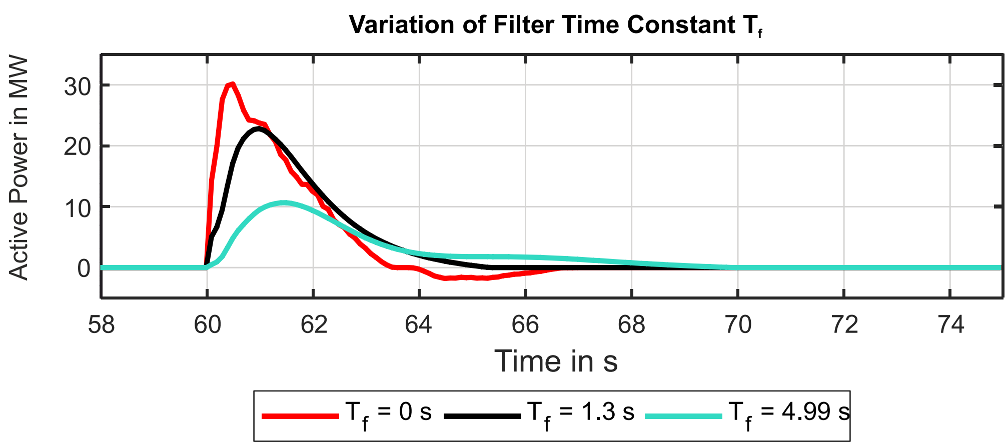

Figure 6.3: Variation of active power output of the BSS with time

Referring to Figure 6.4, the BSS energy output varies only slightly over the course of the active time which peaks at 13.82 kWh for T_f = 0 s, at 13.8 kWh for T_f = 1.3 s, and at 9.05 kWh for T_f = 4.99 s.

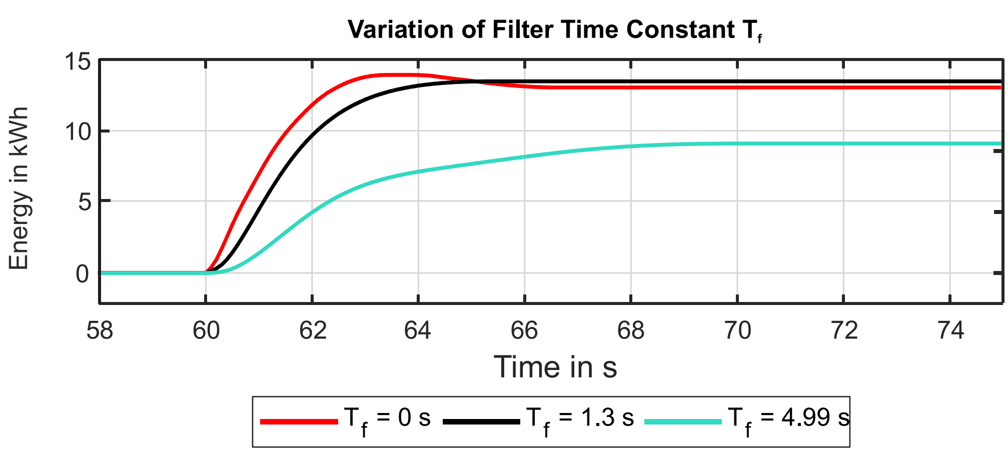

Figure 6.4: Variation of Energy of the BSS with time

Secondly, the proportional gain T_J was varied in the range 1 to 10 in steps of 1 and from 10 to 290 in steps of 10 resulting in 38 scenarios. The relevant parameters are given in Table 6.2 shows the values of the other parameters.

Table 6.2: Parameters of the artificial inertia controller C2.2 for the gain variation

Parameter	Description	Value
T_f	Filter time constant in s	1.3
K_d	Differentiator gain	-1
db	Deadband to avoid activation for small RoCoF	0.002
T_J	Proportional gain; equivalent to acc. time constant	**1 - 290**

The results obtained for frequency variation are illustrated in Figure 6.5 whereas Figure 66 illustrates those for power and Figure 6.7 illustrates energy consumption. Cyan corresponds to the largest proportional gain. It clear that the controller becomes unstable with higher values of gains and leads to oscillations even before the occurrence of the frequency event. To establish the most suitable gain, simple consideration of the frequency nadir is not the best approach. Controller stability is a concern and allowing a slight overshoot as seen with T_f = 110 is a more sensible solution. The difference between a gain of 110 and 210 for the frequency nadir is 0.1 Hz but as can be seen in Figure 6.7, the difference in energy consumption is significant.

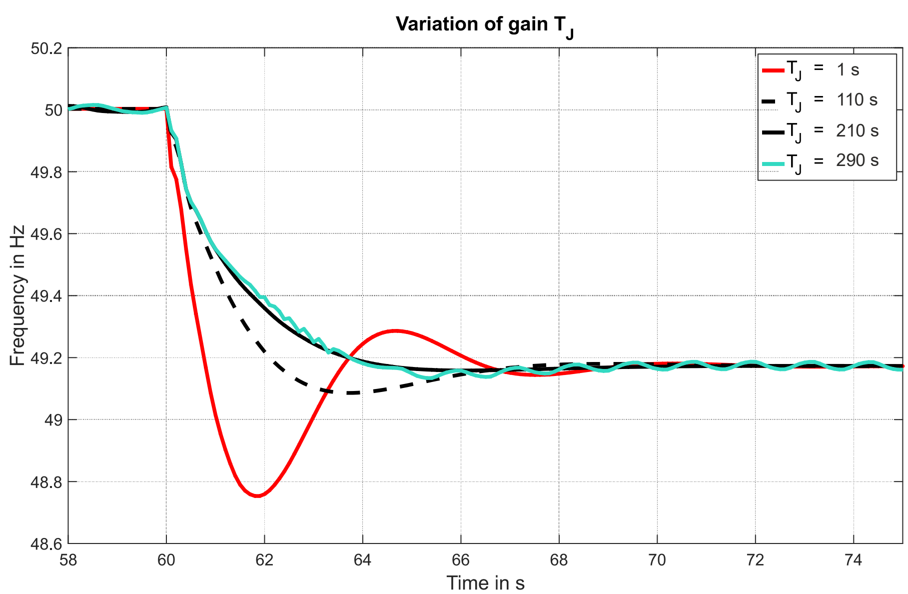

Figure 6.5: Variation of the frequency response of the system with time

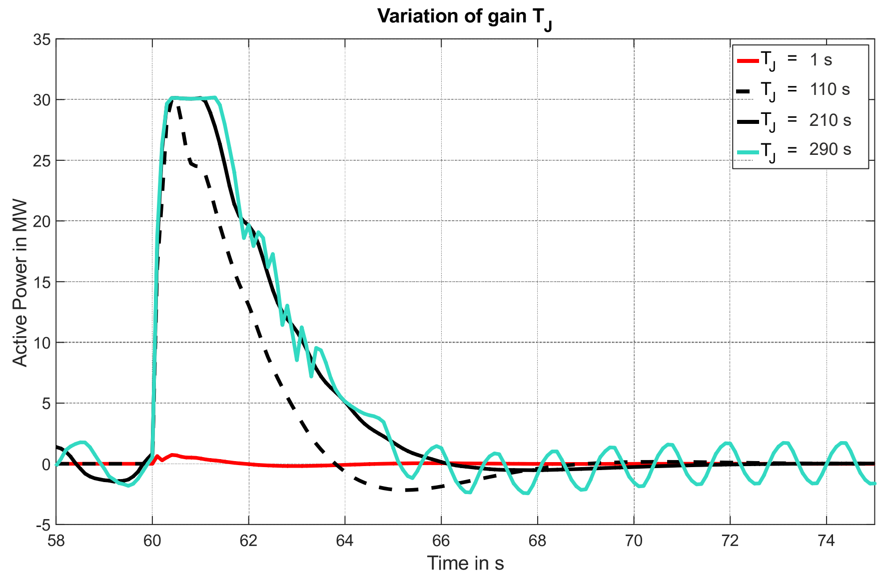

Figure 6.6: Variation of active power output of the BSS with time

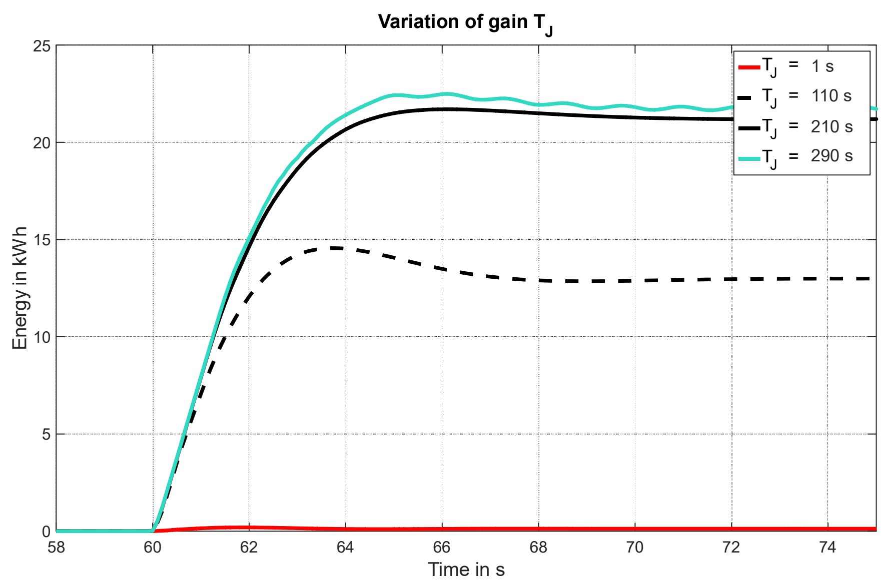

Figure 6.7: Variation of Energy of the BSS with time

6.2 Event Detection Controller C3

This controller activates a specific amount of active power output based on the severity of the frequency event. The time that is taken to assess the event was varied and three representative results are illustrated in Figure 6.8. In all cases the controller recognises the event as severe and activates the maximum power output to highlight the difference between longer and shorter activation times. It is clearly visible, that faster reaction times lead to lower frequency deviations. Technical limitations, such as the fast and correct acquisition of the frequency, however, restrict the actual speed of the controller, so that reaction times of 0.02 s are not achievable. In the network simulation model, with a time delay of one second, the frequency could still be kept above 49 Hz. However, the results clearly show that for fast frequency drops, any time delay is detrimental and should be kept as small as possible.

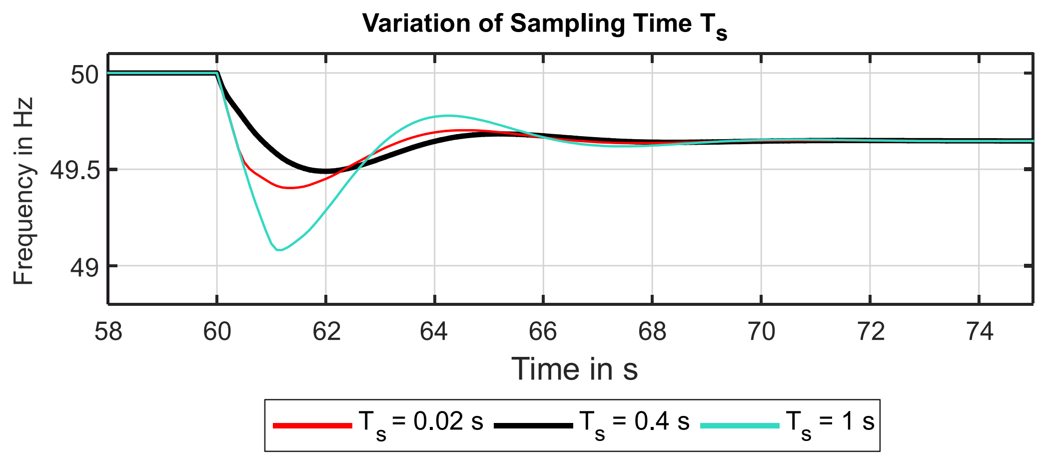

Figure 6.8: Variation of the frequency response of the system

6.3 RAVG Controller C4

Figure 6.9 shows the variation of proportional gain of the controller ranging from Kp = 10 to 400. The smallest frequency deviation is possible with the largest proportional gain. The cyan curve with a much lower gain shows similar results in terms of maximum frequency deviation. The results for a controller gain of 150 also experience less overshoot where the frequency nadir occurs earlier, and the oscillations stop faster.

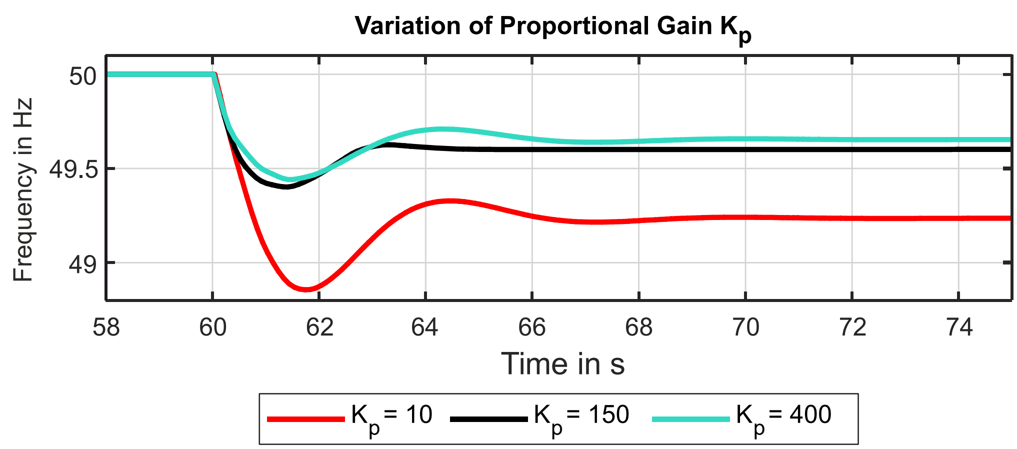

Figure 6.9: Variation of the frequency response of the system

6.4 Conclusion

The results clearly show that several key aspects should be included when implanting FFR. It was found that a slower reacting artificial inertia had a better effect than one without any delay. Artificial inertia showed a great impact on the overall frequency response with the lowest energy consumption. This makes this controller suitable for a wide range of converters that already have some form of energy storage such as wind turbines or the use of larger DC link capacitors in the inverter-based generation systems. For the event detection controller, a direct correlation between sample time and maximum frequency deviation was shown. For the RAVG controller it was shown that a too larger gain does not give the best overall result.

In summary, it can be stated that an automated simulation of different controller settings allows an accurate evaluation of a complex and nonlinear system.

Chapter 7

Conclusion and Recommendations for Future Work

The electricity grids of the future are expected to be weaker from a system inertia and system strength points of view and hence are expected to be more susceptible to disturbances. System separations and islanding scenarios will become more challenging because of unevenly distributed non-synchronous generation in interconnected systems. This thesis illustrated how the introduction of BSS into the power system can help to keep grids stable. With BSS, Fast Frequency Response can be introduced as a new service that takes advantage of their fast reaction times. FFR is the incorporation of rapid active power increase or decrease by generation or load in a frame of two seconds or less, to correct a supply-demand imbalance and assist in managing power system frequency. One of the questions that answered with this work, is how different BSS activation mechanisms compare with each other. For that, the difference between activation methods and technologies that can provide FFR were highlighted which resulted in the development of four different controllers. The basic principles for these controllers were derived from existing concepts for FFR such as the proportional controller or the event-based activation but during the research improvements to these methods were undertaken and further developed.

Although some manufacturers propose BSS with a proportional controller to participate in FCR, the application is limited by the capacity of the storage system. FCR market regulation demands that a participating generation unit must be able to participate in FCR during the whole time slot. There are exemptions for this rule in Austria but only if the BSS is operated in co-operation with a power plant that covers the long-term output. This highlights the fact that BSS are not suitable for FCR operation but should rather be used as FFR devices. Use of a proportional controller for FFR has the disadvantage that there is no inclusion of shut off. The BSS would have a power output if there is a frequency deviation above the deadband threshold. This would lead to the battery shutting off suddenly when the BSS is either full or empty – depending on the direction of power. An improvement to the proportional controller was made in the proposed controller C4 in the thesis. With an included rolling average set-point change, the BSS automatically reduced the power output after a predefined period. The goal for the event-based activation was to automatically detect relevant frequency events and activate according to the severity of the disturbance.

To test the performance of these controllers, a test system was developed that features different levels of renewable generation and therefore system inertia. The focus in this first assessment was on systems with low levels of inertia where FFR should be most impactful. With a loss of generation, the reaction of the controllers was measured and compared with each other. All controllers had a positive effect on the frequency stability of the test system. The battery system with Controller 3 can deliver a fast and predictable power output that is easily customisable for different grids. Controller 4 has the additional advantage that it utilises standard control theory functions which gives the controller the capability to react to changing circumstances where controller C3 would always follow a programmed curve. This gives controller C4 the ability to either reduce the power output alongside the frequency restoration or in a controlled manner following a predefined time. The artificial inertia controller C2.2 showed that a reduction of the RoCoF in a system with low inertia can help to stabilise the frequency by giving conventional power plants more time to react to the disturbance.

To examine if the controllers presented could be useful in a strong interconnected system such as the European mainland grid, an actual disturbance was used as the input to test the controllers. Two approaches were used to evaluate the controllers for this disturbance. The first approach was to use the measured signal as an input for the controllers. The result is the power output of a BSS if it would have been connected during the disturbance but the effect on the frequency cannot be evaluated. The results also represent the output of a single small BSS that participates but has no actual effect on the frequency. To study the effect on the frequency, a second approach was used. The disturbance was simulated with a simplified Central European grid using a single generator setup. Three different stages of BSS installation were considered to analyse the impact of future adoption of BSS in the system. The conclusion of these simulations was that different parameters and thresholds are necessary so that the controllers can operate appropriately. The reasons for this are that lower RoCoF occur and quick reactions by grid operators have in the past resulted in moderately impactful frequency disturbances. Besides that, due to the strong interconnected grid topology, the probability that the worst possible generation loss will occur is less likely, but it cannot be ruled out. Whereas the disconnection of the sole interconnector such as in the Australian grid is much more likely. These benefiting factors were also true for the investigated system separation disturbance examined in the thesis.

The differences between the tested grid topologies and therefore the associated frequency behaviour following a disturbance can be summarised in the difference in RoCoF and in maximum frequency deviation after a disturbance. A system with high levels of renewable generation will experience higher RoCoF due to the lower system inertia. Another factor is the type of generators participating in FCR. Even though there are minimum requirements for rise times, some generators can change the power output faster than others. This leads to differences in maximum frequency deviation when considering grids with the same amount of inertia but have a different generation mix. With this knowledge, Figure 7.1 can be used to identify the most appropriate controller type for FFR and for different grid topologies. It illustrates how well a grid can react to frequency disturbances. A grid with fast acting generators but high RoCoF (greater than 1 Hz/s) may best be helped with additional inertia in the form of artificial inertia. A grid that has relatively slow acting generators or even a momentary lack of FCR can utilise controllers C3 and C4 to provide additional support while generators ramp up.

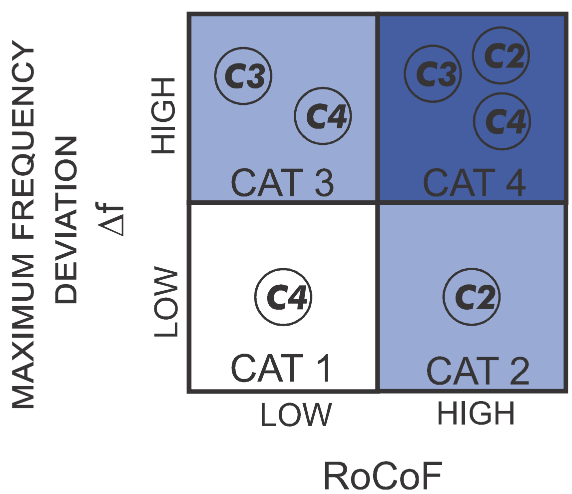

Figure 7.1: Categorisation of grids and the appropriate FFR controller

Besides the type of controller, the results in this thesis demonstrated the importance of correctly parametrising the controllers. It was found that even in a grid with high RoCoF, a slower reacting artificial inertia had a better effect than one without any delay. This was evaluated by automating several controller configurations and comparing the results. This automated approached allows for the assessment of a complex and nonlinear system.

In summary, the addition of a BSS that uses FFR can help mitigate the negative impacts of high rates of change of frequency after a significant grid disturbance linked to ever-increasing levels of inverter-based renewable energy sources. It was shown that all investigated controllers have a positive impact on the frequency drop after a major disturbance in grids with low levels of inertia.

It is possible that a BSS can have a combination of controllers. For example, the artificial inertia controller could be paired with the RAVG controller to provide a power output at different times of the disturbance. Future work could investigate such combinations.

In this thesis the simulations were carried out with a single BSS. It would be useful to investigate several BSS that are placed in key locations in a grid that employing different controllers, parameters and activation times and investigate the interactions and the effect on the frequency stability.

List of Publications arising from the work presented in this Thesis

"Frequency Stability in Future Grids: The Role of Storage Systems and Controller Strategies"

CIGRE South East European Regional Council Conference 2020 in Vienna, Austria

Vienna, Austria

"Frequency ancillary services with Battery Storage Systems"

41. CIGRE International Symposium

Ljubljana, Slovenia

References

[1] UCTE, "Final Report System Disturbance on 4 November 2006," 2007.

[2] J. Cochran, L. Bird, J. Heeter, and D. J. Arent, "Integrating Variable Renewable Energy in Electric Power Markets: Best Practices from International Experience, Summary for Policymakers," 2012.

[3] M. Katsanevakis, R. A. Stewart, and J. Lu, "Energy storage system utilisation to increase photovoltaic penetration in low voltage distribution feeders," *Journal of Energy Storage*, vol. 14, pp. 329–347, 2017, doi: 10.1016/j.est.2017.07.022.

[4] K. Hedegaard and P. Meibom, "Wind power impacts and electricity storage - A time scale perspective," *Renewable Energy*, vol. 37, no. 1, pp. 318–324, 2012, doi: 10.1016/j.renene.2011.06.034.

[5] H. Chen, T. N. Cong, W. Yang, C. Tan, Y. Li, and Y. Ding, "Progress in electrical energy storage system: A critical review," *Progress in Natural Science*, vol. 19, no. 3, pp. 291–312, 2009, doi: 10.1016/j.pnsc.2008.07.014.

[6] Y. W. Shen, D. P. Ke, Y. Z. Sun, D. S. Kirschen, W. Qiao, and X. T. Deng, "Advanced auxiliary control of an energy storage device for transient voltage support of a doubly fed induction generator," *IEEE Transactions on Sustainable Energy*, vol. 7, no. 1, pp. 63–76, 2016, doi: 10.1109/TSTE.2015.2472299.

[7] Aurecon, "Hornsdale Power Reserve - Year 1 Technical and Market Impact Case Study," 2018.

[8] REN21, "Renewables 2021 Global Status Report," Paris, 2021.

[9] Dr. S. Philips and W. Warmuth, "Fraunhofer ISE: Photovoltaics Report, updated: 14 March 2019," *Fraunhofer ISE: Photovoltaics Report, updated: 14 March 2019*, no. March, 2019.

[10] R. Austin, "Solar Energy Costs Trends Over Time," 2019. https://earthtechling.com/solar-energy-costs-trends/

[11] Clean Energy Council, "Progress and status of the renewable energy target," no. June, p. 11, 2016.

[12] Cigre Study Commity C4/C6, *727 Modelling of inverter-based generation for power system dynamic studies*. 2018.

[13] Australian Energy Market Operator (AEMO), “Black System South Australia 28 September 2016,” 2017.

[14] K. E. N. Modig. Erik Ørum, Mikko Kuivaniemi, Minna Laasonen, Alf Ivar Bruseth Erik Alexander Jansson, Anders Danell, “Nordic Report: Future System Inertia,” 2015.

[15] A. Kelly, “Grid Inertia – Fundamental concepts and the Developing Landscape EPRI Mission and Members,” 2020.

[16] Australian Energy Regulator, “Seasonal peak demand,” 2021. https://www.aer.gov.au/wholesale-markets/wholesale-statistics/seasonal-peak-demand-regions

[17] Australian Energy Market Operator (AEMO), “Inertia Requirements Methodology: Inertia Requirements & Shortfalls,” 2018.

[18] AEMC, “Managing power system fault levels,” 2018.

[19] J. Morren, S. W. H. de Haan, W. L. Kling, and J. A. Ferreira, “Wind turbines emulating inertia and supporting primary frequency control,” *IEEE Transactions on Power Systems*, vol. 21, no. 1, pp. 433–434, Feb. 2006, doi: 10.1109/TPWRS.2005.861956.

[20] E. Muljadi, V. Gevorgian, M. Singh, and S. Santoso, “Understanding inertial and frequency response of wind power plants,” *PEMWA 2012 - 2012 IEEE Power Electronics and Machines in Wind Applications*, no. July, 2012, doi: 10.1109/PEMWA.2012.6316361.

[21] NERC, “Fast Frequency Response Concepts and Bulk Power System Reliability Needs,” 2020.

[22] N. Miller, D. Lew, and R. Piwko, “Technology Capabilities for Fast Frequency Response,” 2017.

[23] M. R. Amin, M. Negnevitsky, E. Franklin, K. S. Alam, and S. B. Naderi, “Application of battery energy storage systems for primary frequency control in power systems with high renewable energy penetration,” *Energies (Basel)*, vol. 14, no. 5, 2021, doi: 10.3390/en14051379.

[24] I. F. Azhar, L. M. Putranto, and S. P. Hadi, “Design of Battery Energy Storage System Control Scheme for Frequency Regulation for PV Integrated Power

System," in *2020 FORTEI-International Conference on Electrical Engineering (FORTEI-ICEE)*, 2020, pp. 7–12. doi: 10.1109/FORTEI-ICEE50915.2020.9249865.

[25] Cigre Working Group B4.62, *671 Connection of wind farms to weak AC networks*, no. December. 2016.

[26] P. Kundur, N. J. Balu, and M. G. Lauby, *Power System Stability and Control*. McGraw-Hill Education, 1994. [Online]. Available: https://books.google.at/books?id=2cbvyf8Ly4AC

[27] P. M. Anderson and A. A. Fouad, *Power System Control and Stability*, 2nd Editio. 2003.

[28] A. G. G. Rodríguez, A. G. Rodríguez, and M. B. Payán, "Estimating wind turbines mechanical constants," *Renewable Energy and Power Quality Journal*, vol. 1, no. 5, pp. 697–704, Apr. 2007, doi: 10.24084/repqj05.361.

[29] V. Akhmatov, H. Knudsen, A. H. Nielsen, J. Kaas Pedersen, and N. K. Poulsen, "Modelling and transient stability of large wind farms," 2003. [Online]. Available: www.elsevier.com/locate/ijepes

[30] ENTSO-E, *Network Code on Load-Frequency Control and Reserves*. 2013.

[31] European Commission, *L220 /1 COMMISSION REGULATION (EU) 2017/1485 of 2 August 2017 establishing a guideline on electricity transmission system operation*. 2017.

[32] European Union, "Commission Regulation (Eu) 2016/631," *Official Journal of the European Union*, no. 14 April 2016, p. 68, 2016.

[33] Reliability Panel Australian Energy Market Commission, "The Frequency operating standard," vol. 3, no. November, pp. 1–11, 2017.

[34] K. Clark, N. Miller, and J. Sanchez-Gasca, "Modeling of GE Wind Turbine-Generators for Grid Studies," 2010.

[35] Australian Energy Market Operator (AEMO), "Fast Frequency Response in the NEM," 2017.

[36] Australian Energy Market Commission, "Fast frequency response market ancillary service, Draft rule determination," no. April, 2021.

[37] K. Dallmer-Zerbe, E. Spahic, G. Kuhn, R. Morgenstern, and G. Beck, “Fast frequency response in UK grid — Challenges and solution,” in *13th IET International Conference on AC and DC Power Transmission (ACDC 2017)*, 2017, pp. 1–6. doi: 10.1049/cp.2017.0013.

[38] National Grid ESO, “Response and Reserve Roadmap,” 2019.

[39] S. Homan and S. Brown, “The future of frequency response in Great Britain,” *Energy Reports*, vol. 7, pp. 56–62, 2021, doi: https://doi.org/10.1016/j.egyr.2021.02.055.

[40] National Grid ESO, “Dynamic Containment - Overview,” no. January, 2021.

[41] ENTSO-E, “Fast Frequency Reserve – Solution to the Nordic inertia challenge,” 2019.

[42] Fingrid, “The technical requirements and the prequalification process of Frequency Containment Reserves (FFR),” no. May, p. 14, 2020.

[43] N. Lu, “An Artificial Neural Network-Based Frequency Nadir Estimation Approach for Distributed Virtual Inertia Control,” in *2019 IEEE 4th International Future Energy Electronics Conference (IFEEC)*, Nov. 2019, pp. 1–8. doi: 10.1109/IFEEC47410.2019.9015105.

[44] J. Fang, H. Li, Y. Tang, and F. Blaabjerg, “Distributed Power System Virtual Inertia Implemented by Grid-Connected Power Converters,” *IEEE Transactions on Power Electronics*, vol. 33, no. 10, pp. 8488–8499, 2018, doi: 10.1109/TPEL.2017.2785218.

[45] J. Fang, H. Li, Y. Tang, and F. Blaabjerg, “On the Inertia of Future More-Electronics Power Systems,” *IEEE Journal of Emerging and Selected Topics in Power Electronics*, vol. 7, no. 4, pp. 2130–2146, 2019, doi: 10.1109/JESTPE.2018.2877766.

[46] H. T. Nguyen, G. Yang, A. H. Nielsen, and P. H. Jensen, “Combination of synchronous condenser and synthetic inertia for frequency stability enhancement in low-inertia systems,” *IEEE Transactions on Sustainable Energy*, vol. 10, no. 3, pp. 997–1005, 2019, doi: 10.1109/TSTE.2018.2856938.

[47] R. Ghosh, N. R. Tummuru, B. S. Rajpurohit, and A. Monti, “Virtual Inertia from Renewable Energy Sources: Mathematical Representation and Control Strategy,”

2020 IEEE International Conference on Power Electronics, Smart Grid and Renewable Energy, PESGRE 2020, pp. 1–6, 2020, doi: 10.1109/PESGRE45664.2020.9070733.

[48] I. Vokony, "Effect of inertia deficit on power system stability - Synthetic inertia concepts analysis," *2017 6th International Youth Conference on Energy, IYCE 2017*, 2017, doi: 10.1109/IYCE.2017.8003725.

[49] H. R. Chamorro *et al.*, "Analysis of the Gradual Synthetic Inertia Control on Low-Inertia Power Systems," *IEEE International Symposium on Industrial Electronics*, vol. 2020-June, pp. 816–820, 2020, doi: 10.1109/ISIE45063.2020.9152448.

[50] A. G. Adamczyk, C. D. Barker, M. Ferraz, and R. S. Whitehouse, "Extracting artificial inertia from a HVDC transmission scheme," *IET Conference Publications*, vol. 2019, no. CP751, pp. 1–6, 2019, doi: 10.1049/cp.2019.0009.

[51] ENTSO-E, "Need for synthetic inertia (SI) for frequency regulation," no. January, p. 9, 2018.

[52] A. Tayyebi, F. Dörfler, F. Kupzog, Z. Miletic, and W. Hribernik, *Grid-Forming Converters -- Inevitability, Control Strategies and Challenges in Future Grid Applications*. 2018.

[53] S. Golestan, J. M. Guerrero, and J. C. Vasquez, "Three-Phase PLLs: A Review of Recent Advances," *IEEE Transactions on Power Electronics*, vol. 32, no. 3, pp. 1894–1907, 2017, doi: 10.1109/TPEL.2016.2565642.

[54] C. Liu, X. Tian, K. Chen, Y. Su, and Y. Li, "Effect of PLL on transient performance of wind turbines generator under voltage phase jump," *The Journal of Engineering*, vol. 2019, no. 16, pp. 967–971, 2019, doi: 10.1049/joe.2018.8783.

[55] S.-. Chung, "Phase-locked loop for grid-connected three-phase power conversion systems," *IEE Proceedings - Electric Power Applications*, vol. 147, no. 3, pp. 213–219, 2000, doi: 10.1049/ip-epa:20000328.

[56] D. Arricibita, L. Marroyo, and E. L. Barrios, "Simple and robust PLL algorithm for accurate phase tracking under grid disturbances," in *2017 IEEE 18th Workshop on Control and Modeling for Power Electronics (COMPEL)*, 2017, pp. 1–6. doi: 10.1109/COMPEL.2017.8013305.

[57] M. G. Taul, X. Wang, P. Davari, and F. Blaabjerg, “Robust Fault Ride Through of Converter-Based Generation During Severe Faults With Phase Jumps,” *IEEE Transactions on Industry Applications*, vol. 56, no. 1, pp. 570–583, 2020, doi: 10.1109/TIA.2019.2944175.

[58] M. M. Begović, P. M. Djurić, S. Dunlap, and A. G. Phadke, “Frequency tracking in power networks in the presence of harmonics,” *ICHPS 1992 - International Conference on Harmonics in Power Systems*, vol. 8, no. 2, pp. 151–157, 1992, doi: 10.1109/ICHPS.1992.559016.

[59] E. Chen, H. S. Timorabadi, and F. P. Dawson, “Real-time phasor measurement method including a GPS common time-stamp for distributed power system monitoring and control,” in *Canadian Conference on Electrical and Computer Engineering, 2005.*, 2005, pp. 441–444. doi: 10.1109/CCECE.2005.1556966.

[60] IEEE/IEC, “IEEE/IEC 60255-118-1-2018 - IEEE/IEC International Standard - Measuring relays and protection equipment - Part 118-1: Synchrophasor for power systems - Measurements.” 2018.

[61] G. Rietveld, P. Wright, and A. Roscoe, “Reliable Rate of Change of Frequency (RoCoF) Measurements: Use Cases and Test Conditions,” *IEEE Transactions on Instrumentation and Measurement*, vol. PP, p. 1, 2020, doi: 10.1109/TIM.2020.2986069.

[62] ENTSO-E, “Frequency Measurement Requirements and Usage,” no. January, Final Version 7, pp. 1–11, 2018.

[63] M. Katsanevakis, R. A. Stewart, and J. Lu, “Aggregated applications and benefits of energy storage systems with application-specific control methods: A review,” *Renewable and Sustainable Energy Reviews*, vol. 75, no. November 2016, pp. 719–741, 2017, doi: 10.1016/j.rser.2016.11.050.

[64] A. Malhotra, B. Battke, M. Beuse, A. Stephan, and T. Schmidt, “Use cases for stationary battery technologies: A review of the literature and existing projects,” *Renewable and Sustainable Energy Reviews*, vol. 56, pp. 705–721, 2016, doi: 10.1016/j.rser.2015.11.085.

[65] M. Kloess and K. Zach, “Bulk electricity storage technologies for load-leveling operation - An economic assessment for the Austrian and German power market,”

International Journal of Electrical Power and Energy Systems, vol. 59, pp. 111–122, 2014, doi: 10.1016/j.ijepes.2014.02.002.

[66] D. Zafirakis, K. J. Chalvatzis, G. Baiocchi, and G. Daskalakis, "The value of arbitrage for energy storage: Evidence from European electricity markets," *Applied Energy*, vol. 184, pp. 971–986, 2016, doi: 10.1016/j.apenergy.2016.05.047.

[67] Y. Wang, K. T. Tan, X. Y. Peng, and P. L. So, "Coordinated Control of Distributed Energy-Storage Systems for Voltage Regulation in Distribution Networks," *IEEE Transactions on Power Delivery*, vol. 31, no. 3, pp. 1132–1141, 2016, doi: 10.1109/TPWRD.2015.2462723.

[68] M. Sanduleac, L. Toma, M. Eremia, V. A. Boicea, D. Sidea, and A. Mandis, "Primary Frequency Control in a Power System with Battery Energy Storage Systems," *Proceedings - 2018 IEEE International Conference on Environment and Electrical Engineering and 2018 IEEE Industrial and Commercial Power Systems Europe, EEEIC/I and CPS Europe 2018*, no. 727481, pp. 1–5, 2018, doi: 10.1109/EEEIC.2018.8494490.

[69] M. Aneke and M. Wang, "Energy storage technologies and real life applications – A state of the art review," *Applied Energy*, vol. 179, pp. 350–377, 2016, doi: https://doi.org/10.1016/j.apenergy.2016.06.097.

[70] S. Vazquez, S. M. Lukic, E. Galvan, L. G. Franquelo, and J. M. Carrasco, "Energy Storage Systems for Transport and Grid Applications," *IEEE Transactions on Industrial Electronics*, vol. 57, no. 12, pp. 3881–3895, 2010, doi: 10.1109/TIE.2010.2076414.

[71] F. Milano and Á. O. Manjavacas, *Converter-Interfaced Energy Storage Systems*. Cambridge University Press, 2019.

[72] R. Van Noorden, "The rechargeable revolution: A better battery," *Nature*, vol. 507, no. 7490, pp. 26–28, 2014, doi: 10.1038/507026a.

[73] N. S. Wade, P. C. Taylor, P. D. Lang, and P. R. Jones, "Evaluating the benefits of an electrical energy storage system in a future smart grid," *Energy Policy*, vol. 38, no. 11, pp. 7180–7188, 2010, doi: https://doi.org/10.1016/j.enpol.2010.07.045.

[74] P. Crespo Del Granado, Z. Pang, and S. W. Wallace, “Synergy of smart grids and hybrid distributed generation on the value of energy storage,” *Applied Energy*, vol. 170, pp. 476–488, 2016, doi: https://doi.org/10.1016/j.apenergy.2016.01.095.

[75] Neoen, “Hornsdale Power Reserve,” 2021. https://hornsdalepowerreserve.com.au/

[76] The AES Corporation, “AES Commissions Alamitos Energy Storage Facility in Long Beach, California.” https://www.prnewswire.com/news-releases/aes-commissions-alamitos-energy-storage-facility-in-long-beach-california-301215792.html

[77] X. Li and X. Jia, “Development and Application of Dispatching and Energy Management System for 50MW/100MWh Battery Energy Storage Station,” in *2019 International Conference on Advanced Mechatronic Systems (ICAMechS)*, 2019, pp. 181–185. doi: 10.1109/ICAMechS.2019.8861643.

[78] International Energy Agency, “Energy Storage,” Paris, 2020.

[79] steag, “Large Scale Battery Systems,” 2021. https://www.steag.com/en/services/large-scale-battery-systems

[80] Terna, “THE ROLE OF STORAGE IN GRID MANAGEMENT,” 2021. https://www.terna.it/en/media/news-events/role-storage-grid-management

[81] TransnetBW, “Netzbooster Pilotanlage,” 2021. https://www.transnetbw.de/de/netzentwicklung/projekte/netzbooster-pilotanlage/projektueberblick

[82] International Energy Agency, “Energy Storage: Tracking Clean Energy Progress,” 2021. https://www.iea.org/fuels-and-technologies/energy-storage

[83] IRENA, “Utility-Scale Batteries Innovation Landscape Brief,” 2019.

[84] W. Cole and A. W. Frazier, “Cost Projections for Utility Scale Battery Storage,” 2019.

[85] K. Mongird, V. Viswanathan, J. Alam, C. Vartanian, V. Sprenkle, and R. Baxter, “2020 Grid Energy Storage Technology Cost and Performance Assessment,” 2020.

[86] L. Ruttledge, N. W. Miller, J. O'Sullivan, and D. Flynn, "Frequency Response of Power Systems With Variable Speed Wind Turbines," *IEEE Transactions on Sustainable Energy*, vol. 3, no. 4, pp. 683–691, 2012, doi: 10.1109/TSTE.2012.2202928.

[87] L. Miao, J. Wen, H. Xie, C. Yue, and W. Lee, "Coordinated Control Strategy of Wind Turbine Generator and Energy Storage Equipment for Frequency Support," *IEEE Transactions on Industry Applications*, vol. 51, no. 4, pp. 2732–2742, 2015, doi: 10.1109/TIA.2015.2394435.

[88] M. F. M. Arani and E. F. El-Saadany, "Implementing Virtual Inertia in DFIG-Based Wind Power Generation," *IEEE Transactions on Power Systems*, vol. 28, no. 2, pp. 1373–1384, 2013, doi: 10.1109/TPWRS.2012.2207972.

[89] M. Kayikci and J. V Milanovic, "Dynamic Contribution of DFIG-Based Wind Plants to System Frequency Disturbances," *IEEE Transactions on Power Systems*, vol. 24, no. 2, pp. 859–867, 2009, doi: 10.1109/TPWRS.2009.2016062.

[90] J. F. Conroy and R. Watson, "Frequency Response Capability of Full Converter Wind Turbine Generators in Comparison to Conventional Generation," *IEEE Transactions on Power Systems*, vol. 23, no. 2, pp. 649–656, 2008, doi: 10.1109/TPWRS.2008.920197.

[91] G. Lalor, A. Mullane, and M. O'Malley, "Frequency control and wind turbine technologies," *IEEE Transactions on Power Systems*, vol. 20, no. 4, pp. 1905–1913, Nov. 2005, doi: 10.1109/TPWRS.2005.857393.

[92] E. Waffenschmidt and R. S. Y. Hui, "Virtual inertia with PV inverters using DC-link capacitors," in *2016 18th European Conference on Power Electronics and Applications (EPE'16 ECCE Europe)*, 2016, pp. 1–10. doi: 10.1109/EPE.2016.7695607.

[93] G. Liu *et al.*, "A comparative study of equivalent circuit models and enhanced equivalent circuit models of lithium-ion batteries with different model structures," *IEEE Transportation Electrification Conference and Expo, ITEC Asia-Pacific 2014 - Conference Proceedings*, pp. 1–6, 2014, doi: 10.1109/ITEC-AP.2014.6940946.

[94] S. Grewal and D. A. Grant, "A novel technique for modelling the state of charge of lithium ion batteries using artificial neural networks," *IEE Conference Publication*, no. 484, pp. 174–179, 2001.

[95] Z. Haizhou, “Modeling of lithium-ion battery for charging/discharging characteristics based on circuit model,” *International Journal of Online Engineering*, vol. 13, no. 6, pp. 86–95, 2017, doi: 10.3991/ijoe.v13i06.6799.

[96] A. Rahmoun, A. Armstorfer, J. Helguero, H. Biechl, and A. Rosin, “Mathematical modeling and dynamic behavior of a Lithium-Ion battery system for microgrid application,” *2016 IEEE International Energy Conference, ENERGYCON 2016*, pp. 1–6, 2016, doi: 10.1109/ENERGYCON.2016.7513977.

[97] “Modified IEEE 9-bus test system.” https://www.kios.ucy.ac.cy/testsystems/index.php/dynamic-ieee-test-systems/ieee-9-bus-modified-test-system

[98] ENTSO-E, “System separation in the Continental Europe Synchronous Area on 8 January 2021 – 2nd update,” 2021. https://www.entsoe.eu/news/2021/01/26/system-separation-in-the-continental-europe-synchronous-area-on-8-january-2021-2nd-update/